DRMY1 promotes robust morphogenesis by sustaining translation of a hormone signaling protein

Shuyao Kong,[1,2,†] Mingyuan Zhu,[1,2,3,†] M. Regina Scarpin,[4] David Pan,[1,2] Longfei Jia,[5] Ryan E. Martinez,[4] Simon Alamos,[6,7,8] Batthula Vijaya Lakshmi Vadde,[1,2] Hernan G. Garcia,[9,10,11,12,13] Shu-Bing Qian,[5] Jacob O. Brunkard,[4] Adrienne H. K. Roeder [1,2,14,*]

[1] Weill Institute for Cell and Molecular Biology, Cornell University, Ithaca, NY 14853, USA
[2] Section of Plant Biology, School of Integrative Plant Science, Cornell University, Ithaca, NY 14853, USA
[3] Present address: Department of Biology, Duke University, Durham, NC 27708, USA
[4] Laboratory of Genetics, University of Wisconsin, Madison, WI 53706, USA
[5] Division of Nutritional Sciences, Cornell University, Ithaca, NY 14853, USA
[6] Environmental Genomics and Systems Biology Division, Lawrence Berkeley National Laboratory, Berkeley, CA 94720, USA
[7] Feedstocks Division, Joint BioEnergy Institute, Emeryville, CA 94608, USA
[8] Department of Plant and Microbial Biology, University of California at Berkeley, Berkeley, CA 94720, USA
[9] Biophysics Graduate Group, University of California at Berkeley, Berkeley, CA 94720, USA
[10] Department of Physics, University of California at Berkeley, Berkeley, CA 94720, USA
[11] Institute for Quantitative Biosciences-QB3, University of California at Berkeley, Berkeley, CA 94720, USA
[12] Department of Molecular and Cell Biology, University of California at Berkeley, Berkeley, CA 94720, USA
[13] Chan Zuckerberg Biohub-San Francisco, San Francisco, CA 94158, USA
[14] Lead Contact
[†] These authors contributed equally
[*] Correspondence: ahr75@cornell.edu

SUMMARY

Robustness is the invariant development of phenotype despite environmental changes and genetic perturbations. In the Arabidopsis flower bud, four sepals initiate at robust positions and times and grow to equal size to enclose and protect the inner floral organs. We previously characterized the mutant *development related myb-like1* (*drmy1*), where 3-5 sepals initiate at irregular positions and variable times and grow to different sizes, compromising their protective function. The molecular mechanism underlying this loss of robustness was unclear. Here, we show that *drmy1* has reduced TARGET OF RAPAMYCIN (TOR) activity, ribosomal content, and translation. Translation reduction decreases the protein level of ARABIDOPSIS RESPONSE REGULATOR7 (ARR7), a rapidly synthesized and degraded cytokinin signaling inhibitor. The resultant upregulation of cytokinin signaling disrupts the robust positioning of auxin signaling, causing variable sepal initiation. Our work shows that the homeostasis of translation, a ubiquitous cellular process, is crucial for the robust spatiotemporal patterning of organogenesis.

Keywords: Robustness, TOR, translation, cytokinin, auxin, ARR, ribosomopathy, Arabidopsis, sepal, morphogenesis

INTRODUCTION

Robustness, or canalization, is the invariant, reproducible development of phenotype, unchanged by environmental fluctuations, genetic perturbations, or gene expression noise[1–4]. Commonly, within an individual, a given number of organs develop at well-defined positions to a robust final size and shape, which is crucial for fitness under stabilizing selection[2]. For example, transplanted eyes, limbs, and kidneys in mammals grow to a mature size similar to their donor, irrespective of the mature size of the same type of organ in the recipient[5–7]. The pairs of wings and halteres in Drosophila develop to robust, precisely coordinated final size and shape, which are required for flight[8–11]. The characteristic cruciform flower in *Brassicaceae* consists of four petals[12], a trait that can contribute to pollinator attraction[13]. The robust positioning of leaves around the shoot apical meristem in plants, or phyllotaxis, ensures optimal light capture[14–16]. While these examples of developmental robustness have been documented for a long time, the underlying molecular mechanisms have just begun to be unveiled.

Earlier studies looking for genes involved in maintaining robustness have found *HEAT SHOCK PROTEIN 90* (*HSP90*). Mutations of *HSP90* cause a diverse array of phenotypic changes in plants, fruit fly, zebrafish, worm, and humans[4,17,18]. Notably, the display and severity of these changes vary between individuals and even between different parts of the same individual, indicating that developmental robustness is disrupted[17,18]. *HSP90* encodes a protein chaperone which has clients from nearly all developmental and signaling pathways[4]. *HSP90*, therefore, is a hub gene that affects numerous other genes within the gene network[2]. Disruption of such a hub gene would therefore trigger many defects in numerous developmental processes. Similarly, genes involved in central cellular processes such as chromatin remodelling[19–21], transcription[19,20], translation[22,23], and protein degradation[24,25] are also hub genes, and they have been found to be important for developmental robustness in various systems including fungi, animals, and plants. How these broadly acting hub genes contribute to the robustness of tissue-specific developmental phenotypes is still largely unclear.

We have developed the *Arabidopsis* sepal as a system to elucidate the mechanisms maintaining robustness in organ size and shape[26–28]. Sepals are the outermost floral organs whose function is to enclose buds and protect the developing inner organs, i.e. petals, stamens, and carpels, before the flower blooms. To fulfill this protective function, each flower robustly develops four sepals of equal length, allowing them to close at the top (Figure 1A, middle left); these four sepals are of equal width and positioned 90° from each other, leaving no gap on the sides (Figure 1A, top left). This robustness in sepal size and shape stems from the robust initiation of the four sepal primordia from the floral meristem with precisely coordinated spatiotemporal patterns[26] (Figure 1A, bottom left). The initiated sepal primordia attain robust final size and shape by spatiotemporal averaging of cellular growth variability during sepal elongation, and synchronous progression of a whole-flower growth termination signal from tip to base[27]. In addition, noise in gene expression must be kept low to ensure sepal size robustness[29]. We previously characterized a mutant in *DEVELOPMENT RELATED MYB-LIKE 1* (*DRMY1*) that

87 develops flowers where the inner organs are exposed due to gaps between sepals[26]. The gaps
88 are caused by variability in sepal development. Specifically, some sepals are shorter than others,
89 leaving gaps on the top (Figure 1A, middle right); the arrangement of sepals around the flower
90 deviate from the canonical form such that parts of the flower are not covered by a sepal, leaving
91 gaps on the side (Figure 1A, top right). This variability in the size, number, and position of the
92 mature sepal originates from the earliest stages of floral development where the initiation of sepal
93 primordia is variable in spatiotemporal patterns (Figure 1A, bottom right). Variability in sepal
94 initiation, in turn, is driven by the loss of robust patterning of auxin and cytokinin[26], two plant
95 hormones critical for organ initiation and morphogenesis[30–32], in the floral meristem before sepal
96 initiation. However, the molecular mechanism through which DRMY1 maintains robust hormone
97 patterning is still unknown.
98
99 In this study, we elucidate a mechanism through which DRMY1 maintains robust hormone
100 patterning and thus robust sepal initiation. Specifically, we find that DRMY1 maintains proper
101 activity of TARGET OF RAPAMYCIN (TOR), a crucial regulator of ribosome biogenesis and
102 protein translation[33,34], and thereby sustains translation *in vivo*. When *DRMY1* is mutated, the
103 protein level of ARABIDOPSIS RESPONSE REGULATOR7 (ARR7), a rapidly synthesized and
104 degraded cytokinin signaling inhibitor, is reduced in the floral meristem. Consequently, cytokinin
105 signaling uniformly increases in the meristem periphery, causing variability in auxin patterning
106 and sepal initiation. We further propose that the increase in cytokinin signaling may be a survival
107 mechanism to alleviate the translation rate reduction when ribosomal content is limited. In
108 summary, our work shows that the hub processes of TOR signaling and translation, which occur
109 in every cell, have very specific roles in robust organ primordium initiation by sustaining the rapid
110 synthesis of a hormone signaling protein.
111
112
113 **RESULTS**
114
115 **The *drmy1* mutant has reduced TOR activity, ribosome content, and translation rate**
116
117 *DRMY1* encodes a MYB/SANT domain protein which may exert transcriptional
118 regulation[26]. To look for differentially expressed genes in *drmy1* which may be candidates
119 underlying variable sepal initiation, we performed RNA-sequencing (RNA-seq) in *drmy1* and wild
120 type (WT) of *apetala1* (*ap1) cauliflower (cal) AP1-GR* background[35,36]. The *ap1 cal AP1-GR*
121 inflorescence produces numerous tightly packed ball-shaped meristems, which, upon induction
122 of AP1-GR with dexamethasone, synchronously initiate sepal primordia, allowing us to collect
123 large quantities of floral meristems with sepal primordia initiating (Stage 3)[37] (Figure S1A). We
124 crossed *drmy1* into *ap1 cal AP1-GR* and performed RNA-seq on induced inflorescences of WT
125 and *drmy1* in this background. We detected transcripts from a total of 21,496 genes, of which
126 1,042 (4.8%) were differentially expressed in *drmy1* (Figure S1B; Supplemental Dataset 1). We
127 found that the 443 genes downregulated at the transcript level in *drmy1* were most enriched in
128 the gene ontology (GO) term “Translation”, a fundamental and ubiquitous cellular process that

129 converts genetic information from transcript to protein. Within this term, genes encoding ribosomal
130 components were most downregulated (Figure S1C). The 443 downregulated genes were also
131 enriched in several other GO terms related to ribosome biogenesis and assembly (Figure 1B).
132 We therefore hypothesized that ribosome abundance and translation rate are lower in *drmy1*,
133 potentially altering the accumulation of proteins critical to developmental robustness.
134
135 To determine whether and how ribosome abundance and translation are affected in
136 *drmy1*, we performed polysome profiling in induced inflorescences of WT and *drmy1* in *ap1 cal*
137 *AP1-GR* background. Compared to WT, polysomal peaks are drastically reduced in *drmy1* (Figure
138 1D; Supplemental Dataset 2). To see whether this reduction in ribosomal content affected
139 translation rate (*de novo* protein synthesis) *in vivo*, we performed puromycin labeling. Samples
140 were incubated with puromycin, an amino acid-tRNA analog that is incorporated into nascent
141 polypeptide chains and can be detected using an anti-puromycin antibody to infer global
142 translation rate[38,39]. In both young seedlings and induced *ap1 cal AP1-GR* inflorescences, we
143 found that the puromycin level detected in *drmy1* mutant samples was much reduced compared
144 to WT (Figure 1E), indicating translation rate is reduced. We hypothesized that a reduction in
145 protein translation should likely result in a decrease in protein level. For this, we looked at a
146 ubiquitously expressed membrane marker *UBQ10::mCherry-RCI2A*, and found that it had a small
147 (~25%) but significant decrease in fluorescence intensity in the inflorescence meristem and young
148 floral buds of *drmy1* compared with WT. We also measured its fluorescence intensity in the
149 ribosomal mutant *ul4y* (*rpl4d*)[40] and we found that the decrease in fluorescence intensity in *drmy1*
150 is even greater than in *ul4y* (Figure S1G-J). These results validate our proteomics findings, and
151 show that ribosome content and translation are indeed reduced in the *drmy1* mutant.
152
153 To test how the global repression of translation in *drmy1* impacts its proteome, we
154 extracted total soluble protein from induced inflorescences of WT and *drmy1* in *ap1 cal AP-GR*
155 background and performed mass spectrometry. We identified a total of 5,077 proteins, of which
156 548 (10.8%) were differentially accumulated in *drmy1* (Figure S1B; Supplemental Dataset 1).
157 These differentially accumulated proteins were enriched in GO terms related to translation and
158 ribosomal assembly (Figure 1C). Despite the overall reduction in ribosomes (Figure 1D), relative
159 to other proteins, ribosomal components are more abundant in *drmy1* (Figure S1D; Supplemental
160 Dataset 1). This is not true for all proteins involved in translation; poly-A binding proteins and
161 tRNA synthetases, for example, are relatively less abundant in *drmy1* than in WT. Moreover, the
162 26S proteasome responsible for targeted protein degradation is much more abundant in *drmy1*
163 than in WT (Supplemental Dataset 1). In concert, these results demonstrate that the machinery
164 responsible for maintaining protein homeostasis is substantially dysregulated in *drmy1*.
165
166 A key signaling pathway that regulates protein homeostasis is TARGET OF RAPAMYCIN
167 (TOR)[41,42]. TOR is a hub that integrates information from light, sugars, nutrient availability, etc.,
168 to promote growth-related processes, including ribosome biogenesis and translation, and to
169 repress catabolic processes, including protein degradation by autophagy and the
170 proteasome[33,34,43–45]. We therefore hypothesize that the decrease in ribosomal content and protein

171 translation in *drmy1* may reflect altered TOR signaling. To test for signatures of transcriptomic
172 changes that have been well defined in seedlings under TOR inhibition[34,46,47], we performed RNA-
173 seq on seedlings of WT, *drmy1*, WT treated with AZD-8055 (a potent TOR inhibitor), and mock-
174 treated WT (Supplemental Dataset 3). We found that the *drmy1* mutation causes transcriptomic
175 changes similar to TOR inhibition (Figure 1F). A significant portion of genes differentially
176 expressed under TOR inhibition vs. mock were also differentially expressed in *drmy1* vs. WT
177 (466/2044 = 22.8%; hypergeometric test, $p = 4.7 \times 10^{-108}$). Not only were these 466 genes
178 differentially expressed in both situations, but also most of them were coherently downregulated
179 or upregulated (439/466 = 94.2%, Chi-square test, $p < 2.2 \times 10^{-16}$; Figure S1E). Genes coherently
180 downregulated in both situations were enriched in GO terms related to translation and ribosome
181 biogenesis, and, most strikingly, a quarter of them were under the GO term "translation" (Figure
182 1F, S1F). These similar transcriptomic changes support our hypothesis that TOR activity is
183 reduced in *drmy1*. To further test this hypothesis, we measured TOR activity in WT and *drmy1* by
184 assaying the phosphorylation of its direct substrate, RIBOSOMAL PROTEIN eS6 KINASE
185 (S6K)[48,49]. While the total protein level of S6K did not change in *drmy1*, we found that S6K
186 phosphorylation decreased by half, demonstrating reduced TOR activity (Figure 1G, 1H). Overall,
187 these results are consistent with the idea that *drmy1* has reduced TOR activity—a main pathway
188 controlling ribosome biogenesis and translation—which causes reduced ribosomal content and
189 translation rate.
190
191 **Defects in TOR activity, ribosome integrity, and translation disrupt robust sepal initiation**
192
193 We next asked whether defects in TOR activity, ribosome, or translation have any effects
194 on robust sepal initiation like the *drmy1* mutation does (Figure 2A vs 2B; also see Zhu et al.[26]). In
195 a WT bud, initiation is robust in that four sepal primordia of similar size form evenly spaced around
196 the periphery of the floral meristem (Figure 2A, 2H). Angles between them vary little, i.e., they are
197 all at around 90° angles from each other (Figure 2I, 2J). By contrast, in *drmy1* buds, three to five
198 sepal primordia initiate and grow to different sizes (Figure 2B, 2H; also see Zhu et al.[26]). The
199 *drmy1* sepal primordia are generally unevenly spaced, and angles between them have a high
200 coefficient of variation (CV) (Figure 2I, 2J). To determine whether defects in ribosomes can cause
201 the same sepal initiation defects, we imaged three ribosomal mutants, *ul4z* (*rpl4a*), *ul4y*, and *ul18z*
202 (*rpl5a*)[40], each mutated in a gene encoding a ribosomal component that is also downregulated in
203 *drmy1* at the transcript level (Figure S1C). The *ul4z* mutant bud shows reduced size of the inner
204 sepal primordia relative to the outer sepal primordia (Figure 2C), and slightly more variable spatial
205 distribution of sepal primordia (Figure 2J), although it always develops four sepal primordia
206 (Figure 2H). This is a weaker phenotype than *drmy1* but has similar characteristics. The *ul4y* and
207 *ul18z* mutants show great variability in the number and position of sepal primordia (Figure 2D,
208 2E, 2H, 2J), more similar to *drmy1*. We also crossed these ribosomal mutants with *drmy1* to study
209 sepal variability in the double mutants (Figure S2A-H). In *drmy1 ul4z*, *drmy1 ul4y*, and *drmy1*
210 *ul18z/+*, on average, sepal initiation was as variable as in the *drmy1* single mutant (Figure S2I,
211 SIJ). However, there were buds with no outgrowth in the adaxial or lateral regions of the bud
212 periphery (Figure S2B, S2E, S2G), buds with six sepal primordia (Figure S2C, S2F, S2H), and

213 buds with two outer sepal primordia (Figure S2D, S2H), which were not seen in the single mutants.
214 Note that we were unable to characterize the homozygous *drmy1 ul18z* double mutant because
215 they were embryo-lethal (Figure S2K), further supporting the idea that ribosomal mutations
216 enhance the phenotypic defects in *drmy1*.
217
218 We then imaged mutants with reduced TOR activity to determine whether sepal initiation
219 is also less robust. *lst8-1-1* is a T-DNA insertional mutant of the TOR complex component LST8-
220 1[50] and is weakly hypomorphic in TOR activity. We found that *lst8-1-1* shows variable sepal
221 initiation in a small proportion of buds (4/41, 9.8%) (Figure 2F, 2H, 2J). The *spaghetti-1* mutant
222 defective in TOR complex 1 (TORC1) assembly[51] showed a level of variability comparable to the
223 *drmy1* mutant and the ribosomal mutants *ul4y* and *ul18z* (Figure 2G, 2H, 2J). Mutants with more
224 severe disruption of TOR activity are embryo lethal and could not be analyzed[51,52]. These results
225 show that reduction in TOR activity can cause variability in sepal initiation, similar to *drmy1*.
226
227 To corroborate these findings, we directly inhibited translation by *in vitro* culture of
228 dissected WT inflorescences on 2 μM cycloheximide (CHX, a chemical inhibitor of translation) for
229 9-10 days. This is a low concentration that does not completely block translation, as
230 inflorescences were still alive after 10 days in this condition. Compared with mock, CHX-treated
231 inflorescences develop buds that have 2 to 6 sepal primordia of variable sizes that are unevenly
232 spaced around the bud periphery (Figure 2K, 2M, 2N). These phenotypes are stronger than
233 *drmy1*. Similarly, we directly inhibited TOR activity by continuous bi-daily application of 2 nmol
234 Torin2 to the growing shoot apex for 15 days, and we observed variable sepal initiation (Figure
235 2L, 2M, 2N). Overall, data reported above show that inhibition of TOR activity and translation can
236 disrupt the robustness of sepal initiation, in terms of sepal primordium number, position, and size.
237
238 We previously showed that the *drmy1* mutant bud develops sepals of different sizes
239 because some sepal primordia initiate much later than others[26]. The late-initiating primordia
240 remain smaller throughout development. They end up as smaller sepals relative to those that
241 initiated earlier, leaving gaps that expose the developing inner floral organs[26]. We asked whether
242 TOR or ribosomal defects disrupt the relative timing of sepal initiation just as the *drmy1* mutation
243 does. We live imaged WT and *ul4y* every six hours during sepal initiation and quantified the
244 amount of time the bud takes to initiate the inner and lateral sepals after it initiates the outer sepal.
245 In WT, after the initiation of the outer sepal, most buds initiate the inner sepal within 6 hours and
246 the lateral sepals within 12 hours (Figure 3A, 3C; also see Zhu et al.[26]). In *ul4y*, the initiation times
247 of the inner and lateral sepals are more variable and delayed relative to the outer sepal, with 7.5%
248 of the buds initiating the inner sepal 18 hours after the outer sepal, and 32.5% of the buds initiating
249 the lateral sepals 18 hours after the outer sepal (Figure 3B, 3C). Similarly, we compared the
250 relative timing of sepal initiation in Torin2 vs mock-treated WT buds. While in most mock-treated
251 buds, the inner and lateral sepals initiate within 12 hours after the outer sepal (Figure 3D, 3F), in
252 Torin2-treated buds they are much more variable and delayed (Figure 3E, 3F), to a similar extent
253 as previously observed in *drmy1*[26]. In some cases, the inner and lateral sepals initiate more than

30 hours after the outer sepal. These results show that TOR and ribosomal defects can disrupt the precisely orchestrated initiation timing of sepal primordia.

Does the variability in initiation timing cause variable sizes and gaps in mature sepals, as in *drmy1* (Figure S3A,B,G,H; also see Zhu et al. [26])? We imaged the mature sepals of the ribosomal mutants *ul4z*, *ul4y*, *ul18z*, as well as the TOR component mutant *lst8-1-1*. Surprisingly, unlike *drmy1*, the sepals in *ul4z*, *ul4y*, *ul18z* enclose the inner floral organs perfectly, leaving no gaps, regardless of sepal number (Figure S3C-E). Small gaps still exist in buds of *lst8-1-1*, although sepal size differences appear greatly reduced (Figure S3F). Further dissection shows that in these mutants, sepals within the same flower are of similar sizes, although sepals from different flowers can be of vastly different sizes, most conspicuously for *lst8-1-1* (Figure S3I-N). This is unlike *drmy1*, where sepal size variability is equally high comparing sepals within the same flower or from different flowers (Figure S3H, S3M-N). Upon closer examination, while sepals initiating late in *drmy1* buds remain small, continuously leaving a gap in the sepal whorl (Figure S3O-P), those in *ul4y* were able to catch up with the other sepals and close the gap (Figure S3Q). Our results are consistent with the hypothesis that there exists a size-coordinating mechanism independent of TOR or ribosome function that allows sepals within the same bud to reach the same mature length, and that this mechanism is disrupted in *drmy1*. Such a mechanism requires further investigation in future studies.

Inhibition of TOR activity and translation increase cytokinin signaling and disrupts the robust spatial pattern of auxin and cytokinin signaling

Auxin and cytokinin are two important plant hormones critical to many aspects of plant development[30–32], and there is accumulating evidence that they act synergistically in the shoot apical meristem to promote lateral organ initiation[16,53,54]. We previously showed that, in a WT floral meristem prior to sepal initiation, auxin and cytokinin signaling are concentrated at the four incipient primordia, which is required for robust sepal initiation from these regions (Figure 4A, S4A; Zhu et al.[26]). In the *drmy1* mutant, cytokinin signaling becomes stronger and diffuse around the bud periphery (Figure 4A-B). Auxin signaling also becomes more diffuse, forming irregular auxin maxima that are less focused than those in WT, except at the incipient outer sepal where it remains robust (Figure 4A, S4B; Zhu et al.[26]). These changes in hormone signaling correlate with variable sepal initiation (Figure S4B)[26]. We wondered whether ribosomal mutations have similar effects on auxin and cytokinin signaling. To this end, we imaged the auxin signaling reporter *DR5::3xVENUS-N7* and the cytokinin signaling reporter *TCS::GFP* in floral meristems of the ribosomal mutant *ul4y*. Both reporters lose their robust spatial pattern except in the incipient outer sepal (Figure 4A, S4C). The hormone signaling patterns were quantified by circular histogram analysis (see Methods for details). For each of DR5 and TCS, WT buds showed four clear peaks ~90 degrees apart from each other, with very little signal in between, whereas in *drmy1* and *ul4y*, peaks were barely seen except at the incipient outer sepal (at 45 degrees), and there was greater noise and variation all around the bud (Figure 4C-D). Diffuse bands of auxin signaling that typically occurs in the adaxial or lateral periphery of *drmy1* and *ul4y* buds (Figure S4B and S4C, brackets)

can later resolve into several distinct auxin maxima of various intensity and at various positions, correlated with the initiation of sepal primordia of various sizes at these same positions (Figure S4B and S4C, red arrowheads).

We also tested whether drug treatments that inhibit TOR activity or translation can disrupt the robust hormone patterning. Buds treated *in vitro* with the translation inhibitor CHX (2 μM) for 3 days showed a 50% increase in cytokinin signaling, and both auxin and cytokinin signaling became diffuse around the bud periphery (Figure 4E-H). By day 6, cytokinin signaling was still diffuse all around, and increased to more than two-fold relative to mock (Figure 4I, 4J, 4L). Auxin signaling formed maxima of variable number at variable positions (Figure 4I arrowheads, 4K), correlated with the variable initiation of sepal outgrowth at these positions (Figure S4D-E). Similar changes occurred in buds treated *in vitro* with the TOR inhibitor AZD-8055 (2 μM) for 6 days (Figure 4I-L). For both CHX and AZD-8055, the disruptions of hormone signaling are similar to *drmy1*. *In vivo* treatment using another TOR inhibitor Torin2 for 15 days increased cytokinin signaling by 70%, although it did not make auxin and cytokinin signaling more diffuse (Figure S4F-I). Overall, these results show that defects in TOR activity and translation increase cytokinin signaling, and disrupt the precise spatial patterning of cytokinin and auxin signaling required for robust sepal initiation.

An increase in cytokinin signaling is necessary and sufficient for variable auxin signaling and sepal initiation under translation inhibition

Auxin is a critical hormone in organogenesis[55,56]. As shown above, variable patterning of auxin signaling correlates with variable sepal initiation during inhibition of TOR activity and translation. We wondered what caused auxin to lose its robust patterning under such conditions. It was previously reported that the ribosomal mutants *ul4y*, *ul18z*, and *el24y* have reduced protein levels of AUXIN RESPONSE FACTOR (ARF) 3, 5, and 7[57–59], key transcription factors that mediate the auxin signaling response[60]. The transcripts of these ARFs contain upstream open reading frames (uORFs), requiring translation reinitiation to translate their main open reading frames[61,62], a process defective in *ul4y*, *ul18z*, and *el24y*[57–59]. We therefore hypothesized that *drmy1* loses robust auxin signaling pattern because of reduced translation of uORF-containing transcripts, including those of certain ARFs. To begin, we utilized our transcriptomics and proteomics data, and considered that the protein-transcript ratio of a gene should reflect both its level of translation and stability. Therefore, following our hypothesis, genes containing uORFs should, in general, have a lower protein-transcript ratio in *drmy1* than in WT. We calculated the difference of this ratio between *drmy1* and WT for all 5,086 gene-protein pairs in our inflorescence dataset, and compared the ratio against the number of uORFs in each transcript (Figure S5A; uORF data from von Arnim et al.[62]). We found a small but significant decrease in the protein-transcript ratio in *drmy1* for the 724 genes containing at least 2 uORFs in their transcripts, supporting the hypothesis that *drmy1* has reduced translation reinitiation for uORF-containing transcripts, just like the ribosomal mutants *ul4y*, *ul18z*, and *el24y*[57–59]. Then, we examined whether the translation reinitiation of uORF-containing ARFs are indeed reduced in the *drmy1*

338 mutant. We selected *ARF3/ETTIN*, *ARF5/MONOPTEROS*, and *ARF6*, which have 2, 6, and 6
339 uORFs respectively, and as controls, *ARF8* and *ARF10* which do not contain uORFs. None of
340 these *ARF*s were differentially expressed in *drmy1* at the transcript level, except *ARF10* which
341 was slightly upregulated (Figure S5B). We utilized promoter-fluorescent protein fusion reporters
342 (Figure S5C) which have the same uORFs in the promoter region as the corresponding ARF
343 genes if the genes have them. These reporters reflect transcriptional and uORF-mediated
344 translational regulation. *pARF3::N3xGFP*, *pARF5::ER-EYFP-HDEL*, and *pARF6::N3xGFP*
345 contain uORFs and thus, following our hypothesis, are expected to drastically decrease in
346 fluorescence intensity in *drmy1* compared to WT. *pARF8::N3xGFP* and *pARF10::N3xGFP* do not
347 have uORFs and are thus expected to have comparable or higher fluorescence intensity in *drmy1*.
348 Surprisingly, we saw no correlation between the presence of uORFs and decrease in fluorescent
349 intensity in *drmy1* (Figure S5C). While it might arise from additional layers of regulation on these
350 ARFs, this result suggests that the decrease in translation reinitiation of uORF-containing ARFs
351 is not the main factor explaining the loss of robust auxin signaling pattern in *drmy1*.
352
353 It was previously reported that external application of cytokinin increases auxin
354 biosynthesis in actively growing tissue including the shoot apex, young leaves, and roots[63], and
355 cytokinin application also changes the expression and polarity of PIN-FORMED (PIN) polar auxin
356 transport carriers[64,65]. We previously noticed that external application of 6-benzylaminopurine
357 (BAP), a synthetic cytokinin, induced additional convergence points of PIN1 and increased
358 variability in auxin signaling, causing variability in sepal initiation (Zhu et al.[26], in this reference
359 see Fig. 4e, Extended Data Fig. 7e and 7f). Here, we confirmed this observation by circular
360 histogram analysis (Figure 5A-D). While the mock-treated WT buds showed four clear peaks of
361 DR5 signal with very little signal in between (Figure 5A-B), those treated with 5 μM BAP showed
362 a less robust spatial pattern, with less distinguishable peaks and larger variation all around the
363 bud (Figure 5C-D). Thus, excessive cytokinin is sufficient for the variable spatial pattern of auxin
364 signaling.
365
366 We then wondered whether an increase in cytokinin signaling (Figure 4) is the cause of
367 variable pattern of auxin signaling under translation-limited conditions such as *drmy1*. To test this
368 hypothesis, we crossed *drmy1* containing the DR5 reporter with a triple mutant of *ARABIDOPSIS*
369 *RESPONSE REGULATOR* (*ARR*) *1*, *10*, and *12*, the three most highly expressed B-type ARRs
370 in our RNA-seq (Supplementary Dataset 1) which are crucial for the activation of cytokinin-
371 responsive genes[66]. While buds of *arr1,10,12* did not show apparent phenotypic differences from
372 WT, the quadruple mutant *drmy1 arr1,10,12* largely rescued the *drmy1* phenotype, with much
373 less variability in sepal number and position (Figure 5E-G). While mature buds of *drmy1* have
374 sepals of variable sizes, leaving gaps and exposing the inner floral organs (Figure S6D vs. S6A),
375 those of *drmy1 arr1,10,12* have sepals of robust sizes that are able to close (Figure S6E).
376 Likewise, mutation in a cytokinin receptor *WOODEN LEG* (*WOL*)/*ARABIDOPSIS HISTIDINE*
377 *KINASE 4* (*AHK4*) showed a similar rescue of the *drmy1* sepal phenotype (Figure 5E-G, S6F).
378 While the auxin signaling reporter DR5 was diffuse and variable in *drmy1* except in the incipient
379 outer sepal (Figure 5H-I), in *drmy1 arr1,10,12*, it was focused in all the four incipient sepals that

380 were robustly positioned, although the signal intensity in the incipient outer sepal was much higher
381 than others (Figure 5J-K). These results indicate that cytokinin signaling is required for the
382 variability in auxin signaling pattern and sepal initiation in *drmy1*.
383
384 Furthermore, we wanted to test whether cytokinin signaling is required for variability in
385 more general conditions where translation is inhibited. The translation inhibitor CHX disrupted
386 robustness in auxin signaling and sepal initiation in WT (Figure 2K, 4E, 4I), and we tested whether
387 these effects are still present in *arr1,10,12* and *wol* mutants. We found that, unlike WT, sepal
388 initiation remained mostly robust in *arr1,10,12* and *wol* after ten days of 2 μM CHX treatment
389 (Figure 5L-N). While DR5 in WT became diffuse and occurred in variable positions after three
390 days of CHX treatment (Figure 5O-P, arrow), DR5 in *arr1,10,12* remained robust and
391 concentrated at the four incipient sepal primordia (Figure 5Q-R). These results suggest that
392 elevated cytokinin signaling level is the primary cause for variability in auxin patterning under
393 translation-inhibited conditions. Thus, in WT, maintaining a low level and focused cytokinin
394 signaling is crucial for robust auxin patterning and sepal initiation.
395
396 **Upregulation of cytokinin signaling is required to sustain translation and fitness in *drmy1***
397
398 Why does the plant upregulate cytokinin signaling at the cost of robust morphogenesis
399 under translation-inhibited conditions? Early studies revealed that cytokinin signaling can
400 stimulate translation[67–71], by increasing transcription or protein abundance of ribosomal
401 components or biogenesis factors[72–74] and modification of initiation and elongation factors[75]. We
402 therefore hypothesized that an increase in cytokinin signaling under translation-inhibited
403 conditions such as in *drmy1* serves to sustain a survivable rate of translation in a feedback loop.
404 We first validated that, under our growth conditions, an increase in cytokinin signaling (*arr1*
405 *35S::ARR1*) increases translation rate (Figure 6A; also see Karunadasa et al.[67]) in 14-day-old
406 seedlings. We then tested whether cytokinin signaling is required to sustain translation, especially
407 in *drmy1* (Figure 6B-C). The cytokinin receptor single mutant *wol* does not differ from WT in
408 translation rate 8 days after germination but shows a reduced translation rate at day 14.
409 Conversely, at day 8, *drmy1* seedlings showed a drastically reduced translation rate compared to
410 WT, but by day 14, translation rate in *drmy1* increased and matched WT. In the *drmy1 wol* double
411 mutant, however, translation rate was unable to recover at day 14 and remained lower than either
412 single mutant. Our data suggests that cytokinin signaling is required to sustain translation in
413 *drmy1*, despite reduced ribosomal content (Figure 1D).
414
415 We then examined whether removal of cytokinin signaling and consequent failure to
416 sustain translation in *drmy1* affects plant vitality and reproduction. As expected, at day 14, the
417 *drmy1 wol* double mutant plants were extremely small, with tiny and chlorotic cotyledons and true
418 leaves (Figure 6D). These plants typically produced tiny rosettes and short inflorescences with a
419 few chlorotic buds that develop into small, short siliques (Figure 6E, S6F). Similarly, the *drmy1*
420 *arr1,10,12* quadruple mutant plants are slightly chlorotic and accumulate anthocyanins in the
421 rosette leaves (Figure 6F). They produced a tiny inflorescence composed of very few buds (Figure

422 6F, S6E) and, in the end, siliques in which all seeds had aborted (Figure 6G). Overall, these
423 results show that the growth defects in *drmy1* are exaggerated by downregulation of cytokinin
424 signaling. While it is possible that *drmy1* can be particularly sensitive to other defects caused by
425 cytokinin downregulation, our results are consistent with the hypothesis that the upregulation of
426 protein synthesis by increased cytokinin signaling promotes the survival of mutants with reduced
427 ribosomal content such as *drmy1*.
428
429 **Translation inhibition decreases the level of ARR7, a cytokinin signaling inhibitor protein**
430
431 What causes cytokinin signaling to increase in plants with reduced TOR activity and
432 translation (Figure 4)? It was previously known that *cis*-type cytokinins can be synthesized from
433 tRNAs by the tRNA isopentenyltransferases (IPTs), IPT2 and IPT9[76]. We hypothesized that the
434 decrease in translation rate may increase the availability of tRNAs as substrates for cytokinin
435 biosynthesis, increasing the level of cytokinins. To test this idea, we extracted cytokinins from
436 induced inflorescences of WT and *drmy1* in *ap1 cal AP1-GR* background (Figure S1A). We
437 measured the level of three cytokinin bases, *trans*-Zeatin (tZ), *cis*-Zeatin (cZ), and
438 isopentenyladenine (iP), and their corresponding nucleosides (tZR, cZR, and iPR), using liquid
439 chromatography-mass spectrometry. Surprisingly, we found no significant difference in their
440 levels between WT and *drmy1*, and notably, the amount of *cis*-Zeatin was barely detectable in all
441 samples (Figure S7A). This suggests that the increase in *cis*-type cytokinin synthesis is not the
442 mechanism underlying the increase in cytokinin signaling under our translation-inhibited
443 conditions.
444
445 We then considered the effects that a decrease in translation rate might have on the
446 protein components of the cytokinin signaling pathway. A-type ARR proteins are inhibitors of
447 cytokinin signaling[77–79]. They are rapidly induced upon cytokinin application and serve to dampen
448 cytokinin response in the tissue[80–82]. These proteins also have a fast turnover rate, being rapidly
449 depleted upon blocking translation with a half-life ranging from 60 to 180 min[83]. The rapid
450 synthesis and degradation of these proteins may be crucial for maintaining homeostasis of
451 cytokinin signaling during developmental processes. We therefore hypothesized that, during
452 sepal initiation, translation defects in *drmy1* cause reduced synthesis of A-type ARR proteins,
453 decreasing them to a level insufficient to repress cytokinin signaling (Figure 7A).
454
455 We set out to test whether the level of A-type ARR proteins are reduced in *drmy1*. We
456 were unable to detect fluorescence in the inflorescence of a published GFP-tagged A-type ARR
457 line under the endogenous promoter (*pARR4::ARR4-GFP*)[84]. We reasoned that this was because
458 A-type ARRs have low protein levels in the inflorescence (none was detected in our proteomics
459 dataset) and fast turnover rates[83]. We therefore employed LlamaTagging, a recently developed
460 method to visualize the abundance of nuclear-localized proteins with short half-lives[85]. Rapidly
461 degraded proteins cannot be visualized through fusion with standard fluorescent proteins,
462 because fluorescent proteins take time to fold and mature before they fluoresce, and the protein
463 of interest is degraded before the maturation of the fluorescent protein. On the other hand, the

464 LlamaTag folds immediately. A LlamaTag with a high affinity for GFP can be encoded as a
465 translational fusion with a nuclear-localized protein of interest. In this case, soon after translation,
466 the fusion immediately binds GFP in the cytosol and translocates the GFP with the protein to the
467 nucleus. Thus, increased GFP fluorescence in the nucleus indicates higher abundance of the
468 protein of interest. We decided to focus on ARR7, the A-type ARR that is most highly expressed
469 in our RNA-seq dataset and not differentially expressed in *drmy1* (Figure 7B; Supplemental
470 Dataset 1). We designed a construct with ARR7 fused with GFP-specific LlamaTag by a short
471 linker, driven by the ARR7 native promoter (*pARR7::ARR7-linker-llama-ARR7ter*; *ARR7-llama* for
472 short). This construct was co-transformed with cytosol-localized GFP containing a nuclear
473 exclusion signal (*pUBQ10::sfGFP-nes-UBQ3ter*; *GFP-nes* for short; Figure 7C). When ARR7-
474 llama is produced in the cytosol, LlamaTag binds to cytosolic GFP. ARR7 then localizes to the
475 nucleus, guided by its C-terminal nuclear localization signal[86,87], dragging GFP into the nucleus.
476 Thus, when ARR7-llama is present at a low level, GFP is predominantly cytosol-localized; at an
477 intermediate level, GFP may be nearly equally localized in the cytosol and nucleus; at a high level,
478 most GFP are transported by ARR7-llama into the nucleus, and thus GFP signal is mainly seen
479 in the nucleus (Figure 7D).
480
481 As a proof of concept, we treated this reporter in WT background with 200 μM BAP. We
482 found that GFP signal became more nuclear-localized within 5 hours of the treatment (Figure
483 S7B), agreeing with an increased expression and stability of A-type ARR proteins upon cytokinin
484 application as previously reported[83,88].
485
486 We then compared the localization of GFP signal in floral meristems of WT and *drmy1*
487 before sepal initiation. Following our hypothesis, if the increase in cytokinin signaling in *drmy1* is
488 caused by reduced translation of A-type ARR proteins, there should be a decrease in ARR7 level,
489 and thus an increase in cytosolic GFP signal, in *drmy1* vs WT. On the other hand, if the increase
490 in cytokinin signaling in *drmy1* is caused by any other mechanism, we should see an increase in
491 ARR7 level and nuclear GFP signal because cytokinin signaling increases the gene expression
492 and protein stability of A-type ARRs[81,83,89]. We found that WT buds had slightly more nuclear-
493 localized GFP signal than cytosol-localized GFP signal, with brighter spots corresponding to the
494 nucleus surrounded by darker grooves in between corresponding to the cytosol (Figure 7E-F). In
495 contrast, in the periphery of *drmy1* buds, GFP signal localizes more to the cytosol than to the
496 nucleus, with darker spots surrounded by brighter grooves (Figure 7E-F). More nuclear GFP was
497 present near the center of *drmy1* buds. This result indicates nuclear ARR7 protein concentration
498 is reduced in the *drmy1* mutant, particularly in the zone where sepals initiate. To see whether this
499 conclusion holds in other translation-inhibited conditions, we treated WT plants carrying the
500 *ARR7-llama* and *GFP-nes* reporters with the translation inhibitor CHX and the TOR inhibitor AZD-
501 8055. 2 μM CHX treatment for 24 hours drastically reduced the nuclear localization of the GFP
502 signal and increased its cytosolic localization (Figure 7G). 2 μM AZD-8055 treatment for 72 hours
503 had a milder but similar effect (Figure 7H). These treatments did not affect the localization of the
504 GFP signal in plants without *ARR7-llama* (Figure S7C-D). These results show that conditions that
505 decrease translation rate generally decrease the nuclear level of ARR7 protein. Further, these

results are consistent with our hypothesis that disruption of protein translation upregulates cytokinin signaling in the floral meristem due to depletion of A-type ARR proteins. This suggests that the rapid synthesis of A-type ARR proteins is crucial for maintaining homeostasis of cytokinin signaling during sepal initiation.

Given that the level of nuclear ARR7 was reduced in *drmy1*, we next asked whether increasing the level of ARR7 would restore robustness in *drmy1*. We found that while WT buds carrying the *ARR7-llama* and *GFP-nes* constructs do not phenotypically differ from WT without these constructs (Figure 7I-J, S7E-F), *drmy1* plants with these constructs show a partial restoration of sepal initiation robustness, particularly in terms of sepal primordium position (Figure 7K-N, S7G-H). In stage 9-12 buds, some buds have robustly sized sepals that are able to close properly, while others still have variably sized sepals that leave gaps just like in *drmy1* (Figure S7H). Thus, increasing ARR7 level by adding an extra functional transgene of *ARR7-llama* to the genome can partially restore robustness in both sepal initiation and mature sepal size in *drmy1*. This indicates that the decrease in ARR7 protein level in *drmy1* is at least partially responsible for its variability in these aspects.

We also considered other protein components of auxin and cytokinin signaling that are being rapidly synthesized and degraded during developmental processes, and therefore, may be depleted under translation defects. AUXIN/INDOLE-3-ACETIC ACID INDUCIBLE (Aux/IAA) proteins are auxin signaling inhibitors that are rapidly induced by auxin[90,91]. In the presence of auxin, they are rapidly degraded, mediated by the ubiquitin E3 ligase SKP1, CUL1, F-BOX PROTEIN (SCF) complex involving TRANSPORT INHIBITOR RESPONSE1/AUXIN SIGNALING F-BOX (TIR1/AFB)[92–95]. Degradation is dependent on the Short Linear Motif (SLiM) degron contained within Domain II (DII)[94–96]. We hypothesized that the level of DII-containing proteins including Aux/IAAs would be drastically decreased in *drmy1* because they are unable to be rapidly synthesized to keep up with their degradation. To test this, we used the R2D2 reporter[97], which contains a DII fused with 3xVENUS (*pUS7Y::DII-n3xVENUS*), and as a control, a mutated non-degraded DII fused with tdTomato (*pUS7Y::mDII-ntdTomato*). We compared this reporter in *drmy1* vs. WT. The ratio of *VENUS* to *tdTomato* was not reduced in *drmy1*, but instead slightly but significantly elevated (Figure S7I-J). In addition, *drmy1* has stochastic patches of DII-VENUS degradation, consistent with its often mislocalized auxin maxima (Figure 4A, S4B), unlike WT which had four patches of degradation corresponding to the four incipient sepal primordia where auxin maxima robustly form (Figure 4A, S4A). Overall, these results suggest that the level of DII-containing Aux/IAA proteins is not reduced in *drmy1*, despite the high requirement for synthesis due to their rapid turnover. They also indicate that not all proteins that are rapidly synthesized and depleted in response to hormone signaling are equally affected by translation inhibition, which may result in different changes in hormone signaling output under such condition.

DISCUSSION

548 Robustness, the strikingly reproducible development of phenotype, has fascinated
549 biologists for decades[2]. The Arabidopsis flower robustly develops four sepals of equal size. This
550 stems from the robust initiation of four sepal primordia from the floral meristem, which is in turn
551 dictated by the robust patterning of auxin and cytokinin controlled by DRMY1[26]. Here we
552 elucidated how DRMY1 controls robust hormone patterning and thus robust sepal initiation. We
553 show that DRMY1 sustains TOR activity, ribosomal content, and translation. We further show that
554 inhibition of TOR activity or translation is sufficient to cause variability in the timing, position, and
555 number of sepal primordia, mimicking the *drmy1* phenotype. Our findings are in concert with
556 previous studies that have shown robustness is often maintained by genes involved in central
557 cellular processes[2]. In our case, the rate of translation in wild type maintains a proper level of
558 ARR7, which needs to be rapidly synthesized to dampen cytokinin signaling. ARR7 in turn
559 ensures a normal level and spatial pattern of cytokinin signaling and indirectly auxin signaling,
560 and thus robust sepal initiation (Figure 7O, top). In the *drmy1* mutant, the reduced TOR activity,
561 ribosomal content, and translation rate causes inability to rapidly synthesize ARR7, which are
562 short-lived proteins that are easily depleted[83]. Consequently, cytokinin signaling is elevated,
563 disrupting the robust spatial distribution of both cytokinin and auxin, leading to variable sepal
564 initiation (Figure 7O, bottom). Blocking cytokinin signaling in *drmy1* is sufficient to restore robust
565 initiation of four sepal primordia, but has severe consequences on the overall fitness of the plant.
566 Our results reveal how defects in hub cellular processes such as TOR signaling and translation
567 can have very tissue-specific phenotypic effects.
568
569 It was discovered long ago that extrinsic cytokinin application to plant tissue or cell-free
570 extracts can promote mRNA translation[68–71]. Recent studies further confirmed that the up-
571 regulation of translation by cytokinin is at least in part mediated by the cytokinin signaling
572 pathway[67,75]. Here, we show that cytokinin signaling in floral buds is upregulated in translation-
573 inhibited conditions, such as *drmy1*, AZD-8055 treatment, or CHX treatment (Figure 4; also see
574 Zhu et al.[26]), through reduced level of ARR7 (Figure 7). The enhanced cytokinin signaling
575 maintains translation rate at a level necessary for the survival and reproduction of the plant (Figure
576 6). We propose that there is a homeostasis mechanism where plants leverage increased cytokinin
577 signaling to rescue the translation rate reduction caused by deficient TOR activity and ribosomal
578 content (Figure 7O, bottom). It remains to be tested how widely this mechanism is applicable to
579 other mutants with ribosomal defects, or whether parallel mechanisms operate in other species
580 across kingdoms.
581
582 While translation-inhibited plants likely upregulate cytokinin signaling to maintain protein
583 synthesis, this upregulation negatively affects developmental robustness. We have previously
584 shown that exogenous cytokinin application to the WT floral meristem increases variability in PIN1
585 convergence and auxin signaling patterns, and consequently, in sepal initiation. Mutation of a
586 cytokinin signaling inhibitor *AHP6* causes similar variability in sepal initiation. These effects are
587 more pronounced in the *drmy1* mutant, which by itself has increased and diffuse cytokinin
588 signaling[26]. Here, we provide additional evidence that increased and diffuse cytokinin signaling is
589 necessary for such variability. While *drmy1* and CHX-treated WT floral meristems are variable in

590 auxin signaling pattern and sepal initiation (Figure 2, 4), mutations in *wol* and *arr1,10,12*, which
591 decreases cytokinin signaling, largely restore robustness (Figure 5). Robustness is also restored
592 in the mature sepals of *drmy1 wol* and *drmy1 arr1,10,12*, enabling sepal closure (Figure S6).
593 Similar effects in restoring robustness are seen when an extra functional transgene of *ARR7*
594 (*pARR7::ARR7-llama*) is introduced to the *drmy1* mutant (Figure 7, S7). Our results suggest that
595 cytokinin upregulation is necessary and sufficient for variability in auxin patterning and sepal
596 initiation, indicating that the cytokinin signaling changes are primary defects in *drmy1*, and the
597 auxin signaling changes are secondary. Our results suggest a mechanism different from that
598 previously reported in *ul4y*, *ul18z*, and *el24y*, where ribosomal mutations affect auxin signaling
599 through reduced translation reinitiation of uORF-containing mRNAs, including those of AUXIN
600 RESPONSE FACTOR (ARF) 3, 5, and 7[57–59]. While we found that uORF-containing mRNAs
601 generally have reduced protein-transcript ratio in *drmy1* suggestive of reduced translation, we did
602 not see a consensus reduction in the level of uORF-containing promoter reporters of ARFs (Figure
603 S5). This suggests that the variable auxin signaling pattern in *drmy1* is unlikely to result from
604 changes in uORF-mediated translational regulation of ARFs. Overall, our results suggest that
605 homeostasis in cytokinin signaling is crucial for maintaining robust patterns of auxin signaling and
606 robust morphogenesis in the floral meristem.
607
608 Mutations affecting ribosome biogenesis or translation have long attracted interest due to
609 the surprisingly tissue-specific phenotypes they cause[98]. In humans, these mutations have been
610 associated with diseases collectively known as ribosomopathies, where patients show various
611 abnormalities in blood, skeleton, hair, teeth, and pancreas, as well as intellectual disability and
612 increased risk of cancer[99–104]. Ribosomal protein mutants have been characterized in numerous
613 other species with similarly diverse impacts. They display a range of specific phenotypic changes,
614 such as altered pigmentation and skeletal structure in mouse[105–107] and zebrafish[108], shorter
615 bristles and notched wing margins in fruit fly[22,109], abnormal gonad development in worm[110], and
616 pointed leaves and abnormal vascular patterning in Arabidopsis[57,58,111–113]. Here, we show that
617 the Arabidopsis mutant *drmy1* has reduced TOR activity, ribosomal content, and translation rate,
618 causing variable sepal initiation which phenocopies the ribosomal mutants *ul4y* and *ul18z* and the
619 TORC1 assembly mutant *spaghetti-1* (Figure 2, 3). We therefore propose that *drmy1* is an
620 Arabidopsis ribosomopathy mutant like those previously characterized[112].
621
622 Several mechanisms have been proposed to explain why ribosomopathies do not usually
623 cause a general reduction in growth, but rather affect development in tissue-specific ways. These
624 include extra-ribosomal functions of certain ribosomal proteins[114–118], altered translation behavior
625 of ribosomal variants on certain mRNAs[119], different competitiveness of mRNAs for scarce
626 ribosomes[57–59,120–123], and high translation rate requirement for certain proteins[124,125]. For example,
627 neurotransmitter release in animals relies on constant synthesis of the synaptic vesicle protein
628 Syt1[126]. A Drosophila *Minute* mutant, *uS15/+,* shows reduced synthesis of Syt1, which in turn
629 reduces ecdysone secretion in 5-HT neurons, causing delayed larval-to-pupal transition[124].
630 Similarly, the human apoptosis inhibitor Mcl-1 has a half-life of ~30 min and thus requires a high
631 translation rate to maintain its proper level. Under translation inhibition, Mcl-1 is rapidly degraded,

632 causing apoptosis[125]. Here, we show that the level of ARR7, another rapidly synthesized and
633 degraded protein[83], is drastically reduced under translation inhibition, which underlies the
634 upregulation of cytokinin signaling and loss of robustness in auxin signaling and morphogenesis
635 (Figure 7). This mechanism parallels those previously found in animal systems[124,125], and
636 highlights how defects in translation, which occurs in every cell, can have tissue-specific effects
637 on how cells robustly arrange into organs. Outside the floral meristem, the *drmy1* mutant shows
638 other phenotypic changes such as enlarged shoot apical meristem, reduced apical dominance,
639 phyllotaxy defects, and reduced root system, all of which are related to altered cytokinin/auxin
640 signaling activity[26].
641
642 In addition, we note that not all proteins that are rapidly synthesized and depleted in
643 response to hormone signaling are equally affected under broad translation inhibition. Our data
644 suggest that DII-containing proteins, including auxin signaling inhibitors Aux/IAAs, are not present
645 at a lower level in *drmy1* (Figure S7H-I). Aux/IAAs are degraded by the proteasome in an auxin-
646 dependent manner[96], while A-type ARRs can also be degraded by selective autophagy when
647 phosphorylated, in addition to proteasomal degradation[84]. In addition, the transcription of *Aux/IAA*
648 genes can be induced under translation inhibition, possibly as a feedback mechanism to maintain
649 Aux/IAA protein homeostasis[90]. Therefore, distinct turnover mechanisms and/or transcriptional
650 regulation may shape distinct effects of translational inhibition on the level of these hormone
651 signaling proteins.
652
653
654 **ACKNOWLEDGEMENTS**
655 We thank Bella Burda, Frances Clark, Byron Rusnak, Erich Schwarz, Avilash Yadav, and Maura
656 Zimmermann for comments and suggestions on the manuscript. We thank Frank Wellmer for the
657 *ap1 cal 35S::AP1-GR* (Ler) seeds. We thank Elliot Meyerowitz and Arnavaz Garda for the
658 *DR5::3xVENUS-N7/PIN1::GFP* (Ler) seeds. We thank Teva Vernoux and Géraldine Brunoud for
659 the *TCS::GFP* and *TCS-DR5* (Col) seeds. We thank Jan Smalle for the *arr1-1 35S::ARR1* seeds.
660 We thank Joseph Kieber, Jamie Winshell, and Kwame Acheampong for the *pARR4::ARR4-GFP*
661 seeds. We thank Thomas Greb and Min-Hao Chiang for the *pARF5::ER-ARF5-HDEL* seeds. We
662 thank Georg Jander for advice and protocol for cytokinin extraction. We thank Brian Curtis and
663 Frank Schroeder for help on mass spectrometry. We thank Sheng Zhang and Qin Fu for help on
664 Xcalibur. We thank Richie Ragas, Yanã Rizzieri, and Ziqing Wei for assistance on experiments
665 and data analysis. We thank Vicky Spencer and Minsung Kim for sharing the *in vivo* Torin2
666 treatment protocol. We thank Arabidopsis Biological Resource Center for providing seed stocks
667 and plasmids used in this research. Research reported in this publication was supported by the
668 National Institute of General Medical Sciences of the National Institutes of Health (NIH) under
669 award numbers R01GM134037, DP5OD023072, and R01GM145814; Cornell Graduate School
670 new student fellowship (S.K.); and in part by a Schmittau-Novak Grant from the School of
671 Integrative Plant Science, Cornell University (M.Z.). H.G.G. was supported by NIH Director's New
672 Innovator Award (DP2 OD024541-01) and NSF CAREER Award (1652236), NIH R01 Award
673 (R01GM139913), and the Koret-UC Berkeley-Tel Aviv University Initiative in Computational

674 Biology and Bioinformatics. H.G.G. is also a Chan Zuckerberg Biohub Investigator. We thank the
675 Biotechnology Resource Center (BRC) Genomics Facility (RRID:SCR_021727) of Cornell
676 University for performing RNA-seq on *ap1 cal AP1-GR* inflorescence samples. We thank
677 Novogene for performing seedling RNA-Seq library synthesis and sequencing. We thank the BRC
678 Proteomics Facility (RRID:SCR_021743) of Cornell University for performing mass spectrometry
679 on *ap1 cal AP1-GR* inflorescence samples, and NIH SIG Grant 1S10 OD017992-01 for supporting
680 the Orbitrap Fusion mass spectrometer. The content is solely the responsibility of the authors and
681 does not necessarily represent the official views of the National Institutes of Health.
682
683

684 **AUTHOR CONTRIBUTIONS**

685 S.K.: Conceptualization, Investigation, Formal Analysis, Visualization, Writing - Original Draft,
686 Writing - Review & Editing. M.Z.: Conceptualization, Investigation, Formal Analysis, Writing -
687 Review & Editing. M.R.S: Investigation, Visualization. D.P.: Investigation, Formal Analysis,
688 Visualization. L.J.: Investigation. R.E.M.: Investigation, Formal Analysis. S.A.: Methodology,
689 Resources. B.V.L.V.: Methodology, Resources, Writing - Review & Editing. H.G.: Methodology,
690 Resources, Writing - Review & Editing, Supervision. S.B.Q: Writing - Review & Editing,
691 Supervision. J.O.B.: Resources, Writing - Review & Editing, Supervision. A.H.K.R:
692 Conceptualization, Writing - Review & Editing, Supervision, Project administration, Funding
693 acquisition.
694
695

696 **DECLARATION OF INTERESTS**

697 The authors declare no competing interests.

698 **FIGURE TITLES AND LEGENDS**

699

700 **Figure 1. *drmy1* has reduced ribosome abundance, translation rate, and TOR activity.**
701 **(A)** Top row, stage 12 buds of WT (left) and *drmy1* (right) viewed from the top. Arrowheads point
702 to sepals. Note that the *drmy1* bud has 5 sepals of unequal size and unevenly spaced, exposing
703 the stamens and carpels. Middle row, stage 12 buds of WT (left) and *drmy1* (right) viewed from
704 the side. Asterisk shows the gap between sepals with petals and carpels exposed. Bottom row,
705 stage 5 buds of WT (left) and *drmy1* (right) containing *35S::mCitrine-RCI2A* (plasma membrane
706 marker). Arrowheads point to sepal primordia. Note that the *drmy1* bud has 5 sepal primordia of
707 different sizes. Scale bars are 0.5 mm for stage 12 bud images and 25 µm for stage 5 bud images.
708 **(B-C)** Gene ontology (GO) enrichment of downregulated genes **(B)** and differentially accumulated
709 proteins **(C)** in *drmy1* compared to WT, in the *ap1 cal AP1-GR* background. Shown are the top 8
710 GO terms and their enrichment p-values. A complete list can be found in Supplemental Dataset
711 1. Arrowheads highlight terms related to ribosome biogenesis or translation.
712 **(D)** Ribosome profiles of WT (blue) and *drmy1* (red) in the *ap1 cal AP1-GR* background,
713 representative of 3 biological replicates each. Polysomal peaks are highlighted. All replicates can
714 be found in Supplemental Dataset 2.
715 **(E)** Puromycin labeling of WT vs *drmy1*. Left, puromycin labeling in WT and *drmy1* seedlings.
716 From left to right: WT pre-treated with CHX, two biological replicates of WT pre-treated with mock,
717 and two biological replicates of *drmy1* pre-treated with mock. All groups were then treated with
718 puromycin. For seedlings to match in size, WT seedlings were 8 days old and *drmy1* seedlings
719 were 10 days old. Right, puromycin labeling in WT and *drmy1* inflorescences of induced *ap1 cal*
720 *AP1-GR* background. From left to right: WT co-treated with puromycin and CHX, three biological
721 replicates of WT treated with puromycin, and three biological replicates of *drmy1* treated with
722 puromycin. In both experiments, RuBisCO large subunit on Ponceau S-stained membrane is
723 shown as a loading control (bottom).
724 **(F)** Coherent alteration of gene expression by *drmy1* and AZD-8055 TOR inhibitor treatment.
725 Shown here is a scatterplot of RNA log 2 fold change in *drmy1* vs WT (x-axis), and WT+AZD vs
726 WT+Mock (y-axis), in 7-day-old seedlings. Genes are color-coded based on the following
727 categories: genes in "Structural constituents of the ribosome" (GO:0003735) and its offspring
728 terms (magenta); all other genes in "Translation" (GO:0006412) and its offspring terms (orange);
729 all other genes (gray). Blue line shows a linear regression of all points ($R^2 = 0.1446$, $p < 2.2x10^{-}$
730 ^{16}). Note that the axes were trimmed to (-3,3) for ease of display.
731 **(G-H)** Phosphorylation of the direct TOR substrate, S6K-pT449, in WT and *drmy1*. Representative
732 images are shown in **(G)**. Top, Western blot against S6K-pT449. Middle, Western blot against
733 total S6K protein. Bottom, Ponceau S staining as a loading control. **(H)** Quantification of the
734 intensity of S6K-pT449 over Ponceau normalized by WT, in three experiments, shows that TOR
735 activity decreased by half in *drmy1*. (mean ± SD; *, $p<0.05$).
736

737 **Figure 2. Defects in TOR activity, ribosome integrity, and translation cause variable sepal**
738 **initiation.**
739 **(A-G)** Representative images of stage 5 buds in WT (A), *drmy1* (B), *ul4z* (C), *ul4y* (D), *ul18z* (E),
740 *lst8-1-1* (F), and *spaghetti-1* (G). Tissue morphology is visualized by either propidium iodide (a
741 cell wall-staining dye) or a plasma membrane marker. Arrowheads indicate sepal primordia that
742 are variable in number, position, and size. Note that *ul4z* flowers always develop four sepal
743 primordia, although of different sizes; *lst8-1-1* occasionally (4/41, 9.8%) develops buds with more
744 than four sepal primordia. Scale bars, 25 μm.
745 **(H)** Quantification of sepal primordium number, comparing *ul4z* (n = 52 buds), *ul4y* (n = 53 buds),
746 *ul18z* (n = 52 buds), *lst8-1-1* (n = 41 buds), and *spaghetti-1* (n = 84 buds) with WT (n = 51 buds).
747 Asterisks indicate statistically significant ($p < 0.05$) differences from WT in Fisher's contingency
748 table tests.
749 **(I)** Illustration of robust versus variable positioning of sepal primordia. Primordia are considered
750 robustly positioned if they are evenly distributed around the edge of the bud. Within each bud,
751 angles between adjacent primordia with respect to the center of the bud are measured, and
752 coefficient of variation (CV) is calculated. A bud with robustly positioned primordia would have
753 similar angular values and a low CV value. A bud with variably positioned primordia would have
754 very different angular values and a high CV value.
755 **(J)** Quantification of variability in primordium positioning (CV) in the same buds as in (H), following
756 illustration in (I). Asterisks indicate statistically significant ($p < 0.05$) differences from WT in
757 Wilcoxon's rank sum tests.
758 **(K)** Representative images of buds from *in vitro*-cultured WT inflorescences treated with mock or
759 2 μM CHX for 9 days (see Material and Methods). Arrowheads indicate sepal primordia that are
760 variable in number, position, and size. Scale bars, 25 μm.
761 **(L)** Representative images of buds from WT plants treated with mock or 2 nmol Torin2 for 15 days
762 (see Material and Methods). Arrowheads indicate sepal primordia that are variable in number,
763 position, and size. Scale bars, 25 μm.
764 **(M-N)** Quantification of variability in primordium number (M) and positional variability (N) similar
765 to (H,J), comparing CHX-treated (n = 31 buds), CHX-mock (n = 42 buds), Torin2-treated (n = 51
766 buds) and Torin2-mock buds (n = 56 buds).
767

768 **Figure 3. TOR and ribosomal defects cause variability in the timing of sepal initiation.**
769 **(A-C)** 6h-interval live imaging of the sepal initiation process in WT (A) and *ul4y* (B), which is
770 quantified in (C). n = 48 buds for WT; n = 40 buds for *ul4y*.
771 **(D-F)** 6h-interval live imaging of the sepal initiation process in buds from WT plants treated with
772 mock or 2 nmol Torin2 bi-daily for 15 days, which is quantified in (F). n = 31 buds for mock; n =
773 15 buds for Torin2.
774 In **(A,B,D,E)**, top rows show the *35S::mCitrine-RCI2A* membrane marker, and bottom rows show
775 Gaussian curvature heatmaps calculated from the same image stacks. Asterisks indicate sepal
776 initiation events, defined as a dark red band (primordium with positive curvature) separated from
777 the floral meristem by a dark blue band (boundary with negative curvature) in the Gaussian
778 curvature heatmap. Scale bars, 25 μm.
779 In **(C,F)**, the amount of time between outer and inner sepal initiation (left) and between outer and
780 lateral sepal initiation (right) were calculated for each bud, and summarized over all the buds.
781 Asterisks indicate statistically significant ($p < 0.05$) differences in the distribution of relative
782 initiation timing in Fisher's contingency table tests.
783

Figure 4. Defects in TOR activity, ribosome integrity, and translation cause variability in auxin and cytokinin signaling.

(A-D) The ribosomal mutant *ul4y* loses robustness in auxin and cytokinin signaling. (A) Representative images of late stage 2 buds of WT, *drmy1*, and *ul4y*, showing the auxin signaling reporter *DR5::3xVENUS-N7* in yellow, the cytokinin signaling reporter *TCS::GFP* in cyan, and both merged with Chlorophyll (in WT) or *UBQ10::mCherry-RCI2A* (in *drmy1* and *ul4y*) in magenta. (B) Quantification of TCS intensity (integrated density divided by area) from maximum intensity projection images, normalized to mean of WT. Shown are mean ± SD. Asterisks show statistically significant differences from WT in two-tailed Student's t-tests (*drmy1*, $p = 2.1 \times 10^{-6}$; *ul4y*, $p = 3.4 \times 10^{-5}$). (C) Circular histogram of DR5 distribution around the bud. Each bud was divided into 360 sectors of 1° each. Within each sector, DR5 signal measured in pixel intensity units (0-255 range) was summed. This sum was plotted along the x-axis starting from the sector at 1:30 position (between the incipient outer sepal and incipient lateral sepal on the right) going counterclockwise. I.e. in WT, the outer sepal is near 45°, the inner sepal near 225°, and the lateral sepals near 45° and 135° (vertical dotted lines). The mean was plotted as a solid line, and mean ± SD was plotted as a shaded area. (D) Circular histogram of TCS distribution around the bud. Sample size for (A-D): WT, n = 12 buds; *drmy1*, n = 15 buds; *ul4y*, n = 10 buds.

(E-H) 3 days of translation inhibition causes increased and diffuse cytokinin signaling, and diffuse auxin signaling. (E) Representative images of late stage 2 buds from dissected and cultured WT inflorescences treated with mock or 2 µM CHX for 3 days. Shown are *DR5::3xVENUS-N7* in yellow, *TCS::GFP* in cyan, and both merged with Chlorophyll in magenta. (F) Quantification of TCS intensity from maximum intensity projection images, normalized to mean of WT mock day 3. Shown are mean ± SD. Asterisk shows statistically significant difference in a two-tailed Student's t-test ($p = 2.0 \times 10^{-4}$). (G) Circular histogram of DR5 distribution around the bud. (H) Circular histogram of TCS distribution around the bud. Sample size for (E-H): WT mock day 3, n = 10 buds; WT CHX day 3, n = 12 buds.

(I-L) 6 days of TOR or translation inhibition causes increased and diffuse cytokinin signaling, and randomly positioned auxin signaling maxima. (I) Representative images of late stage 2 buds from dissected and cultured WT inflorescences treated with mock, 2 µM CHX, or 2 µM AZD for 6 days. Shown are *DR5::3xVENUS-N7* in yellow, *TCS::GFP* in cyan, and both merged with Chlorophyll in magenta. Arrowheads point to randomly positioned auxin maxima in buds of the CHX or AZD group. (J) Quantification of TCS intensity from maximum intensity projection images, normalized to mean of WT mock day 6. Shown are mean ± SD. Asterisks show statistically significant differences from mock in two-tailed Student's t-tests (CHX, $p = 1.0 \times 10^{-3}$; AZD, $p = 1.2 \times 10^{-4}$). (K) Circular histogram of DR5 distribution around the bud. (L) Circular histogram of TCS distribution around the bud. Sample size for (I-L): WT mock day 6, n = 12 buds; WT CHX day 6, n = 11 buds; WT AZD day 6, n = 10 buds. Scale bars in (A,E,I) represent 25 µm.

822 **Figure 5. Cytokinin signaling is required for variability in auxin signaling and sepal**
823 **initiation under translation inhibition.**
824 **(A-D)** Cytokinin treatment makes auxin signaling diffuse. Shown are late stage 2 WT buds under
825 mock (A,B) or 5 µM cytokinin (BAP) treatment (C,D) for 4 days. (A,C) Representative images of
826 the auxin signaling reporter *DR5::3xVENUS-N7* in yellow, and *DR5* merged with Chlorophyll in
827 magenta. (B,D) Circular histograms of the *DR5::3xVENUS-N7* signal, showing mean (solid line)
828 and mean ± SD (shaded area). Arrows point to DR5 signal in variable positions. Sample size: WT
829 Mock n = 10, WT BAP n = 10. Also see Zhu et al. (2020), Extended Data Figure 7e.
830 **(E-G)** Cytokinin signaling is required for variable sepal initiation in *drmy1*. (E) Representative
831 images of stage 5 buds in WT, *drmy1*, *arr1,10,12*, *drmy1 arr1,10,12*, *wol*, and *drmy1 wol*.
832 Arrowheads indicate initiated sepal primordia that are variable in number, position, and size. (F,G)
833 Quantification of sepal primordium number (F) and positional variability (G), comparing WT (n =
834 58) with *drmy1* (n = 31), *arr1,10,12* (n = 24) with *drmy1 arr1,10,12* (n = 20), and *wol* (n = 36) with
835 *drmy1 wol* (n = 39). Asterisks indicate statistically significant ($p < 0.05$) differences in Fisher's
836 contingency table tests (F) and Wilcoxon's rank sum tests (G) respectively. ns indicates no
837 significant difference.
838 **(H-K)** Cytokinin signaling is required for variable patterning of auxin signaling in *drmy1*. Shown
839 are late stage 2 buds of WT vs *drmy1* (H,I), and *arr1,10,12* vs *drmy1 arr1,10,12* (J,K). (H,J)
840 Representative images of the auxin signaling reporter *DR5::3xVENUS-N7* in yellow, and *DR5*
841 merged with propidium iodide in magenta. Arrows point to diffuse DR5 signal in variable positions
842 in the *drmy1* bud. Arrowheads show four robust DR5 maxima in *drmy1 arr1,10,12*. (I,K) Circular
843 histograms of the *DR5::3xVENUS-N7* signal, showing mean (solid line) and mean ± SD (shaded
844 area). For ease of visualization, circular histograms of *drmy1* and *drmy1 arr1,10,12* between 90
845 and 360 degrees are enlarged and shown as insets (y-axis range 0-0.4). Sample size: WT n =
846 19, *drmy1* n = 16, *arr1,10,12* n = 13, *drmy1 arr1,10,12* n = 9.
847 **(L-N)** Cytokinin signaling is required for variable sepal initiation under translation inhibition. (L)
848 Representative images of stage 6 buds in WT, *arr1,10,12*, and *wol*, treated with Mock or 2 µM
849 CHX for 10 days. Arrowheads indicate variable initiation of sepal primordia. (M,N) Quantification
850 of sepal primordium number (M) and positional variability (N), comparing Mock and CHX within
851 each genotype. Sample size: WT Mock n = 29, WT CHX n = 19, *arr1,10,12* Mock n = 18,
852 *arr1,10,12* CHX n = 19, *wol* Mock n = 15, *wol* CHX n = 19. Asterisks indicate statistically significant
853 ($p < 0.05$) differences in Fisher's contingency table tests (M) and Wilcoxon's rank sum tests (N)
854 respectively. ns indicates no significant difference.
855 **(O-R)** Cytokinin signaling is required for diffuse auxin signaling under translation inhibition. Shown
856 are late stage 2 buds of WT (O,P) and *arr1,10,12* (Q,R), treated with Mock or 2 µM CHX for 3
857 days. (O,Q) Representative images of the auxin signaling reporter *DR5::3xVENUS-N7* in yellow,
858 and *DR5* merged with Chlorophyll in magenta. Arrows point to diffuse DR5 signal in variable
859 positions in CHX-treated WT. Arrowheads show four robust DR5 maxima in CHX-treated
860 *arr1,10,12*. (P,R) Circular histograms of the *DR5::3xVENUS-N7* signal, showing mean (solid line)
861 and mean ± SD (shaded area). Sample size: WT Mock n = 17, WT CHX n = 18, *arr1,10,12* Mock
862 n = 7, *arr1,10,12* CHX n = 7. Scale bars in (A,C,E,H,J,L,O,Q) represent 25 µm.
863

Figure 6. Upregulation of cytokinin signaling is required to maintain translation and fitness in *drmy1*.

(A) Puromycin labeling of WT seedlings with 4 h CHX pre-treatment (control), and three biological replicates each of WT and *arr1 35S::ARR1* seedlings with 4 h mock pre-treatment. All seedlings are 14 days old. RuBisCO large subunit in Ponceau S-stained membrane is shown as a loading control. Also see Karunadasa et al. (2020).

(B,C) Puromycin labeling of WT seedlings with 4 h CHX pre-treatment (control), and two biological replicates of WT, *drmy1*, *wol*, and *drmy1 wol* seedlings with 4 h mock pre-treatment. Seedlings are 8 days old in (B) and 14 days old in (C). RuBisCO large subunit in Ponceau S-stained membrane is shown as a loading control.

(D) Representative 14 days old seedling images of WT, *drmy1*, *wol*, and *drmy1 wol* used in (C). Notice that *drmy1 wol* is very small and pale. Scale bars, 5 mm.

(E) Representative aerial part images of 42 days old plants of WT, *drmy1*, *wol*, and *drmy1 wol*. Inset shows enlarged *drmy1 wol* plant; notice that it has a tiny rosette and inflorescence. Scale bars, 5 cm. See also Supplemental Figure 6F.

(F) Representative aerial part images of 74 days old plants of WT, *drmy1*, *arr1*,*10*,*12*, and *drmy1 arr1*,*10*,*12*. Inset shows enlarged *drmy1 arr1*,*10*,*12* plant; notice its pale leaves accumulating anthocyanin, and short inflorescence. Scale bars, 5 cm. See also Supplemental Figure 6E.

(G) Dissected siliques of *arr1,10,12* (left) and *drmy1 arr1,10,12* (right) showing developing seeds. Notice that while *arr1,10,12* occasionally have aborted seeds, all seeds in the *drmy1 arr1,10,12* silique were aborted. Scale bars, 0.2 mm.

886 **Figure 7. A-type ARR protein levels are sensitive to TOR and translation inhibition.**
887 **(A)** The hypothesis. A-type ARRs are rapidly synthesized and degraded to dampen cytokinin
888 signaling. Translation inhibition causes inability to rapidly synthesize these proteins in response
889 to cytokinin signaling, resulting in an upregulation of cytokinin signaling.
890 **(B)** Expression of A-type ARR genes in WT vs *drmy1* inflorescences (*ap1 cal AP1-GR*) measured
891 in RNA-seq. Shown are the five A-type ARR genes with the highest expression, ranked by mean
892 expression level in WT. Asterisk indicates statistically significant difference, while ns means no
893 significant difference. P-values: ARR7, p = 0.807; ARR4, p = 0.611; ARR15, p = 0.532; ARR8, p
894 = 0.0115; ARR9, p = 0.0416.
895 **(C)** A GFP-channel image of a stage 2 bud of GFP-nes (*pUBQ10::sfGFP-nes-UBQ3ter*). For this
896 panel and (E-H), each image was brightened to reveal GFP distribution patterns. A square region
897 taken from the image containing 5-10 cells is enlarged and shown on the top right. Within the
898 enlargement, GFP intensity was quantified along the dotted line and plotted on the bottom right.
899 X-axis, pixels (range 0-238). Y-axis, GFP intensity in gray value (smoothened by taking the
900 average intensity of 11-pixel neighborhoods; range 90-210). Scale bars, 25 μm.
901 **(D)** Illustration of the Llama Tag system used in this study. Plants were co-transformed with *ARR7-*
902 *llama* (*pARR7::ARR7-linker-llama-ARR7ter*) and *GFP-nes* (*pUBQ10::sfGFP-nes-UBQ3ter*).
903 Without ARR7-llama, the GFP is localized in the cytosol. ARR7-llama is produced in the cytosol
904 and translocates into the nucleus. When this happens, the Llama Tag capable of binding GFP
905 drags GFP into the nucleus (note that from our observation it is excluded from the nucleolus).
906 Therefore, at low ARR7-llama levels, GFP signal is mainly seen in the cytosol. At intermediate
907 ARR7-llama levels, GFP is at comparable intensities between the cytosol and the nucleus, and
908 no clear pattern can be seen. At high ARR7-llama levels, GFP is mainly seen in the nucleus.
909 **(E,F)** GFP channel images of stage 2 buds from two independent transgenic lines of *ARR7-llama*
910 *GFP-nes*, 7-4 (E) and 7-6 (F), in WT (top) vs *drmy1* (bottom). Images are representative of n =
911 17 (line 7-4, WT), n = 40 (line 7-4, *drmy1*), n = 9 (line 7-6, WT), and n = 6 (line 7-6, *drmy1*) buds.
912 **(G)** GFP channel images of WT *ARR7-llama GFP-nes* buds treated with mock (top) or 2 μM CHX
913 (bottom) for 24 hours. The mock image is representative of n = 20 buds (12 from line 7-4, 5 from
914 line 7-6, and 3 from line 7-12). The CHX image is representative of n = 19 buds (11 from line 7-
915 4, 5 from line 7-6, and 3 from line 7-12).
916 **(H)** GFP channel images of WT *ARR7-llama GFP-nes* buds treated with mock (top) or 2 μM AZD-
917 8055 (bottom) for 72 hours. The mock image is representative of n = 13 buds (8 from line 7-4 and
918 5 from line 7-6). The AZD-8055 image is representative of n = 11 buds (8 from line 7-4 and 3 from
919 line 7-6).
920 **(I-N)** *ARR7-llama* partially restores robustness in *drmy1* sepal primordia. (I-L) Representative
921 stage 5 or 6 buds from WT (I), WT with the *ARR7-llama* and *GFP-nes* constructs (J), *drmy1* (K),
922 and *drmy1* with these constructs (L). (M) Quantification of sepal primordium number. ns indicates
923 no significance difference in a Fisher's exact test (WT vs *ARR7-llama*, p = 1; *drmy1* vs *drmy1*
924 *ARR7-llama*, p = 0.44). (N) Quantification of variability in sepal primordium position. Asterisk
925 indicates statistically significant difference ($p = 5.7 \times 10^{-6}$), while ns indicates no statistically
926 significant difference (p = 0.91). Data for WT and *drmy1* were reused from Figure 2H, 2J. Data
927 for *ARR7-llama GFP-nes* and *drmy1 ARR7-llama GFP-nes* were pooled from line 7-4 and 7-6.

928 Sample size: WT n = 51, *ARR7-llama GFP-nes* n = 16, *drmy1* n = 67, *drmy1 ARR7-llama GFP-*
929 *nes* n = 20. Scale bars, 25 µm.
930 **(O)** Working model. In WT, DRMY1 maintains TOR activity and translation, which sustains the
931 rapid translation of A-type ARRs in response to cytokinin signaling. This suppresses excessive
932 cytokinin signaling, allowing auxin and cytokinin signaling to interact and form robust spatial
933 patterns. Robust patterning of auxin and cytokinin signaling gives rise to robustly numbered,
934 positioned, and sized sepal primordia. In *drmy1*, A-type ARR protein levels are reduced due to
935 insufficient TOR activity, ribosome content, and translation rate. Cytokinin signaling is
936 upregulated, which rescues the translation rate reduction in a homeostatic mechanism. This
937 upregulation of cytokinin signaling disrupts the robust spatial pattern of both cytokinin and auxin
938 signaling, which in turn causes variable sepal initiation.
939

940 **MATERIALS AND METHODS**

941

942 **Plant material**

943 Most Arabidopsis plants were in Col-0 background (WT). *ap1 cal 35S::AP1-GR* was in Ler
944 background. *drmy1* (Col-0) was backcrossed to Ler twice and then crossed with *ap1 cal*
945 *35S::AP1-GR* to obtain *drmy1 ap1 cal 35S::AP1-GR*. R2D2 was originally in Col-Utrecht
946 background and was backcrossed twice into WT (Col-0) and *drmy1* (Col-0). The following mutants
947 and reporters were previously described: *drmy1-2*[26], *wol-1*[127], *spaghetti-1* (*tpr5-1*)[128], *ap1 cal*
948 *35S::AP1-GR* (Ler)[35,36], *arr1-1 35S::ARR1*[67], *DR5::3xVENUS-N7*[129], *TCS::GFP*[130], *pARF5::ER-*
949 *EYFP-HDEL*[131], *pUS7Y-mDII-NtdTomato-pUS7Y-DII-N3xVENUS* (R2D2)[97], *35S::mCirtine-*
950 *RCI2A*[26], *UBQ10::mCherry-RCI2A*[26]. The following mutants and reporter lines were obtained from
951 Arabidopsis Biological Resource Center (ABRC): *ul4z* (SALK_130595), *ul4y* (SALK_029203),
952 *ul18z* (SALK_089798), *arr1-3 arr10-5 arr12-1*[132] (CS39992), *lst8-1-1* (SALK_002459),
953 *pARF3::N3xGFP*[133] (CS67072), *pARF6::N3xGFP*[133] (CS67078), *pARF8::N3xGFP*[133] (CS67082),
954 *pARF10::N3xGFP*[133] (CS67086).

955

956 **Llama-tagged ARR7 construct**

957 For the LlamaTag system, we first generated plasmid *pVV13* containing linker-llama. We
958 amplified the LlamaTag (from a plasmid containing vhhGFP4[134]) and added a linker sequence of
959 tccggagcagctgcggctgccgctgcggcagcggccactagt at its 5' end by two rounds of overlap PCRs.
960 Primers for the first round were oVV64 and oVV53, and primers for the second round were oVV35
961 and oVV53. After the second round, we A-tailed the PCR product according to the Promega
962 manufacturer's protocol. A-tailed product was ligated to the pGEMTeasy vector according to the
963 Promega ligation protocol, to create the plasmid *pVV13*.

964 To make *pARR7::ARR7-llama*, a genomic fragment of *pARR7::ARR7* minus the stop
965 codon and terminator was amplified from the Arabidopsis (Col-0) genome using the primers
966 oSK197 and oSK198. The linker-llama fragment was PCR-amplified from *pVV13* using the
967 primers oSK199 and oSK200. The *ARR7* stop codon, 3' UTR, and terminator was amplified from
968 the Arabidopsis (Col-0) genome using the primers oSK201 and oSK202. *pMLBART* backbone
969 was digested with NotI, and all fragments were assembled into *pMLBART* using NEBuilder
970 according to the manufacturer's protocol.

971 To make *pUBQ10::sfGFP-NES:UBQ3ter*, sfGFP sequence was amplified from the *35S-*
972 *sfGFP-nosT* plasmid[135] (Addgene # 80129) using primers UsfGM-F1 and UsfGnes-R1. The
973 UBQ10 promoter was amplified from the *UPG* plasmid[136] (Addgene # 161003) using primers
974 OutALFd and UsfGM-R1. The UBQ3 terminator was amplified from the *UPG* plasmid[136] (Addgene
975 # 161003) using primers UsfGnes-F1 and OutALRb. Primer overhangs spanning the junction
976 between sfGFP and the UBQ3 terminator contain the sequence of the mouse PKIα NES.
977 *pCambia1300* backbone was digested with BamHI and KpnI, and all fragments were Gibson-
978 assembled into the backbone. Sequences of primers, *pARR7::ARR7-llama*, and *pUBQ10::sfGFP-*
979 *NES:UBQ3ter* can be found in Supplemental Dataset 5.

980 Col-0 plants were co-transformed with *pARR7::ARR7-llama* and *pUBQ10::sfGFP-*
981 *NES:UBQ3ter*, and selected with Basta (for *pARR7::ARR7-llama*) + Hygromycin (for

982 *pUBQ10::sfGFP-NES:UBQ3ter*). Surviving T1 plants were screened for clear nuclear signal in the
983 inflorescence, and 5 independent T1 plants were selected and crossed into *drmy1*. F2 plants from
984 each line were again selected with Basta + Hygromycin and genotyped. One line showed co-
985 segregation with the *DRMY1* locus. Two lines showed severe silencing in the F2 and could not
986 be used. Two lines (7-4 and 7-6), though with minor silencing in F2, were used for imaging and
987 image analysis. F3 plants of 7-4 and 7-6 had severe silencing, and therefore only F2 were imaged.
988
989 **Plant growth conditions**
990 For most experiments, seeds were sown in wetted Lamber Mix LM-111 soil and stratified
991 at 4°C for 3-5 days. For experiments including *drmy1 wol* and *drmy1 arr1,10,12*, all seeds were
992 sown onto ½ MS plates with 0.05% (w/v) MES, 1% (w/v) sucrose, 1.2% (w/v) agar, pH 5.7, and
993 stratified at 4°C for a week. They were grown for 7-10 days before being transplanted to soil (for
994 imaging of inflorescence or aerial part of the plant) or left on the plates until desired time of the
995 experiment (for seedling imaging or puromycin labeling).
996 Most plants were grown under 16 h – 8 h light-dark cycles (fluorescent light, ~100 μmol
997 m^{-1} s^{-1}) at 22°C in a Percival walk-in growth chamber. We found that the *drmy1* phenotype is more
998 pronounced in this condition than under continuous light. The *ap1 cal 35S::AP1-GR* and *drmy1*
999 *ap1 cal 35S::AP1-GR* plants were grown in soil under continuous light at 16°C to prevent
1000 premature floral induction.
1001
1002 **Flower staging**
1003 Flower buds were staged as previously described[37]. Briefly, stage 1 is when the floral
1004 meristem emerges, but not yet separated, from the inflorescence meristem. Stage 2 is when the
1005 floral meristem separates from the inflorescence meristem but with no floral organs initiated.
1006 Stage 3 is when sepal primordia initiate. Stage 4 is when sepal primordia bend to cover part of
1007 the floral meristem. Stage 5 is when stamen primordia initiate. Stage 6 is when sepal primordia
1008 completely cover the floral meristem.
1009
1010 **RNA-seq data collection and analysis**
1011 For RNA-seq in the inflorescence, bolting *ap1 cal 35S::AP1-GR* and *drmy1 ap1 cal*
1012 *35S::AP1-GR* plants were induced daily with an aqueous solution containing 10 μM
1013 dexamethasone (Sigma-Aldrich), 0.01% (v/v) ethanol, and 0.015% (v/v) Silwet L-77
1014 (Rosecare.com). When sepals initiated from the floral meristems, usually on the fourth day after
1015 three daily inductions, three inflorescence samples per genotype (including inflorescence
1016 meristems and buds under stage 6) were collected and immediately put into liquid nitrogen. RNA
1017 extraction, library preparation, RNA-seq, and data analysis for inflorescence samples were done
1018 as previously described[26] with a few changes. After read mapping, genes with at least two raw
1019 reads in at least two biological replicates in either WT or *drmy1* were kept for downstream
1020 analysis. For differentially expressed genes, we set a log2 fold change threshold of ±1 and a BH-
1021 adjusted p-value threshold of 0.05. For GO term enrichment, gene-GO mapping data was
1022 obtained from TAIR (https://www.arabidopsis.org
1023 /download_files/GO_and_PO_Annotations/Gene_Ontology_Annotations/ATH_GO_GOSLIM.txt)

1024 . The R package "topGO"[137] (version 2.38.1) was used for the enrichment, with statistic "fisher",
1025 algorithm "weight01", annotation function "annFUN.gene2GO", and minimum node size 10. The
1026 results were ranked by their p-value, and the first 8 terms were plotted.
1027 For RNA-seq in seedlings, WT and *drmy1* seedlings were grown to quiescence (7 days)
1028 in ½ MS liquid media as previously described[34]. After 7 days, the media was replaced with ½ MS
1029 liquid media containing 15 mM glucose and incubated for 24 hours to activate TOR. Seedlings
1030 were then incubated with or without AZD-8055 in addition to 15 mM glucose in ½ MS liquid media
1031 for 2 hours before collecting tissue. RNA was extracted from 100 mg pooled seedlings using the
1032 Spectrum Plant Total RNA Kit (Sigma). This RNA was used as a template for RNA-Seq library
1033 synthesis and sequencing, which was performed by Novogene. RNA-seq data for AZD-8055
1034 treated WT and *drmy1* seedlings were preprocessed with fastp (v. 0.22.0) using default
1035 parameters. Preprocessed reads were then mapped to the TAIR10 reference genome using
1036 STAR (v. 2.7.10z_alpha_220314). Following alignment, BAM output files from STAR were used
1037 to generate feature counts for transcripts using subread-featureCounts (v. 2.0.3) and the
1038 Araport11 transcriptome. TPMs were generated using TPMCalculator (v. 0.0.3). Differential
1039 expression analysis was performed using feature count data and DESeq2 (v. 1.36.0).
1040 A list of genes with uORFs based on gene models of the TAIR10 Arabidopsis genome
1041 assembly were downloaded from von Arnim et al.[62]. For each gene, within each genotype, protein-
1042 transcript ratio was calculated as the ratio between mean protein abundance and mean transcript
1043 TPM across all bio-reps in our proteomics and RNA-seq datasets, respectively. This was log2-
1044 transformed, and the difference between *drmy1* and WT was calculated. This was used as an
1045 indicator of translation rate difference between *drmy1* and WT, although we acknowledge that
1046 other factors such as protein stability may affect this number. This was plotted against the number
1047 of uORFs in each gene model (0, 1, or ≥ 2).
1048
1049 **Proteomics**
1050 Five induced inflorescence samples of WT and *drmy1* in *ap1 cal AP1-GR* background
1051 were collected as described above. Samples were ground in liquid nitrogen. Total soluble proteins
1052 were extracted in ice-cold extraction buffer (50 mM PBS-HCl (pH 8.0) buffer with 150 mM NaCl,
1053 2% NP-40, 1 mM PMSF, 1x Roche cOmplete protease inhibitor cocktail (Sigma 11697498001),
1054 and 1x Halt TM Phosphatase inhibitor cocktail (ThermoFisher 78420)) and filtered through
1055 Pierce™ Micro-Spin Columns (30 µm pore size; Thermo Scientific 89879). Extracts were
1056 RuBisCO-depleted using Seppro Bubisco Kit (Sigma SEP070-1KT), concentrated, denatured,
1057 reduced, cysteine blocked, trypsin-digested, and TMT 10-plex labeled. Then, mass spectrometry
1058 was done using an UltiMate 3000 RSLCnano / Orbitrap Fusion system (Thermo Scientific). Raw
1059 data was searched against the NCBI protein database using PD 2.3 (Thermo Scientific) with
1060 Sequest HT searching engine. Precursor-based protein identification and relative quantification
1061 was done using the standard processing workflow in PD 2.3, with an additional node of Minora
1062 Feature Detector. Proteins with at least 2 supporting peptides were kept for downstream analysis.
1063 For each protein, data was fit with an ANOVA model and a p-value was calculated. Proteins with
1064 a p-value < 0.05 were considered differentially accumulated in *drmy1*. GO term enrichment was
1065 done as above, using genes corresponding to the differentially accumulated proteins.

1066
1067 **Polysome extraction and profiling**
1068 Three induced inflorescence samples of WT and *drmy1* in *ap1 cal AP1-GR* background
1069 were collected as described above, and polysomes were extracted as previously described[138].
1070 Briefly, samples were ground in liquid nitrogen, mixed with an extraction buffer (0.2 M Tris pH 9.0,
1071 0.2 M KCl, 0.025 M EGTA, 0.035 M $MgCl_2$, 1% (w/v) Brij-35, 1% (v/v) Triton X-100, 1% (v/v) Igepal
1072 CA-630, 1% (v/v) Tween-20, 1% (w/v) Sodium deoxycholate, 1% (v/v) Polyoxyethylene 10 tridecyl
1073 ether, 5 mM Dithiothreitol, 1 mM Phenylmethylsulfonyl fluoride, 100 µg/ml cycloheximide, 100
1074 µg/ml chloramphenicol, 40 U/ml RNasin, 0.5 mg/ml Heparin), and let sit on ice for 10 min. Samples
1075 were centrifuged at 4°C 4,000 g for 5 min, supernatant was transferred to a new tube, centrifuged
1076 at 4°C 16,000 g for 15 min, and supernatant was filtered through Miracloth.
1077 Polysome extracts were profiled as previously described[139]. Briefly, samples were loaded
1078 onto 15%-45% sucrose density gradients and centrifuged at 4°C 38,000 rpm in a SW41 rotor.
1079 Separated samples were fractionated at a rate of 0.375 mL/min in an Isco fractionation system,
1080 and absorbance at 254 nm was recorded.
1081
1082 **Puromycin labeling**
1083 Puromycin labeling was done as previously described[39], with slight modifications.
1084 In seedlings, when comparing WT and *drmy1*, in order to control for plant size, WT
1085 seedlings were grown for 8 days and *drmy1* seedlings were grown for 10 days (Figure 1E). When
1086 comparing WT, *drmy1*, *wol*, and *drmy1 wol*, we were unable to control for plant size because
1087 *drmy1 wol* seedlings were too small. We therefore controlled for plant age, and seedlings were
1088 grown to specified age (8 days for Figure 6B and 14 days for Figure 6C). Seedlings were
1089 harvested from plates and incubated with an incubation buffer (½ MS, 0.05% (w/v) MES, 1% (w/v)
1090 sucrose, 0.1% (v/v) Tween-20, 0.1% (v/v) DMSO, 1x Gamborg vitamin mix, pH 5.7), with or
1091 without 50 µM CHX, for 4 hours in an illuminated growth chamber. Then, the buffer was replaced
1092 with a fresh incubation buffer (which is same as above, but contains 50 µM puromycin (GoldBio
1093 P-600-100)), and incubation continued for another 45 min.
1094 In inflorescences of WT and *drmy1* in *ap1 cal AP1-GR* background, inflorescences were
1095 DEX-induced as described above. Inflorescence samples were collected and put in an incubation
1096 buffer (½ MS, 1% (w/v) sucrose, 0.02% (v/v) Silwet L-77, 0.1% (v/v) DMSO, 50 µM puromycin,
1097 1x Gamborg vitamin mix, pH 5.7), with or without 100 µM CHX. Samples were vacuum infiltrated
1098 for 15 minutes and then put on a rocking shaker in an illuminated growth chamber for 45 minutes.
1099 In both cases, at the end of the incubation, samples were washed three times with water,
1100 blot dry, weighed, and frozen in liquid nitrogen. Soluble proteins were extracted as described
1101 above. Puromycin incorporated into the proteins were detected in a Western blot using a mouse-
1102 origin anti-puromycin monoclonal antibody (12D10, Sigma MABE343, lot # 3484967) and a goat-
1103 anti-mouse HRP-conjugated secondary antibody (Abcam ab6789, lot # 3436981). RuBisCO large
1104 subunit in Ponceau S-stained membrane was used as a loading control.
1105
1106 **TOR activity assay**

1107 WT and *drmy1* seedlings were grown in a six-well plate containing ½ MS liquid media.
1108 After seven days, the media were replaced with half-strength MS liquid media plus 15 mM glucose
1109 and incubated for 24 hours. At least 120 quiescent seedlings per sample were collected and
1110 frozen in liquid nitrogen. Protein was then extracted from the plant tissue in 100 mM MOPS (pH
1111 7.6), 100 mM NaCl, 5% SDS, 0.5% b-mercaptoethanol, 10% glycerin, 2 mM PMSF, and 1x
1112 PhosSTOP phosphatase inhibitor (Sigma). S6K-pT449 was detected by Western blot using a
1113 phosphospecific antibody (Abcam ab207399) and an HRP-conjugated goat anti-rabbit IgG
1114 secondary antibody (Jackson Immuno Research 111-035-003). Total S6K was detected using a
1115 custom monoclonal antibody described by Busche et al.[140]. Total protein visualized in Ponceau
1116 S-stained membrane was used as a loading control.
1117
1118 **Confocal microscopy**
1119 Confocal imaging of reporter lines in the inflorescence were done as previously
1120 described[26]. Briefly, main inflorescences (not side branches) were cut and dissected with a
1121 Dumont tweezer (Electron Microscopy Sciences, style 5, no. 72701-D) to remove buds older than
1122 stage 9 or 10. The inflorescences were then inserted upright into a small petri dish (VWR, 60 x
1123 15 mm) containing inflorescence culture medium (1/2 MS, 1% (w/v) sucrose, 1x Gamborg vitamin
1124 mixture, 0.1% (v/v) plant preservative mixture (Plant Cell Technology) 1% (w/v) agarose, pH 5.8),
1125 leaving most of the stem inside the medium and the buds outside. They were then further
1126 dissected to reveal stage 6 and younger buds, immersed with water, and imaged under a
1127 Zeiss710 upright confocal microscope with a 20x Plan-Apochromat water-dipping lens (1.0 NA).
1128 For live imaging experiments, inflorescence samples were put in a continuous-light growth
1129 chamber between time points. To prevent bacterial growth, samples were transferred onto fresh
1130 media every 2 to 3 days, and for live imaging experiments lasting longer than 6 days, once in the
1131 middle, plants were incubated with an aqueous solution of 100 µg/ml Carbenicillin (GoldBio, C-
1132 103-5, lot # 0129.091814A) for 30 minutes.
1133 To visualize tissue morphology of inflorescence samples without a reporter, samples were
1134 stained for 5 minutes with an aqueous solution of 0.1 mg/ml propidium iodide (PI) and 0.1% (v/v)
1135 Tween-20, washed three times with water, and imaged.
1136 The following laser and wavelength were used in confocal imaging. Chlorophyll, excitation
1137 488 nm, emission 647-721 nm. PI, excitation 514 nm, emission 566-659 nm. mCherry, excitation
1138 594 nm, emission 600-659 nm. tdTomato, excitation 561 nm, emission 566-595 nm. For
1139 EYFP/VENUS/mCitrine, in *35S::mCirtine-RCI2A*, excitation 514 nm, emission 519-580 nm; in
1140 *DR5::3xVENUS-N7*, excitation 514 nm, emission 519-569 nm; in *pARF5::ER-EYFP-HDEL*,
1141 excitation 514 nm, emission 519-550 nm; in *R2D2*, excitation 488 nm, emission 493-551 nm. For
1142 GFP/sfGFP, in *pARR7::ARR7-llama UBQ10::sfGFP-NES*, excitation 488 nm, emission 493-569
1143 nm; in *pARF3::N3xGFP*, *pARF6::*N3xGFP, *pARF8::N3xGFP*, and *pARF10::N3xGFP*, excitation
1144 488 nm, emission 493-564 nm; in *TCS::GFP*, excitation 488 nm, emission 493-513 nm.
1145
1146 **Visualization of tissue morphology**
1147 For single-channel image stacks intended for the visualization of tissue morphology
1148 (*35S::mCitrine-RCI2A* or PI), stacks were 3D-rendered using the ZEN confocal software

1149 (Processing -> 3D). Parameters were set to best visualize tissue morphology, typically, minimum
1150 5-10, ramp 60-80, maximum 100. Buds were rotated to desired orientation, and screenshots were
1151 taken using the "Create Image" button. For fluorophores that are dimmer, less sharp, or have a
1152 noisy background (*UBQ10::mCherry-RCI2A* or Chlorophyll), stacks were converted from LSM to
1153 TIF using ImageJ[141,142], loaded into MorphoGraphX[143], and screenshots were taken using the
1154 built-in screenshot function in MorphoGraphX.
1155 To aid visualizing tissue morphology and determine the timing of sepal initiation, each
1156 stack was fitted with a surface, and a Gaussian curvature heatmap was calculated from the
1157 surface (see below). We consider a sepal primordium as initiated when we see a dark red band
1158 of positive Gaussian curvature (primordium) separated from the center of the floral meristem by
1159 a dark blue band of negative Gaussian curvature (boundary)[26].
1160 Gaussian curvature heatmaps were calculated as previously described[26], with slight
1161 modifications. Briefly, stacks underwent the following processes in MorphoGraphX: Gaussian blur
1162 (3 times; X/Y/Z sigma = 1 μm for the first 2 times, and 2 μm for the third time), edge detection
1163 (threshold = 2000-8000 depending on the brightness of the stack, multiplier = 2.0, adapt factor =
1164 0.3, fill value = 30000), marching cube surface (cube size = 8 μm, threshold = 20000), subdivide
1165 mesh, smooth mesh (passes = 5), subdivide mesh, smooth mesh (passes = 5), project mesh
1166 curvature (type = Gaussian, neighborhood = 10 μm, autoscale = no, min curv = -0.0015, max curv
1167 = 0.0015). For ease of visualization, the lookup table "jet" was applied to the mesh.
1168
1169 **Quantification of sepal initiation robustness**
1170 For sepal primordium number, screenshots were taken of stage 3-6 buds of indicated
1171 genotypes, in either ZEN or MorphoGraphX. The number of sepal primordia initiated were
1172 counted from these screenshots.
1173 For variability in sepal primordium positioning, within each bud, an angular distance was
1174 measured between each pair of adjacent sepal primordia (with vertex at the center of the bud),
1175 using ImageJ. Note that the last pair was not measured – the angular distance was calculated as
1176 the sum of all other angular distances subtracted from 360°. A CV value (standard deviation
1177 divided by mean) was calculated from all the measured or calculated angular distances. Buds
1178 with sepal primordia evenly distributed around the bud periphery should have a small CV value,
1179 i.e. all angles are around 90° for four-sepal buds (or 72° for five-sepal buds, etc.). Buds whose
1180 sepal primordia distributed variably or randomly around the bud periphery will have widely varying
1181 angular distances between adjacent sepal primordia, and thus large CV values.
1182 Relative sepal initiation timing was quantified as previously described[26]. Briefly, dissected
1183 inflorescence samples were live-imaged every 6 hours. A Gaussian curvature heatmap was
1184 generated for each sample at each time point and was used to determine the time point at which
1185 a sepal primordium initiates. A sepal primordium is considered initiated at time point Tn if it is
1186 absent at time point T(n-1) but becomes present at time point Tn. Within the same bud, we
1187 counted the number of time points between outer and inner sepal initiation, and between outer
1188 and lateral sepal initiation, and multiplied them by 6 hours to get the relative initiation timing of
1189 these sepals.
1190

1191 **Quantification of fluorescent reporters**

1192 For *TCS::GFP*, *pARF3::N3xGFP*, *pARF5::ER-YFP-HDEL*, *pARF6::N3xGFP*,
1193 *pARF8::N3xGFP*, *pARF10::N3xGFP*, *pUS7Y::mDII-NtdTomato, pUS7Y::DII-N3xVENUS*, and
1194 *UBQ10::mCherry-RCI2A*, total signal (integrated density) was quantified from maximum intensity
1195 projection images using ImageJ[141,142]. Fluorescence intensity was measured in pixel intensity
1196 units (0-255 range). Signal intensity was calculated as total signal divided by area.

1197 For both *TCS::GFP* and *DR5:3xVENUS-N7*, circular histogram analysis was done as
1198 previously described[26]. Briefly, individual buds were cropped out of image stacks, channels were
1199 split using FIJI and saved in TIF format, and TIF stacks were imported into MorphoGraphX. Signal
1200 from outside the buds (e.g. inflorescence meristem, parts of other buds within the same image)
1201 was manually removed using the Voxel Edit function. Buds were positioned so that the incipient
1202 sepal primordia are in the XY plane: the incipient outer sepal is at 45°, the incipient inner sepal
1203 and the inflorescence meristem are at 225°, and the incipient lateral sepals are at 135° and 315°,
1204 respectively. Fluorescence intensity was measured in pixel intensity units (0-255 range). A circular
1205 histogram of bin width 1° centered around the Z axis was exported for each replicate expressing
1206 DR5 and/or TCS. Multiple circular histograms of the same reporter and genotype were pooled
1207 and mean ± SD were plotted.

1208 For GFP signal in plants carrying *pUBQ10::sfGFP-nes-UBQ3ter* and *pARR7::ARR7-*
1209 *linker-llama-ARR7ter* reporters, screenshots were taken in MorphoGraphX as described above.
1210 Screenshots were subtracted of a background determined using blank regions with no tissue, and
1211 brightened to the same level to reveal differences in GFP distribution patterns. A square region
1212 containing 5-10 cells were taken from each screenshot, and GFP intensity (in gray value ranging
1213 from 0 to 255) along a straight line of 239 pixels in length was quantified using ImageJ[141,142]
1214 (Analyze -> Plot profile). For ease of visualization, the curves were smoothed by taking the
1215 average of the gray value of 11 neighboring pixels (including itself) as the value of each pixel.

1216

1217 ***In vitro* drug treatments on inflorescence samples**

1218 For cycloheximide (CHX) treatment, a stock solution of 10 mM CHX was made from
1219 powder (Sigma C1988) in pH 4.0 water. The stock solution was filter-sterilized and stored in -
1220 20°C and replaced every six months to prevent degradation. The stock solution was added to an
1221 autoclaved and cooled (but not solidified) inflorescence culture medium (see above) to a final
1222 concentration of 2 μM. The medium was not pH-buffered. The medium was made at the beginning
1223 of each experiment and was stored at 4°C. After each imaging session (at day 3 and day 6), new
1224 medium was taken out of 4°C, warmed to room temperature, and inflorescence samples were
1225 transferred onto the new medium.

1226 For AZD-8055 treatment, a stock solution of 16 mM AZD-8055 was prepared from powder
1227 (Cayman Chemical 16978) in DMSO within days of use, and stored in -80°C. The stock was serial-
1228 diluted with water to 2 mM, and added to autoclaved and cooled (but not solidified) inflorescence
1229 culture medium (see above) to a final concentration of 2 μM. For the mock medium, DMSO was
1230 added to the inflorescence culture medium to a final concentration of 0.0125% (v/v).

1231 For 6-benzylaminopurine (BAP) treatment, a stock solution of 50 mM BAP was prepared
1232 from powder (Alfa Aesar A14678) in DMSO, and stored in -80°C. The stock was added to an

1233 autoclaved and cooled (but not solidified) inflorescence culture medium (see above) to a final
1234 concentration of 5 μM. For the mock medium, DMSO was added to the inflorescence culture
1235 medium to a final concentration of 0.01% (v/v).
1236 Inflorescences were dissected and inserted into regular inflorescence culture medium
1237 without drugs, and pre-treatment image stacks were captured. Then, they were transferred into
1238 specified treatment or mock media, and imaged at the specified time points.
1239
1240 ***In vivo* Torin2 treatment**
1241 Starting at 14 days after germination, twice each day for 15 days, 2 nmol of Torin2
1242 (Cayman Chemical 14185) in 20 μl of aqueous solution containing 0.5% DMSO and 0.5% Tween-
1243 20 was applied to the center of the rosette using a pipette. For mock, 20 μl aqueous solution
1244 containing 0.5% DMSO and 0.5% Tween-20 was applied. At the end of the 15-day treatment
1245 period, inflorescences were dissected and put in the inflorescence culture medium for imaging.
1246 To prevent Torin2 degradation, throughout the duration of this experiment, the Torin2
1247 stock solution in DMSO was kept in -80°C and replaced each week, and the treatment and mock
1248 solutions were kept in 4°C and replaced each day.
1249
1250 **Imaging of whole plant, whole inflorescence, silique, and mature sepals**
1251 For whole-plant imaging, aerial parts of the plants were removed from the pots, flattened,
1252 put on a dark cloth, and imaged with a cell phone (iPhone 12, iOS 16.2).
1253 For whole-inflorescence imaging, inflorescences consisting of open flowers and unopened
1254 buds were removed from the plant and held with forceps. Images were taken under a Zeiss Stemi
1255 2000-C Stereo Microscope with a cell phone (iPhone 12, iOS 16.2).
1256 For silique imaging, siliques on inflorescences sufficiently distant from the shoot apex that
1257 were developed and started to ripen were picked with forceps, opened with a razor blade, and
1258 imaged under a Zeiss Stemi 2000-C Stereo Microscope with a cell phone (iPhone 12, iOS 16.2).
1259 Mature sepal imaging was done as previously described[26,27]. Briefly, mature sepals from
1260 stage 15 flowers (10th to 25th flower on the inflorescence) were dissected and sandwiched
1261 between two slides to flatten. Images were taken using a Canon Powershot A640 camera
1262 attached to a Zeiss Stemi 2000-C Stereo Microscope. Minor damages were manually fixed, and
1263 undesired objects such as pollen grains were manually removed from these images. Sepals with
1264 major damages were discarded. Then, a contour was extracted from each sepal using custom
1265 python scripts[27]. This gave us measurements such as length, width, area, etc. of each sepal. To
1266 measure between-flower variability of length, within each genotype and for each of outer, inner,
1267 and lateral positions, a CV (standard deviation divided by mean) of all sepals was calculated (for
1268 example, a CV of length of all outer sepals in WT). To determine statistical significance, genotypes
1269 were compared pairwise using permutation tests. To measure within-flower variability of length,
1270 a CV was calculated for all sepals within each flower (for example, a CV of length of outer, inner,
1271 and two lateral sepals in WT bud #10). For accurate calculation of CV, flowers with length data of
1272 at least four sepals were included in the analysis. To determine statistical significance, genotypes
1273 were compared pairwise using Wilcoxon rank sum tests.
1274

1275 **Cytokinin extraction and measurement**

1276 Cytokinin extraction was based on a previously published protocol[144] with modifications.
1277 Briefly, five inflorescence samples of induced *ap1 cal 35S::AP1-GR*, and six inflorescence
1278 samples of induced *drmy1 ap1 cal 35S::AP1-GR* were collected as described above. Samples
1279 were ground in liquid nitrogen and twice extracted in methanol : water : formic acid (15:4:1). 200
1280 pg of BAP per sample was added as an internal control. Extracts were centrifuged at 14,650 rpm
1281 in -4°C for 30 min, and supernatant was evaporated of methanol and reconstituted in 1% (v/v)
1282 acetic acid. Samples were passed through an Oasis MCX SPE column (Waters 186000252),
1283 washed with 1% acetic acid, washed with methanol, and eluted with 0.35 M ammonia in 70%
1284 methanol. Eluents were evaporated to complete dryness, reconstituted in 5% acetonitrile, and
1285 sent for LC-MS.

1286 LC-MS was done as previously described[145], with modifications. Briefly, 1 µl of each
1287 sample was injected into a Thermo Fisher Scientific Vanquish Horizon UHPLC System coupled
1288 with a Thermo Q Exactive HF hybrid quadropole-orbitrap high-resolution mass spectrometer
1289 equipped with a HESI ion source. Samples were separated on a C18 ODS column (AQUITY
1290 UPLC BEH C18, 1.7 µm, 2.1 × 100 mm, Waters), at a flow rate of 0.3 ml/min, with linear gradients
1291 of solvent A (0.1% formic acid) and solvent B (0.1% formic acid in methanol) according to the
1292 following profile: 0 min, 99.0% A + 1.0% B; 4.0 min, 55.0% A + 45.0% B; 7 min, 30.0% A + 70.0%
1293 B; and then with isocratic conditions: 8 min, 1.0% A + 99.0% B; 12 min, 99.0% A + 1.0% B.
1294 Cytokinins were detected using the positive ion mode.

1295 For tZ, tZR, iP, iPR, and the internal control BAP, peaks were identified from an external
1296 standard mix composed of 0.1 µg/ml each of BAP (Alfa Aesar A14678), tZ (Sigma Z0876), tZR
1297 (Sigma Z3541), iP (Cayman Chemical 17906), and iPR (Cayman chemical 20522) in 5%
1298 acetonitrile. For cZ and cZR, peaks were identified based on previously reported precursor m/z
1299 and retention time[146]. Using Xcalibur (Thermo Scientific), peak area was quantified for each
1300 cytokinin in each sample, normalized against the peak area of BAP (internal control) and sample
1301 fresh weight, and then normalized against the average abundance of tZ in WT samples.

1302

1303 **Software**

1304 Image processing was done in ImageJ (version 2.9.0/1.53t, build a33148d777)[141,142] and
1305 MorphoGraphX (version 2.0, revision 1-294, CUDA version 11.40)[143].

1306 Data processing was done in RStudio (R version 4.0.5 “Shake and Throw” (2021-03-
1307 31))[147]. Graphs were made using the package ggplot2 (version 3.3.3)[148]. Fisher’s contingency
1308 table tests were done using the function fisher.test in R. Wilcoxon rank sum tests were done using
1309 the function wilcox.test in R. Hypergeometric tests were done using the function phyper in R. Data
1310 fitting with ANOVA was done using the function aov in R.

1311 Figures were assembled in Adobe Illustrator (version 25.4.1). An RGB color profile “Image
1312 P3” was used for all the figures.

1313

1314 **SUPPLEMENTAL INFORMATION TITLES AND LEGENDS**

1315

1316 **Supplemental Figure 1. Evidence that the *drmy1* mutant has ribosomal and translation**
1317 **defects, associated with Figure 1.**
1318 **(A)** The *drmy1* phenotype is reproduced in the *ap1 cal AP1-GR* system (Ler background). Shown
1319 are representative buds of *ap1 cal AP1-GR* (top row) *and drmy1 ap1 cal AP1-GR* (bottom row) at
1320 day 0 (before DEX induction), day 3 (after 3 DEX inductions, when tissue is collected for RNA,
1321 protein, or cytokinin extraction), and day 5 (after 5 DEX inductions). Arrowheads show sepal
1322 primordia that are of variable number, position, and sizes. Asterisks indicate periphery of the floral
1323 meristem that has limited or no sepal outgrowth in *drmy1 ap1 cal AP1-GR* compared with *ap1 cal*
1324 *AP1-GR*. Scale bars, 25 µm.
1325 **(B)** Summary of the inflorescence RNA-seq and proteomics datasets. Shown are numbers of
1326 genes in each category. Down, downregulated in *drmy1*; NS, not significantly changed between
1327 *drmy1* and WT; Up, upregulated in *drmy1*; NA, not available. Note that in the combined dataset
1328 (gene-protein pairs), different genes encoding for the same protein were separately counted, so
1329 were different proteins encoded by the same gene. See also Supplemental Dataset 1.
1330 **(C)** Violin and box plots of log2 fold change in RNA between *drmy1* and WT in induced *ap1 cal*
1331 *AP1-GR* inflorescence, for genes encoding ribosomal components ("Structural constituents of the
1332 ribosome" GO:0003735, and its offspring terms) and all other genes involved in translation
1333 ("Translation" GO:0006412, and its offspring terms). The following genes are labeled on the
1334 graph: *UL4Z* (AT3G09630), log2FC = -0.492; *UL4Y* (AT5G02870), log2FC = -0.509; *UL18Z*
1335 (AT3G25520), log2FC = -0.459. Note that the x-axis was trimmed to (-2,2) for ease of display.
1336 **(D)** Violin and box plots of log2 fold change in protein level between *drmy1* and WT in induced
1337 *ap1 cal AP1-GR* inflorescence, for genes in the same categories as in (C). The following genes
1338 are labeled on the graph: *UL4Z* (AT3G09630), log2FC = 0.352; *UL4Y* (AT5G02870), log2FC =
1339 0.811; *UL18Z* (AT3G25520), log2FC = 0.742.
1340 **(E)** Coherent regulation of gene expression by *drmy1* and AZD-8055. Shown is a contingency
1341 table of genes downregulated (Down), not significantly changed (NS), and upregulated (Up) in
1342 *drmy1* vs WT (columns), and in AZD-8055-treated WT vs mock-treated WT (rows). Bold font
1343 shows the number of genes in each category, and gray font shows the expected number of genes
1344 if there were no correlation between two conditions (calculated as row margin × column margin /
1345 total number of genes). Categories where the number of genes is above expectation are
1346 highlighted blue, and categories where the number of genes is below expectation are highlighted
1347 red. Chi-square test $p < 2.2 \times 10^{-16}$.
1348 **(F)** Gene ontology enrichment of genes coherently downregulated by both *drmy1* and AZD-8055.
1349 Shown are the top 8 terms and their enrichment p-values. A complete list can be found in
1350 Supplementary Dataset 3.
1351 **(G-J)** Fluorescence of a constitutively expressed marker supports the hypothesis that *drmy1* has
1352 reduced translation rate. (G-I) are representative confocal images of *UBQ10::mCherry-RCI2A* in
1353 dissected inflorescences of WT (G), *drmy1* (H), and *ul4y* (I). Numbers show how the signal is
1354 divided based on the stage of floral meristem when quantified (IM+1, inflorescence meristem plus
1355 stage 1; 2, stage 2; 3, stage 3). Scale bars, 25µm. (J) shows quantification of signal intensity (i.e.

integrated density divided by area) in all images divided as in (G-I). Mean $\pm$ SD are shown. Data was fit using a two-way ANOVA model with genotype and stage as two additive factors. Asterisks show statistically significant pairwise contrasts between WT and *drmy1* ($p < 2x10^{-16}$) and between WT and *ul4y* ($p = 2.1x10^{-15}$). Sample sizes: WT IM+1, n = 30; *drmy1* IM+1, n = 22; *ul4y* IM+1, n = 18; WT stage 2, n = 99; *drmy1* stage 2, n = 100; *ul4y* stage 2, n = 52; WT stage 3, n = 39; *drmy1* stage 3, n = 27; *ul4y* stage 3, n = 26.

1363 **Supplemental Figure 2. Ribosomal mutations enhance the *drmy1* phenotype, associated**
1364 **with Figure 2.**
1365 **(A-H)** Examples of stage 5 buds from *drmy1* (A), *drmy1 ul4z* (B-D), *drmy1 ul4y* (E-F), and *drmy1*
1366 *ul18z/+* (G-H). In (B,E,G) sepal primordia within each bud have bigger size differences than typical
1367 *drmy1* single mutant buds; asterisks show giant outer sepal primordia and brackets show bud
1368 peripheral regions with little or no primordium outgrowth. In (C,F,H), arrowheads show 6 sepal
1369 primordia within each bud, which does not occur in *drmy1*. In (D,H), asterisks show the presence
1370 of two outer sepal primordia within a bud, instead of one in *drmy1*. Scale bars, 25μm.
1371 **(I-J)** Quantification of sepal primordium number (I) and positional variability (J), comparing each
1372 of *drmy1 ul4z* (n = 60), *drmy1 ul4y* (n = 61), and *drmy1 ul18z/+* (n = 69) with *drmy1* (n = 67). “ns”
1373 indicates no significant difference in Fisher’s contingency table tests (I) and Wilcoxon’s rank sum
1374 tests (J) respectively. Data of *drmy1* is reproduced from the same dataset presented in Figure 2.
1375 **(K)** Dissected young silique of *drmy1 ul18z/+* mother plant. Arrowheads point to aborted ovules.
1376 Scale bar, 200 μm.
1377

1378 **Supplemental Figure 3. Sepal primordia in ribosome and TOR mutants catch up in growth**
1379 **to form uniformly sized mature sepals within the bud, associated with Figure 3.**
1380 **(A-F)** Representative inflorescences images (left) of WT (A), *drmy1* (B), *ul4z* (C), *ul4y* (D), *ul18z*
1381 (E), and *lst8-1-1* (F), with boxed regions enlarged (right). Blue arrowheads show sepals of regular
1382 length, and red arrowheads show sepals shorter than others. Note that sepals in *drmy1* were
1383 unable to close due to unequal lengths, while sepals in *ul4z*, *ul4y*, and *ul18z*, and close like in
1384 WT. Sepals in *lst8-1-1* were unable to close although there is no apparent variation in length.
1385 Scale bars, 0.5 mm.
1386 **(G-L)** Dissected sepals from a representative bud of WT (G), *drmy1* (H), *ul4z* (I), *ul4y* (J), *ul18z*
1387 (K), and two buds of *lst8-1-1* (L). Note that sepals in the *drmy1* bud are of different sizes. Sepals
1388 within each bud of *ul4z*, *ul4y*, *ul18z*, and *lst8-1-1* are of similar sizes, although there can be
1389 variation between different buds of the same genotype. O, outer sepal. I, inner sepal. L, lateral
1390 sepal. Scale bars, 200 μm.
1391 **(M)** Quantification of between-flower variability of sepal length. Length was measured from all
1392 imaged outer sepals of each genotype, and coefficient of variation (CV) was calculated. A two-
1393 sided permutation test (100,000 permutations) for CV difference not equating to zero was done
1394 for each pair of genotypes, and results were represented by letters (left). Similar analysis was
1395 done for the inner sepal (middle), and the lateral sepal (right). Sample size: Outer sepal, WT n =
1396 35, *drmy1* n = 43, *ul4z* n = 37, *ul4y* n = 42, *ul18z* n = 39, *lst8-1-1* n = 43. Inner sepal, WT n = 34,
1397 *drmy1* n = 46, *ul4z* n = 38, *ul4y* n = 44, *ul18z* n = 37, *lst8-1-1* n = 44. Lateral sepal, WT n = 65,
1398 *drmy1* n = 84, *ul4z* n = 81, *ul4y* n = 89, *ul18z* n = 76, *lst8-1-1* n = 82.
1399 **(N)** Quantification of within-flower variability of length. Flowers with length data from at least four
1400 sepals were analyzed. A CV of length from all sepals within each flower was calculated, and mean
1401 ± SD was plotted, grouped by genotype. A Wilcoxon rank sum test was done for each pair of
1402 genotypes, and results were represented by letters. Sample size: WT n = 31 buds, *drmy1* n = 38
1403 buds, *ul4z* n = 33 buds, *ul4y* n = 36 buds, *ul18z* n = 32 buds, *lst8-1-1* n = 39 buds.
1404 **(O-Q)** Live imaging of sepal development from stage 3 to 6 in a bud each of WT, *drmy1*, and *ul4y*,
1405 showing chlorophyll or propidium iodide channel, and Gaussian curvature calculated from the
1406 surface. Note that both *drmy1* and *ul4y* have inner sepals that initiate late (day 2, asterisk). The
1407 *drmy1* inner sepal develops slowly, and leaves the bud open at day 3 (red arrowhead). The *ul4y*
1408 inner sepal catches up with the rest of the sepals and closes the bud (blue arrowhead). Scale
1409 bars, 25 μm.
1410

1411 **Supplemental Figure 4. Inhibition of TOR activity and translation causes auxin maxima**
1412 **formation at variable positions, correlated with variable positions of sepal primordia,**
1413 **associated with Figure 4.**
1414 **(A-E)** Variable patterning of auxin signaling in *drmy1*, *ul4y*, and CHX-treated WT buds
1415 corresponds to variable sepal initiation. Shown are a representative bud each of the labeled
1416 genotype or treatment live-imaged over three or four days. In all but the last time point, in the top
1417 row is *DR5::3xVENUS-N7* (yellow), in the middle row is a composite of *DR5::3xVENUS-N7*
1418 (yellow) and Chlorophyll (magenta), and in the bottom row is Gaussian curvature calculated from
1419 a surface extracted from the Chlorophyll channel. In the last time point, propidium iodide is shown
1420 on the top, and Gaussian curvature calculated from a surface extracted from the propidium iodide
1421 channel is shown on the bottom. (A) In WT, four robustly positioned auxin maxima at day 1
1422 correlates with four robustly positioned sepal primordia at day 4 (blue arrowheads). (B) In *drmy1*,
1423 at day 1 there are three robustly positioned auxin maxima (blue arrowheads). At day 2, a diffuse
1424 band of auxin signaling occurs in the adaxial periphery of the bud, joining with one of the lateral
1425 auxin maxima (red bracket). At day 3, this diffuse band splits into three auxin maxima (red
1426 arrowheads), making a total of 5. The maxima correlate with the five sepal primordia at day 4,
1427 three at robust positions (blue arrowheads) and two at irregular positions (red arrowheads). (C)
1428 In *ul4y*, at day 1 there are two auxin maxima at robust positions (blue arrowheads), one at robust
1429 lateral position but much weaker (red arrowhead), and a band of weak auxin signaling in the
1430 adaxial periphery of the bud (red bracket). At day 2, the weak auxin maxima at lateral position got
1431 stronger, and the weak band split into two auxin maxima on the adaxial side (red arrowheads).
1432 These five auxin maxima correspond to the five sepal primordia at day 3, three in robust positions
1433 (blue arrowheads) and two in irregular positions (red arrowheads). (D) In the WT bud treated with
1434 Mock, four robust auxin maxima at day 6 of the treatment corresponds to four robust sepal
1435 primordia seen at day 9 (blue arrowheads). (E) In the WT bud treated with CHX, at day 6 there
1436 are three stronger auxin maxima (blue arrowheads) and two weaker ones (red arrowheads),
1437 corresponding to three bigger primordium outgrowth regions (blue arrowheads) and two smaller
1438 ones (red arrowheads) at day 9. For ease of display, the DR5 channel in CHX-treated WT was
1439 brightened three times relative to mock. Scale bars, 25 μm.
1440 **(F-I)** TOR inhibition using Torin2 causes increased cytokinin signaling, and occasional variability
1441 in both auxin and cytokinin signaling. (F) Representative images of late stage 2 buds from WT
1442 plants treated with mock or 2 nmol Torin2 for 15 days. Shown are *DR5::3xVENUS-N7* in yellow,
1443 *TCS::GFP* in cyan, and both merged with propidium iodide in magenta. Note that 3/16 (19%) buds
1444 had variable number and position of DR5 and TCS maxima, and 13/16 (81%) had robust DR5
1445 and TCS maxima, although TCS intensity is higher in both cases compared with mock-treated
1446 buds. Scale bars, 25 μm. (G) Quantification of TCS intensity from maximum intensity projection
1447 images, normalized to the mean of WT mock. Shown are mean ± SD. Asterisk shows statistical
1448 significance in a two-tailed Student's t-test compared with WT mock ($p = 1.2x10^{-4}$). (H) Circular
1449 histograms of DR5 distribution around the bud (mean ± SD). (I) Circular histograms of TCS
1450 distribution around the bud (mean ± SD). For calculation of circular histograms, please see Figure
1451 4 legends and Materials and Methods. Sample size: WT mock, n = 11 buds; WT Torin2, n = 16
1452 buds.

1453 **Supplemental Figure 5. Translation of uORF-containing ARFs is not universally**
1454 **downregulated in *drmy1*, associated with Figure 5.**
1455 **(A)** *drmy1* has a lower protein-transcript ratio than WT for genes with at least 2 uORFs. 5,086
1456 transcript-protein pairs in our dataset were grouped according to the maximum number of uORFs
1457 in all transcript isoforms (0, n = 3,485; 1, n = 874; ≥ 2, n = 724)[62]. For each pair, protein-transcript
1458 ratio was calculated, log-transformed, and the difference between *drmy1* and WT was plotted. A
1459 negative value means this gene has less protein per transcript in *drmy1* than WT, and could
1460 indicate reduced translation or protein stability. Medians for each group: 0 uORF, -0.00367; 1
1461 uORF, -0.00808; ≥ 2 uORFs, -0.0243. Asterisk show statistically significant difference from Group
1462 0 in a Wilcoxon rank sum test ($p = 3.167 \times 10^{-4}$), while ns means no significant difference from
1463 Group 0 (p = 0.167).
1464 **(B-D)** There is no universal decrease in the expression of uORF-containing ARF reporters. (B)
1465 Transcript level of three activator *ARF*s (*ARF5*, *ARF6*, *ARF8*) and two repressor *ARF*s (*ARF3*,
1466 *ARF10*) in RNA-seq (n = 3 per genotype). Note that *ARF3*, *ARF5*, and *ARF6* contain uORFs
1467 before the main ORF, and *ARF8* and *ARF10* do not. Asterisks show statistically significant
1468 differences between WT and *drmy1*, and ns means no significance difference. p values: *ARF3*, p
1469 = 0.583; *ARF5*, p = 0.497; *ARF6*, p = 0.603; *ARF8*, p = 0.058; *ARF10* p = 0.019. (C)
1470 Transcriptional reporters for these ARFs (*pARF3::n3xGFP*, *pARF5::erYFP*, *pARF6::n3xGFP*,
1471 *pARF8::n3xGFP* and *pARF10::n3xGFP*) were imaged in WT and *drmy1*, and representative late
1472 stage 2 buds were shown (cyan, GFP or YFP; magenta, propidium iodide). Note that the *pARF3*,
1473 *pARF5*, and *pARF6* reporters contain the same uORFs as the genes, reflecting a combination of
1474 transcriptional and uORF regulations. Scale bars, 20 μm. (D) Quantification of GFP intensity.
1475 Sample size: *pARF3* WT, n = 22; *pARF3 drmy1*, n = 25; *pARF5* WT, n = 22; *pARF5 drmy1*, n =
1476 22; *pARF6* WT, n = 19; *pARF6 drmy1*, n = 28; *pARF8* WT, n = 25; *pARF8 drmy1*, n = 31; *pARF10*
1477 WT, n = 20; *pARF10 drmy1*, n = 29. Asterisks show statistically significant differences between
1478 WT and *drmy1* in Wilcoxon rank sum tests, and ns means no significance difference. p values:
1479 *pARF3*, p = 0.3797; *pARF5*, $p = 6.22 \times 10^{-5}$; *pARF6*, $p = 2.868 \times 10^{-13}$; *pARF8*, p = 0.5127; *pARF10*
1480 $p = 7.073 \times 10^{-14}$.
1481

1482 **Supplemental Figure 6. Cytokinin signaling causes variability in mature sepal number and**
1483 **size in *drmy1*, associated with Figure 5.**
1484 Shown are top-view inflorescence images of WT (A), *arr1,10,12* (B), *wol* (C), *drmy1* (D), *drmy1*
1485 *arr1,10,12* (E), and *drmy1 wol* (F), with boxed areas of individual buds enlarged and shown on
1486 the right. In the enlarged views, blue arrowheads point to sepals of regular size, and red
1487 arrowheads point to sepals that are much smaller. Scale bars, 0.5 mm.
1488

1489 **Supplemental Figure 7. ARR7-llama partially restores robustness in mature sepal number**
1490 **and size, associated with Figure 7.**
1491 **(A)** Cytokinin abundance does not significantly change in *drmy1*. Shown is mean ± SD of levels
1492 of trans-zeatin (tZ), cis-Zeatin (cZ), N^6-(Δ^2-Isopentenyl)adenine (iP), trans-Zeatin riboside (tZR),
1493 cis-Zeatin riboside (cZR), and N^6-(Δ^2-Isopentenyl)adenosine (iPR) quantified by LC-MS in
1494 induced WT and *drmy1* inflorescences of *ap1 cal AP1-GR* background. Levels are normalized to
1495 the mean tZ level in WT. Sample size: n = 5 for WT; n = 6 for *drmy1*. ns means no significant
1496 difference between WT and *drmy1* in a two-sided Wilcoxon rank sum test. P-values: tZ, p =
1497 0.2468; cZ, p = 0.7922; iP, p = 0.2468; tZR, p = 0.1775; cZR, p = 0.6623; iPR, p = 0.6623.
1498 **(B)** The *ARR7-llama* reporter responds to externally applied cytokinin. Shown are GFP channel
1499 images of stage 2 buds from *ARR7-llama GFP-nes* line 7-4 in WT, before (top) or after (bottom)
1500 5 hours of 200 μM BAP treatment. Images are representative of n = 6 buds from line 7-4 and n =
1501 3 buds from line 7-6.
1502 **(C)** CHX treatment does not change the localization of GFP-nes. Shown are GFP channel images
1503 of stage 2 buds from *GFP-nes* in WT, treated with mock (top) or 2 μM CHX (bottom) for 24 hours.
1504 Images are representative of n = 10 buds (mock) and n = 9 buds (CHX).
1505 **(D)** AZD-8055 treatment does not change the localization of GFP-nes. Shown are GFP channel
1506 images of stage 2 buds from *GFP-nes* in WT, treated with mock (top) or 2 μM AZD-8055 (bottom)
1507 for 72 hours. Images are representative of n = 10 buds (mock) and n = 11 buds (AZD-8055). For
1508 (B-D), each image was brightened to reveal patterns of GFP distribution. A square region taken
1509 from the image containing 5-10 cells is enlarged and shown on the top right. Within the
1510 enlargement, GFP intensity was quantified along the dotted line and plotted on the bottom right.
1511 X-axis, pixels (range 0-238). Y-axis, GFP intensity in gray value (smoothened by taking the
1512 average intensity of 11-pixel neighborhoods; range 90-175). Scale bars, 25 μm.
1513 **(E-H)** The ARR7-llama construct partially rescues the mature sepal variability in *drmy1*. Shown
1514 are inflorescence images of WT (E), *ARR7-llama GFP-nes* (F), *drmy1* (G), and *drmy1 ARR7-*
1515 *llama GFP-nes* (H). The boxed regions were enlarged and shown on the right of each panel. Note
1516 that while *drmy1* buds have normal-sized (blue arrowheads) and smaller (red arrowheads) sepals,
1517 some buds in *drmy1 ARR7-llama GFP-nes* have robustly sized sepals (H, middle) while others
1518 still show variability (H, right). Scale bars, 0.5 mm.
1519 **(I-J)** *drmy1* has decreased and disrupted pattern of DII degradation. (I) Representative late stage
1520 2 buds of WT and *drmy1* showing *DII-n3xVENUS* (cyan), *mDII-ntdTomato* (magenta), and merge.
1521 For ease of display, the *VENUS* channel was brightened 3 times relative to the *tdTomato* channel.
1522 Scale bars, 25 μm. (J) Quantification of VENUS/tdTomato ratio using ImageJ. Note that a
1523 universal background of 6 gray value per pixel (determined in blank regions without tissue) were
1524 subtracted from each image before quantification. Sample size: WT, n = 8 buds; *drmy1*, n = 19
1525 buds. Asterisk shows statistically significant difference in a Wilcoxon rank sum test (p = 0.01335).
1526

1527 **Supplemental Dataset 1. Inflorescence RNA-seq and proteomics.**
1528
1529 **Supplemental Dataset 2. Unprocessed ribosome profiles.**
1530
1531 **Supplemental Dataset 3. Seedling RNA-seq.**
1532
1533 **Supplemental Dataset 4. Data used in graphs.**
1534
1535 **Supplemental Dataset 5. DNA sequences.**
1536

1537 **REFERENCES**

1538 1. Kaneko, K. (2007). Evolution of robustness to noise and mutation in gene expression
1539 dynamics. PLoS One *2*, e434. 10.1371/journal.pone.0000434.
1540 2. Lachowiec, J., Queitsch, C., and Kliebenstein, D.J. (2016). Molecular mechanisms
1541 governing differential robustness of development and environmental responses in plants.
1542 Ann. Bot. *117*, 795–809. 10.1093/aob/mcv151.
1543 3. Waddington, C.H. (1942). Canalization of Development and the Inheritance of Acquired
1544 Characters. Nature *150*, 563–656.
1545 4. Zabinsky, R.A., Mason, G.A., Queitsch, C., and Jarosz, D.F. (2019). It's not magic –
1546 Hsp90 and its effects on genetic and epigenetic variation. Semin. Cell Dev. Biol. *88*, 21–
1547 35. 10.1016/j.semcdb.2018.05.015.
1548 5. Twitty, V.C., and Schwind, J.L. (1931). The growth of eyes and limbs transplanted
1549 heteroplastically between two species of <i>Amblystoma. J. Exp. Zool. *59*, 61–86.
1550 10.1002/jez.1400590105.
1551 6. Silber, S.J. (1976). Growth of Baby Kidneys Transplanted Into Adults. Arch. Surg. *111*,
1552 75–77. 10.1001/archsurg.1976.01360190077014.
1553 7. Summerbell, D., and Lewis, J.H. (1975). Time, place and positional value in the chick
1554 limb bud. J. Embryol. Exp. Morphol. *33*, 621–643. 10.1242/dev.33.3.621.
1555 8. Parker, J., and Struhl, G. (2020). Control of *Drosophila* wing size by morphogen range
1556 and hormonal gating. Proc. Natl. Acad. Sci. U. S. A. *117*, 31935–31944.
1557 10.1073/pnas.2018196117.
1558 9. Garelli, A., Gontijo, A.M., Miguela, V., Caparros, E., and Dominguez, M. (2012). Imaginal
1559 discs secrete insulin-like peptide 8 to mediate plasticity of growth and maturation.
1560 Science *336*, 579–582. 10.1126/science.1216735.
1561 10. Crickmore, M.A., and Mann, R.S. (2006). Hox control of organ size by regulation of
1562 morphogen production and mobility. Science *313*, 63–68. 10.1126/science.1128650.
1563 11. Recasens-Alvarez, C., Ferreira, A., and Milán, M. (2017). JAK/STAT controls organ size
1564 and fate specification by regulating morphogen production and signalling. Nat. Commun.
1565 *8*, 10–12. 10.1038/ncomms13815.
1566 12. Irish, V.F. (2008). The Arabidopsis petal: a model for plant organogenesis. Trends Plant
1567 Sci. *13*, 430–436. 10.1016/j.tplants.2008.05.006.
1568 13. Fenster, C.B., Armbruster, W.S., Wilson, P., Dudash, M.R., and Thomson, J.D. (2004).
1569 Pollination syndromes and floral specialization. Annu. Rev. Ecol. Evol. Syst. *35*, 375–403.
1570 10.1146/annurev.ecolsys.34.011802.132347.
1571 14. King, S., Beck, F., and Lüttge, U. (2004). On the mystery of the golden angle in
1572 phyllotaxis. Plant, Cell Environ. *27*, 685–695. 10.1111/j.1365-3040.2004.01185.x.
1573 15. Smith, R.S., Guyomarc'h, S., Mandel, T., Reinhardt, D., Kuhlemeier, C., and
1574 Prusinkiewicz, P. (2006). A plausible model of phyllotaxis. Proc. Natl. Acad. Sci. U. S. A.
1575 *103*, 1301–1306. 10.1073/pnas.0510457103.
1576 16. Besnard, F., Refahi, Y., Morin, V., Marteaux, B., Brunoud, G., Chambrier, P., Rozier, F.,
1577 Mirabet, V., Legrand, J., Lainé, S., et al. (2014). Cytokinin signalling inhibitory fields
1578 provide robustness to phyllotaxis. Nature *505*, 417–421. 10.1038/nature12791.
1579 17. Queitsch, C., Sangster, T.A., and Lindquist, S. (2002). Hsp90 as a capacitor of
1580 phenotypic variation. Nature *417*, 618–624. 10.1038/nature749.
1581 18. Rutherford, S.L., and Lindquist, S. (1998). Hsp90 as a capacitor for morphological
1582 evolution. Nature *396*, 336–342. 10.1038/24550.
1583 19. Lehner, B., Crombie, C., Tischler, J., Fortunato, A., and Fraser, A.G. (2006). Systematic
1584 mapping of genetic interactions in *Caenorhabditis elegans* identifies common modifiers of
1585 diverse signaling pathways. Nat. Genet. *38*, 896–903. 10.1038/ng1844.
1586 20. Levy, S.F., and Siegal, M.L. (2008). Network hubs buffer environmental variation in

1587 *Saccharomyces cerevisiae*. PLoS Biol. *6*, 2588–2604. 10.1371/journal.pbio.0060264.
1588 21. Folta, A., Severing, E.I., Krauskopf, J., van de Geest, H., Verver, J., Nap, J.P., and
1589 Mlynarova, L. (2014). Over-expression of Arabidopsis AtCHR23 chromatin remodeling
1590 ATPase results in increased variability of growth and gene expression. BMC Plant Biol.
1591 *14*, 76. 10.1186/1471-2229-14-76.
1592 22. Marygold, S.J., Roote, J., Reuter, G., Lambertsson, A., Ashburner, M., Millburn, G.H.,
1593 Harrison, P.M., Yu, Z., Kenmochi, N., Kaufman, T.C., et al. (2007). The ribosomal protein
1594 genes and Minute loci of *Drosophila melanogaster*. Genome Biol. *8*, R216. 10.1186/gb-
1595 2007-8-10-r216.
1596 23. Hintze, M., Katsanos, D., Shahrezaei, V., and Barkoulas, M. (2021). Phenotypic
1597 Robustness of Epidermal Stem Cell Number in C. elegans Is Modulated by the Activity of
1598 the Conserved N-acetyltransferase nath-10/NAT10. Front. Cell Dev. Biol. *9*, 640856.
1599 10.3389/fcell.2021.640856.
1600 24. Wang, S., Kurepa, J., and Smalle, J.A. (2009). The *Arabidopsis* 26S proteasome subunit
1601 RPN1a is required for optimal plant growth and stress responses. Plant Cell Physiol. *50*,
1602 1721–1725. 10.1093/pcp/pcp105.
1603 25. Gallois, J.L., Guyon-Debast, A., Lecureuil, A., Vezon, D., Carpentier, V., Bonhomme, S.,
1604 and Guerche, P. (2009). The *Arabidopsis* proteasome RPT5 subunits are essential for
1605 gametophyte development and show accession-dependent redundancy. Plant Cell *21*,
1606 442–459. 10.1105/tpc.108.062372.
1607 26. Zhu, M., Chen, W., Mirabet, V., Hong, L., Bovio, S., Strauss, S., Schwarz, E.M.,
1608 Tsugawa, S., Wang, Z., Smith, R.S., et al. (2020). Robust organ size requires robust
1609 timing of initiation orchestrated by focused auxin and cytokinin signalling. Nat. Plants *6*,
1610 686–698. 10.1038/s41477-020-0666-7.
1611 27. Hong, L., Dumond, M., Tsugawa, S., Sapala, A., Routier-Kierzkowska, A.L., Zhou, Y.,
1612 Chen, C., Kiss, A., Zhu, M., Hamant, O., et al. (2016). Variable Cell Growth Yields
1613 Reproducible Organ Development through Spatiotemporal Averaging. Dev. Cell *38*, 15–
1614 32. 10.1016/j.devcel.2016.06.016.
1615 28. Roeder, A.H.K. (2021). Arabidopsis sepals: A model system for the emergent process of
1616 morphogenesis. Quant. Plant Biol. *2*. 10.1017/qpb.2021.12.
1617 29. Trinh, D.-C., Martin, M., Bald, L., Maizel, A., Trehin, C., and Hamant, O. (2022). Paf1C
1618 denoises transcription and growth patterns to achieve organ shape reproducibility.
1619 bioRxiv, 2022.03.25.485770.
1620 30. Jing, H., and Strader, L.C. (2019). Interplay of auxin and cytokinin in lateral root
1621 development. Int. J. Mol. Sci. *20*, 486. 10.3390/ijms20030486.
1622 31. Hussain, S., Nanda, S., Zhang, J., Rehmani, M.I.A., Suleman, M., Li, G., and Hou, H.
1623 (2021). Auxin and Cytokinin Interplay during Leaf Morphogenesis and Phyllotaxy. Plants
1624 *10*, 1732. 10.3390/plants10081732.
1625 32. Schaller, G.E., Bishopp, A., and Kieber, J.J. (2015). The yin-yang of hormones: Cytokinin
1626 and auxin interactions in plant development. Plant Cell *27*, 44–63.
1627 10.1105/tpc.114.133595.
1628 33. Ingargiola, C., Duarte, G.T., Robaglia, C., Leprince, A.S., and Meyer, C. (2020). The plant
1629 target of rapamycin: A conduc TOR of nutrition and metabolism in photosynthetic
1630 organisms. Genes (Basel). *11*, 1285. 10.3390/genes11111285.
1631 34. Scarpin, M.R., Leiboff, S., and Brunkard, J.O. (2020). Parallel global profiling of plant tor
1632 dynamics reveals a conserved role for LARP1 in translation. eLife *9*, e58795.
1633 10.7554/eLife.58795.
1634 35. Yu, H., Ito, T., Wellmer, F., and Meyerowitz, E.M. (2004). Repression of AGAMOUS-LIKE
1635 24 is a crucial step in promoting flower development. Nat. Genet. *36*, 157–161.
1636 10.1038/ng1286.
1637 36. Wellmer, F., Alves-Ferreira, M., Dubois, A., Riechmann, J.L., and Meyerowitz, E.M.

(2006). Genome-wide analysis of gene expression during early *Arabidopsis* flower development. PLoS Genet. *2*, 1012–1024. 10.1371/journal.pgen.0020117.

37. Smyth, D.R., Bowman, J.L., and Meyerowitz, E.M. (1990). Early flower development in Arabidopsis. Plant Cell *2*, 755–767. 10.1105/tpc.2.8.755.
38. Goodman, C.A., and Hornberger, T.A. (2013). Measuring protein synthesis with SUnSET: A valid alternative to traditional techniques? Exerc. Sport Sci. Rev. *41*, 107–115. 10.1097/JES.0b013e3182798a95.
39. Van Hoewyk, D. (2016). Use of the non-radioactive SUnSET method to detect decreased protein synthesis in proteasome inhibited Arabidopsis roots. Plant Methods *12*, 20. 10.1186/S13007-016-0120-Z.
40. Scarpin, M.R., Busche, M., Martinez, R.E., Harper, L.C., Reiser, L., Szakonyi, D., Merchante, C., Lan, T., Xiong, W., Mo, B., et al. (2023). An updated nomenclature for plant ribosomal protein genes. Plant Cell *35*, 640–643. 10.1093/plcell/koac333.
41. Schepetilnikov, M., and Ryabova, L.A. (2018). Recent discoveries on the role of tor (Target of rapamycin) signaling in translation in plants. Plant Physiol. *176*, 1095–1105. 10.1104/pp.17.01243.
42. Scarpin, M.R., Simmons, C.H., and Brunkard, J.O. (2022). Translating across kingdoms: target of rapamycin promotes protein synthesis through conserved and divergent pathways in plants. J. Exp. Bot. *73*, 7016–7025. 10.1093/jxb/erac267.
43. Brunkard, J.O. (2020). Exaptive Evolution of Target of Rapamycin Signaling in Multicellular Eukaryotes. Dev. Cell *54*, 142–155. 10.1016/j.devcel.2020.06.022.
44. Battaglioni, S., Benjamin, D., Wälchli, M., Maier, T., and Hall, M.N. (2022). mTOR substrate phosphorylation in growth control. Cell *185*, 1814–1836. 10.1016/j.cell.2022.04.013.
45. Valvezan, A.J., and Manning, B.D. (2019). Molecular logic of mTORC1 signalling as a metabolic rheostat. Nat. Metab. *1*, 321–333. 10.1038/s42255-019-0038-7.
46. Xiong, Y., McCormack, M., Li, L., Hall, Q., Xiang, C., and Sheen, J. (2013). Glucose-TOR signalling reprograms the transcriptome and activates meristems. Nature *496*, 181–186. 10.1038/nature12030.
47. Riegler, S., Servi, L., Scarpin, M.R., Godoy Herz, M.A., Kubaczka, M.G., Venhuizen, P., Meyer, C., Brunkard, J.O., Kalyna, M., Barta, A., et al. (2021). Light regulates alternative splicing outcomes via the TOR kinase pathway. Cell Rep. *36*, 109676. 10.1016/j.celrep.2021.109676.
48. Obomighie, I., Lapenas, K., Murphy, B.E., Bowles, A.M.C., Bechtold, U., and Prischi, F. (2021). The Role of Ribosomal Protein S6 Kinases in Plant Homeostasis. Front. Mol. Biosci. *8*, 636560. 10.3389/fmolb.2021.636560.
49. Xiong, Y., and Sheen, J. (2012). Rapamycin and glucose-target of rapamycin (TOR) protein signaling in plants. J. Biol. Chem. *287*, 2836–2842. 10.1074/jbc.M111.300749.
50. Moreau, M., Azzopardi, M., Clé ment, G., Dobrenel, T., Marchive, C., Renne, C., Martin-Magniette, M.L., Taconnat, L., Renou, J.P., Robaglia, C., et al. (2012). Mutations in the *Arabidopsis* homolog of LST8/GβL, a partner of the target of Rapamycin kinase, impair plant growth, flowering, and metabolic adaptation to long days. Plant Cell *24*, 463–481. 10.1105/tpc.111.091306.
51. Brunkard, J.O., Xu, M., Regina Scarpin, M., Chatterjee, S., Shemyakina, E.A., Goodman, H.M., and Zambryski, P. (2020). TOR dynamically regulates plant cell-cell transport. Proc. Natl. Acad. Sci. U. S. A. *117*, 5049–5058. 10.1073/pnas.1919196117.
52. Menand, B., Desnos, T., Nussaume, L., Bergert, F., Bouchez, D., Meyer, C., and Robaglia, C. (2002). Expression and disruption of the *Arabidopsis TOR* (target of rapamycin) gene. Proc. Natl. Acad. Sci. U. S. A. *99*, 6422–6427. 10.1073/pnas.092141899.
53. Zhao, Z., Andersen, S.U., Ljung, K., Dolezal, K., Miotk, A., Schultheiss, S.J., and

1689 Lohmann, J.U. (2010). Hormonal control of the shoot stem-cell niche. Nature *465*, 1089–
1690 1092. 10.1038/nature09126.
1691 54. Yoshida, S., Mandel, T., and Kuhlemeier, C. (2011). Stem cell activation by light guides
1692 plant organogenesis. Genes Dev. *25*, 1439–1450. 10.1101/gad.631211.
1693 55. Du, F., Guan, C., and Jiao, Y. (2018). Molecular Mechanisms of Leaf Morphogenesis.
1694 Mol. Plant *11*, 1117–1134. 10.1016/j.molp.2018.06.006.
1695 56. Taylor-Teeples, M., Lanctot, A., and Nemhauser, J.L. (2016). As above, so below:
1696 Auxin's role in lateral organ development. Dev. Biol. *419*, 156–164.
1697 10.1016/j.ydbio.2016.03.020.
1698 57. Rosado, A., Li, R., Van De Ven, W., Hsu, E., and Raikhel, N. V. (2012). *Arabidopsis*
1699 ribosomal proteins control developmental programs through translational regulation of
1700 auxin response factors. Proc. Natl. Acad. Sci. U. S. A. *109*, 19537–19544.
1701 10.1073/pnas.1214774109.
1702 58. Nishimura, T., Wada, T., Yamamoto, K.T., and Okada, K. (2005). The *Arabidopsis* STV1
1703 protein, responsible for translation reinitiation, is required for auxin-mediated gynoecium
1704 patterning. Plant Cell *17*, 2940–2953. 10.1105/tpc.105.036533.
1705 59. Zhou, F., Roy, B., and von Arnim, A.G. (2010). Translation reinitiation and development
1706 are compromised in similar ways by mutations in translation initiation factor eIF3h and the
1707 ribosomal protein RPL24. BMC Plant Biol. *10*, 193. 10.1186/1471-2229-10-193.
1708 60. Cancé, C., Martin-Arevalillo, R., Boubekeur, K., and Dumas, R. (2022). Auxin response
1709 factors are keys to the many auxin doors. New Phytol. *235*, 402–419.
1710 10.1111/nph.18159.
1711 61. Kim, B.H., Cai, X., Vaughn, J.N., and Von Arnim, A.G. (2007). On the functions of the h
1712 subunit of eukaryotic initiation factor 3 in late stages of translation initiation. Genome Biol.
1713 *8*, R60. 10.1186/gb-2007-8-4-r60.
1714 62. Von Arnim, A.G., Jia, Q., and Vaughn, J.N. (2014). Regulation of plant translation by
1715 upstream open reading frames. Plant Sci. *214*, 1–12. 10.1016/j.plantsci.2013.09.006.
1716 63. Jones, B., Ljung, K., Gunnerås, S.A., Petersson, S. V., Tarkowski, P., Graham, N., May,
1717 S., Dolezal, K., and Sandberg, G. (2010). Cytokinin regulation of auxin synthesis in
1718 Arabidopsis involves a homeostatic feedback loop regulated via auxin and cytokinin
1719 signal transduction. Plant Cell *22*, 2956–2969. 10.1105/tpc.110.074856.
1720 64. Marhavý, P., Duclercq, J., Weller, B., Feraru, E., Bielach, A., Offringa, R., Friml, J.,
1721 Schwechheimer, C., Murphy, A., and Benková, E. (2014). Cytokinin controls polarity of
1722 PIN1-dependent Auxin transport during lateral root organogenesis. Curr. Biol. *24*, 1031–
1723 1037. 10.1016/j.cub.2014.04.002.
1724 65. Růzĭčka, K., Šimášková, M., Duclercq, J., Petrášek, J., Zažímalová, E., Simon, S., Friml,
1725 J., Van Montagu, M.C.E., and Benková, E. (2009). Cytokinin regulates root meristem
1726 activity via modulation of the polar auxin transport. Proc. Natl. Acad. Sci. U. S. A. *106*,
1727 4284–4289. 10.1073/pnas.0900060106.
1728 66. Müller, B., and Sheen, J. (2007). Advances in cytokinin signaling. Science *318*, 68–69.
1729 10.1126/science.1145461.
1730 67. Karunadasa, S.S., Kurepa, J., Shull, T.E., and Smalle, J.A. (2020). Cytokinin-induced
1731 protein synthesis suppresses growth and osmotic stress tolerance. New Phytol. *227*, 50–
1732 64. 10.1111/nph.16519.
1733 68. Szweykowska, A., Gwoidi, E., and Spychala, M. (1980). The Cytokinin Control of Protein
1734 Synthesis in Plants. In Metabolism and Molecular Activities of Cytokinins, J. Guern and C.
1735 Peaud-Lenoel, eds. (Springer-Verlag Berlin Heidelberg), pp. 212–217. 10.1007/978-3-
1736 642-68035-9.
1737 69. Woźny, A., and Gwóźdź, E.A. (1980). The effect of cytokinin on the polyribosome
1738 formation in cucumber cotyledons. Biochem. und Physiol. der Pflanz. *175*, 476–480.
1739 10.1016/s0015-3796(80)80032-1.

1740 70. Klyachko, N.L., Yakovleva, L.A., Shakirova, F.M., and Kulaeva, O.N. (1982). Cell-free
1741 translation of polyribosomes from detached pumpkin cotyledons: Effects of starvation and
1742 cytokinin. Biol. Plant. *24*, 374–380. 10.1007/BF02909106.
1743 71. Short, K.C., Tepfer, D.A., and Fosket, D.E. (1974). Regulation of polyribosome formation
1744 and cell division in cultured soybean cells by cytokinin. J. Cell Sci. *15*, 75–87.
1745 72. Brenner, W.G., and Schmülling, T. (2012). Transcript profiling of cytokinin action in
1746 *Arabidopsis* roots and shoots discovers largely similar but also organ-specific responses.
1747 BMC Plant Biol. *12*, 112. 10.1186/1471-2229-12-112.
1748 73. Kiba, T., Naitou, T., Koizumi, N., Yamashino, T., Sakakibara, H., and Mizuno, T. (2005).
1749 Combinatorial microarray analysis revealing Arabidopsis genes implicated in cytokinin
1750 responses through the His→Asp phosphorelay circuitry. Plant Cell Physiol. *46*, 339–355.
1751 10.1093/pcp/pci033.
1752 74. Černý, M., Kuklová, A., Hoehenwarter, W., Fragner, L., Novák, O., Rotková, G., Jedelský,
1753 P.L., Žáková, K., Šmehilová, M., Strnad, M., et al. (2013). Proteome and metabolome
1754 profiling of cytokinin action in Arabidopsis identifying both distinct and similar responses
1755 to cytokinin down- and up-regulation. J. Exp. Bot. *64*, 4193–4206. 10.1093/jxb/ert227.
1756 75. Cerný, M., Dycka, F., Bobál'Ová, J., and Brzobohatý, B. (2011). Early cytokinin response
1757 proteins and phosphoproteins of Arabidopsis thaliana identified by proteome and
1758 phosphoproteome profiling. J. Exp. Bot. *62*, 921–937. 10.1093/jxb/erq322.
1759 76. Miyawaki, K., Tarkowski, P., Matsumoto-Kitano, M., Kato, T., Sato, S., Tarkowska, D.,
1760 Tabata, S., Sandberg, G., and Kakimoto, T. (2006). Roles of Arabidopsis ATP/ADP
1761 isopentenyltransferases and tRNA isopentenyltransferases in cytokinin biosynthesis.
1762 Proc. Natl. Acad. Sci. U. S. A. *103*, 16598–16603. 10.1073/pnas.0603522103.
1763 77. Ren, B., Liang, Y., Deng, Y., Chen, Q., Zhang, J., Yang, X., and Zuo, J. (2009). Genome-
1764 wide comparative analysis of type-A Arabidopsis response regulator genes by
1765 overexpression studies reveals their diverse roles and regulatory mechanisms in
1766 cytokinin signaling. Cell Res. *19*, 1178–1190. 10.1038/cr.2009.88.
1767 78. Ferreira, F.J., and Kieber, J.J. (2005). Cytokinin signaling. Curr. Opin. Plant Biol. *8*, 518–
1768 525. 10.1016/j.pbi.2005.07.013.
1769 79. Kakimoto, T. (2003). Perception and Signal Transduction of Cytokinins. Annu. Rev. Plant
1770 Biol. *54*, 605–627. 10.1146/annurev.arplant.54.031902.134802.
1771 80. Jain, M., Tyagi, A.K., and Khurana, J.P. (2006). Molecular characterization and
1772 differential expression of cytokinin-responsive type-A response regulators in rice (*Oryza*
1773 *sativa*). BMC Plant Biol. *6*, 1. 10.1186/1471-2229-6-1.
1774 81. To, J.P.C., Haberer, G., Ferreira, F.J., Deruère, J., Mason, M.G., Schaller, G.E., Alonso,
1775 J.M., Ecker, J.R., and Kieber, J.J. (2004). Type-A Arabidopsis response regulators are
1776 partially redundant negative regulators of cytokinin signaling. Plant Cell *16*, 658–671.
1777 10.1105/tpc.018978.
1778 82. Kiba, T., Yamada, H., Sato, S., Kato, T., Tabata, S., Yamashino, T., and Mizuno, T.
1779 (2003). The type-A response regulator, ARR15, acts as a negative regulator in the
1780 cytokinin-mediated signal transduction in *Arabidopsis thaliana*. Plant Cell Physiol. *44*,
1781 868–874. 10.1093/pcp/pcg108.
1782 83. To, J.P.C., Deruère, J., Maxwell, B.B., Morris, V.F., Hutchison, C.E., Ferreira, F.J.,
1783 Schaller, G.E., and Kieber, J.J. (2007). Cytokinin regulates type-A Arabidopsis response
1784 regulator activity and protein stability via two-component phosphorelay. Plant Cell *19*,
1785 3901–3914. 10.1105/tpc.107.052662.
1786 84. Acheampong, A.K., Shanks, C., Cheng, C.Y., Eric Schaller, G., Dagdas, Y., and Kieber,
1787 J.J. (2020). EXO70D isoforms mediate selective autophagic degradation of type-A ARR
1788 proteins to regulate cytokinin sensitivity. Proc. Natl. Acad. Sci. U. S. A. *117*, 27034–
1789 27043. 10.1073/pnas.2013161117.
1790 85. Bothma, J.P., Norstad, M.R., Alamos, S., and Garcia, H.G. (2018). LlamaTags: A

1791 Versatile Tool to Image Transcription Factor Dynamics in Live Embryos. Cell *173*, 1810-
1792 1822.e16. 10.1016/j.cell.2018.03.069.
1793 86. Imamura, A., Yoshino, Y., and Mizuno, T. (2001). Cellular Localization of the Signaling
1794 Components of Arabidopsis His-to-Asp Phosphorelay. Biosci. Biotechnol. Biochem. *65*,
1795 2113–2117. 10.1271/bbb.65.2113.
1796 87. Lee, D.J., Kim, S., Ha, Y.M., and Kim, J. (2008). Phosphorylation of Arabidopsis
1797 response regulator 7 (ARR7) at the putative phospho-accepting site is required for ARR7
1798 to act as a negative regulator of cytokinin signaling. Planta *227*, 577–587.
1799 10.1007/s00425-007-0640-x.
1800 88. Buechel, S., Leibfried, A., To, J.P.C., Zhao, Z., Andersen, S.U., Kieber, J.J., and
1801 Lohmann, J.U. (2010). Role of A-type Arabidopsis Response Regulators in meristem
1802 maintenance and regeneration. Eur. J. Cell Biol. *89*, 279–284.
1803 10.1016/j.ejcb.2009.11.016.
1804 89. Xie, M., Chen, H., Huang, L., O'Neil, R.C., Shokhirev, M.N., and Ecker, J.R. (2018). A B-
1805 ARR-mediated cytokinin transcriptional network directs hormone cross-regulation and
1806 shoot development. Nat. Commun. *9*, 1604. 10.1038/s41467-018-03921-6.
1807 90. Abel, S., Nguyen, M.D., and Theologis, A. (1995). The *PS-IAA4/5-like* Family of Early
1808 Auxin-inducible mRNAs in *Arabidopsis thaliana*. J. Mol. Biol. *251*, 533–549.
1809 10.1006/jmbi.1995.0454.
1810 91. Park, J.Y., Kim, H.J., and Kim, J. (2002). Mutation in domain II of IAA1 confers diverse
1811 auxin-related phenotypes and represses auxin-activated expression of Aux/IAA genes in
1812 steroid regulator-inducible system. Plant J. *32*, 669–683. 10.1046/j.1365-
1813 313X.2002.01459.x.
1814 92. Abel, S., Oeller, P.W., and Theologis, A. (1994). Early auxin-induced genes encode
1815 short-lived nuclear proteins. Proc. Natl. Acad. Sci. U. S. A. *91*, 326–330.
1816 10.1073/pnas.91.1.326.
1817 93. Zenser, N., Ellsmore, A., Leasure, C., and Callis, J. (2001). Auxin modulates the
1818 degradation rate of Aux/IAA proteins. Proc. Natl. Acad. Sci. U. S. A. *98*, 11795–11800.
1819 10.1073/pnas.211312798.
1820 94. Worley, C.K., Zenser, N., Ramos, J., Rouse, D., Leyser, O., Theologis, A., and Callis, J.
1821 (2000). Degradation of Aux/IAA proteins is essential for normal auxin signalling. Plant J.
1822 *21*, 553–562. 10.1046/j.1365-313X.2000.00703.x.
1823 95. Ramos, J.A., Zenser, N., Leyser, O., and Callis, J. (2001). Rapid degradation of
1824 auxin/indoleacetic acid proteins requires conserved amino acids of domain II and is
1825 proteasome dependent. Plant Cell *13*, 2349–2360. 10.1105/tpc.13.10.2349.
1826 96. Figueiredo, M.R.A. de, and Strader, L.C. (2022). Intrinsic and extrinsic regulators of
1827 Aux/IAA protein degradation dynamics. Trends Biochem. Sci. *47*, 865–874.
1828 10.1016/j.tibs.2022.06.004.
1829 97. Liao, C.Y., Smet, W., Brunoud, G., Yoshida, S., Vernoux, T., and Weijers, D. (2015).
1830 Reporters for sensitive and quantitative measurement of auxin response. Nat. Methods
1831 *12*, 207–210. 10.1038/nmeth.3279.
1832 98. Mills, E.W., and Green, R. (2017). Ribosomopathies: There's strength in numbers.
1833 Science *358*, eaan2755. 10.1126/science.aan2755.
1834 99. Warren, A.J. (2018). Molecular basis of the human ribosomopathy Shwachman-Diamond
1835 syndrome. Adv. Biol. Regul. *67*, 109–127. 10.1016/j.jbior.2017.09.002.
1836 100. Hawer, H., Mendelsohn, B.A., Mayer, K., Kung, A., Malhotra, A., Tuupanen, S., Schleit,
1837 J., Brinkmann, U., and Schaffrath, R. (2020). Diphthamide-deficiency syndrome: a novel
1838 human developmental disorder and ribosomopathy. Eur. J. Hum. Genet. *28*, 1497–1508.
1839 10.1038/s41431-020-0668-y.
1840 101. Armistead, J., Patel, N., Wu, X., Hemming, R., Chowdhury, B., Basra, G.S., Del Bigio,
1841 M.R., Ding, H., and Triggs-Raine, B. (2015). Growth arrest in the ribosomopathy, bowen-

1842 conradi syndrome, is due to dramatically reduced cell proliferation and a defect in mitotic
1843 progression. Biochim. Biophys. Acta - Mol. Basis Dis. *1852*, 1029–1037.
1844 10.1016/j.bbadis.2015.02.007.
1845 102. Zhou, C., Zang, D., Jin, Y., Wu, H., Liu, Z., Du, J., and Zhang, J. (2011). Mutation in
1846 ribosomal protein L21 underlies hereditary hypotrichosis simplex. Hum. Mutat. *32*, 710–
1847 714. 10.1002/humu.21503.
1848 103. Dixon, M.J. (1995). Treacher Collins syndrome. J. Med. Genet. *32*, 806–808.
1849 10.1136/jmg.32.10.806.
1850 104. Gazda, H.T., Sheen, M.R., Vlachos, A., Choesmel, V., O'Donohue, M.F., Schneider, H.,
1851 Darras, N., Hasman, C., Sieff, C.A., Newburger, P.E., et al. (2008). Ribosomal Protein L5
1852 and L11 Mutations Are Associated with Cleft Palate and Abnormal Thumbs in Diamond-
1853 Blackfan Anemia Patients. Am. J. Hum. Genet. *83*, 769–780. 10.1016/j.ajhg.2008.11.004.
1854 105. Oliver, E.R., Saunders, T.L., Tarlé, S.A., and Glaser, T. (2004). Ribosomal protein L24
1855 defect in belly spot and tail (*Bst*), a mouse *Minute*. Development *131*, 3907–3920.
1856 10.1242/dev.01268.
1857 106. McGowan, K.A., Li, J.Z., Park, C.Y., Beaudry, V., Tabor, H.K., Sabnis, A.J., Zhang, W.,
1858 Fuchs, H., De Angelis, M.H., Myers, R.M., et al. (2008). Ribosomal mutations cause p53-
1859 mediated dark skin and pleiotropic effects. Nat. Genet. *40*, 963–970. 10.1038/ng.188.
1860 107. Oristian, D.S., Slooíman, L.G., Zhou, X., Wang, L., Farach-Carson, M.C., and Kirn-
1861 Safran, C.B. (2009). Ribosomal protein L29/HIP deficiency delays osteogenesis and
1862 increases fragility of adult bone in mice. J. Orthop. Res. *27*, 28–35. 10.1002/jor.20706.
1863 108. Uechi, T., Nakajima, Y., Nakao, A., Torihara, H., Chakraborty, A., Inoue, K., and
1864 Kenmochi, N. (2006). Ribosomal protein gene knockdown causes developmental defects
1865 in zebrafish. PLoS One *1*, e37. 10.1371/journal.pone.0000037.
1866 109. Marygold, S.J., Coelho, C.M.A., and Leevers, S.J. (2005). Genetic analysis of RpL38 and
1867 RpL5, two minute genes located in the centric heterochromatin of chromosome 2 of
1868 *Drosophila melanogaster*. Genetics *169*, 683–695. 10.1534/genetics.104.034124.
1869 110. Lee, C.C., Tsai, Y.T., Kao, C.W., Lee, L.W., Lai, H.J., Ma, T.H., Chang, Y.S., Yeh, N.H.,
1870 and Lo, S.J. (2014). Mutation of a Nopp140 gene *dao-5* alters rDNA transcription and
1871 increases germ cell apoptosis in *C. elegans*. Cell Death Dis. *5*, e1158.
1872 10.1038/cddis.2014.114.
1873 111. Ito, T., Kim, G.T., and Shinozaki, K. (2000). Disruption of an Arabidopsis cytoplasmic
1874 ribosomal protein S13-homologous gene by transposon-mediated mutagenesis causes
1875 aberrant growth and development. Plant J. *22*, 257–264. 10.1046/j.1365-
1876 313X.2000.00728.x.
1877 112. Horiguchi, G., Mollá-Morales, A., Pérez-Pérez, J.M., Kojima, K., Robles, P., Ponce, M.R.,
1878 Micol, J.L., and Tsukaya, H. (2011). Differential contributions of ribosomal protein genes
1879 to *Arabidopsis thaliana* leaf development. Plant J. *65*, 724–736. 10.1111/j.1365-
1880 313X.2010.04457.x.
1881 113. Zhao, H., Lü, S., Li, R., Chen, T., Zhang, H., Cui, P., Ding, F., Liu, P., Wang, G., Xia, Y.,
1882 et al. (2015). The Arabidopsis gene *DIG6* encodes a large 60S subunit nuclear export
1883 GTPase 1 that is involved in ribosome biogenesis and affects multiple auxin-regulated
1884 development processes. J. Exp. Bot. *66*, 6863–6875. 10.1093/jxb/erv391.
1885 114. Takagi, M., Absalon, M.J., McLure, K.G., and Kastan, M.B. (2005). Regulation of p53
1886 translation and induction after DNA damage by ribosomal protein L26 and nucleolin. Cell
1887 *123*, 49–63. 10.1016/j.cell.2005.07.034.
1888 115. Deisenroth, C., and Zhang, Y. (2010). Ribosome biogenesis surveillance: Probing the
1889 ribosomal protein-Mdm2-p53 pathway. Oncogene *29*, 4253–4260.
1890 10.1038/onc.2010.189.
1891 116. Warner, J.R., and McIntosh, K.B. (2009). How Common Are Extraribosomal Functions of
1892 Ribosomal Proteins? Mol. Cell *34*, 3–11. 10.1016/j.molcel.2009.03.006.

1893 117. Dutt, S., Narla, A., Lin, K., Mullally, A., Abayasekara, N., Megerdichian, C., Wilson, F.H.,
1894 Currie, T., Khanna-Gupta, A., Berliner, N., et al. (2011). Haploinsufficiency for ribosomal
1895 protein genes causes selective activation of p53 in human erythroid progenitor cells.
1896 Blood *117*, 2567–2576. 10.1182/blood-2010-07-295238.
1897 118. Danilova, N., Sakamoto, K.M., and Lin, S. (2008). Ribosomal protein S19 deficiency in
1898 zebrafish leads to developmental abnormalities and defective erythropoiesis through
1899 activation of p53 protein family. Blood *112*, 5228–5237. 10.1182/blood-2008-01-132290.
1900 119. Girardi, T., Vereecke, S., Sulima, S.O., Khan, Y., Fancello, L., Briggs, J.W., Schwab, C.,
1901 De Beeck, J.O., Verbeeck, J., Royaert, J., et al. (2018). The T-cell leukemia-associated
1902 ribosomal RPL10 R98S mutation enhances JAK-STAT signaling. Leukemia *32*, 809–819.
1903 10.1038/leu.2017.225.
1904 120. Ludwig, L.S., Gazda, H.T., Eng, J.C., Eichhorn, S.W., Thiru, P., Ghazvinian, R., George,
1905 T.I., Gotlib, J.R., Beggs, A.H., Sieff, C.A., et al. (2014). Altered translation of GATA1 in
1906 Diamond-Blackfan anemia. Nat. Med. *20*, 748–753. 10.1038/nm.3557.
1907 121. Khajuria, R.K., Munschauer, M., Ulirsch, J.C., Fiorini, C., Ludwig, L.S., McFarland, S.K.,
1908 Abdulhay, N.J., Specht, H., Keshishian, H., Mani, D.R., et al. (2018). Ribosome Levels
1909 Selectively Regulate Translation and Lineage Commitment in Human Hematopoiesis.
1910 Cell *173*, 90-103.e19. 10.1016/j.cell.2018.02.036.
1911 122. In, K., Zaini, M.A., Müller, C., Warren, A.J., Von Lindern, M., and Calkhoven, C.F. (2016).
1912 Shwachman-Bodian-Diamond syndrome (SBDS) protein deficiency impairs translation re-
1913 initiation from C/EBPα and C/EBPβ mRNAs. Nucleic Acids Res. *44*, 4134–4146.
1914 10.1093/nar/gkw005.
1915 123. Kondrashov, N., Pusic, A., Stumpf, C.R., Shimizu, K., Hsieh, A.C., Xue, S., Ishijima, J.,
1916 Shiroishi, T., and Barna, M. (2011). Ribosome-mediated specificity in Hox mRNA
1917 translation and vertebrate tissue patterning. Cell *145*, 383–397.
1918 10.1016/j.cell.2011.03.028.
1919 124. Deliu, L.P., Turingan, M., Jadir, D., Lee, B., Ghosh, A., and Grewal, S.S. (2022).
1920 Serotonergic neuron ribosomal proteins regulate the neuroendocrine control of
1921 Drosophila development. PLoS Genet. *18*, e1010371. 10.1371/journal.pgen.1010371.
1922 125. Adams, K.W., and Cooper, G.M. (2007). Rapid turnover of Mcl-1 couples translation to
1923 cell survival and apoptosis. J. Biol. Chem. *282*, 6192–6200. 10.1074/jbc.M610643200.
1924 126. Truckenbrodt, S., Viplav, A., Jähne, S., Vogts, A., Denker, A., Wildhagen, H., Fornasiero,
1925 E.F., and Rizzoli, S.O. (2018). Newly produced synaptic vesicle proteins are preferentially
1926 used in synaptic transmission. EMBO J. *37*, e98044. 10.15252/embj.201798044.
1927 127. Mähönen, A.P., Bonke, M., Kauppinen, L., Riikonen, M., Benfey, P.N., and Helariutta, Y.
1928 (2000). A novel two-component hybrid molecule regulates vascular morphogenesis of the
1929 Arabidopsis root. Genes Dev. *14*, 2938–2943. 10.1101/gad.189200.
1930 128. Sotta, N., Shantikumar, L., Sakamoto, T., Matsunaga, S., and Fujiwara, T. (2016). TPR5
1931 is involved in directional cell division and is essential for the maintenance of meristem cell
1932 organization in *Arabidopsis thaliana*. J. Exp. Bot. *67*, 2401–2411. 10.1093/jxb/erw043.
1933 129. Heisler, M.G., Ohno, C., Das, P., Sieber, P., Reddy, G. V., Long, J.A., and Meyerowitz,
1934 E.M. (2005). Patterns of auxin transport and gene expression during primordium
1935 development revealed by live imaging of the Arabidopsis inflorescence meristem. Curr.
1936 Biol. *15*, 1899–1911. 10.1016/j.cub.2005.09.052.
1937 130. Müller, B., and Sheen, J. (2008). Cytokinin and auxin interaction in root stem-cell
1938 specification during early embryogenesis. Nature *453*, 1094–1097. 10.1038/nature06943.
1939 131. Brackmann, K., Qi, J., Gebert, M., Jouannet, V., Schlamp, T., Grünwald, K., Wallner,
1940 E.S., Novikova, D.D., Levitsky, V.G., Agustí, J., et al. (2018). Spatial specificity of auxin
1941 responses coordinates wood formation. Nat. Commun. *9*, 875. 10.1038/s41467-018-
1942 03256-2.
1943 132. Argyros, R.D., Mathews, D.E., Chiang, Y.H., Palmer, C.M., Thibault, D.M., Etheridge, N.,

Argyros, D.A., Mason, M.G., Kieber, J.J., and Schallera, G.E. (2008). Type B response regulators of Arabidopsis play key roles in cytokinin signaling and plant development. Plant Cell *20*, 2102–2116. 10.1105/tpc.108.059584.

133. Rademacher, E.H., Möller, B., Lokerse, A.S., Llavata-Peris, C.I., Van Den Berg, W., and Weijers, D. (2011). A cellular expression map of the *Arabidopsis AUXIN RESPONSE FACTOR* gene family. Plant J. *68*, 597–606. 10.1111/j.1365-313X.2011.04710.x.

134. Saerens, D., Pellis, M., Loris, R., Pardon, E., Dumoulin, M., Matagne, A., Wyns, L., Muyldermans, S., and Conrath, K. (2005). Identification of a universal VHH framework to graft non-canonical antigen-binding loops of camel single-domain antibodies. J. Mol. Biol. *352*, 597–607. 10.1016/j.jmb.2005.07.038.

135. Fujii, Y., and Kodama, Y. (2015). *In planta* comparative analysis of improved green fluorescent proteins with reference to fluorescence intensity and bimolecular fluorescence complementation ability. Plant Biotechnol. *32*, 81–87. 10.5511/plantbiotechnology.15.0120a.

136. Alamos, S., Reimer, A., Niyogi, K.K., and Garcia, H.G. (2021). Quantitative imaging of RNA polymerase II activity in plants reveals the single-cell basis of tissue-wide transcriptional dynamics. Nat. Plants *7*, 1037–1049. 10.1038/s41477-021-00976-0.

137. Alexa, A., Rahnenführer, J., and Lengauer, T. (2006). Improved scoring of functional groups from gene expression data by decorrelating GO graph structure. Bioinformatics *22*, 1600–1607. 10.1093/bioinformatics/btl140.

138. Mustroph, A., Juntawong, P., and Bailey-Serres, J. (2009). Isolation of Plant Polysomal mRNA by Differential Centrifugation and Ribosome Immunopurification Methods. In Methods in molecular biology (vol. 553) (Humana Press, a part of Springer Science+Business Media, LLC), pp. 109–126. 10.1007/978-1-60327-563-7_6.

139. Gao, X., Wan, J., Liu, B., Ma, M., Shen, B., and Qian, S.B. (2015). Quantitative profiling of initiating ribosomes *in vivo*. Nat. Methods *12*, 147–153. 10.1038/nmeth.3208.

140. Busche, M., Regina Scarpin, M., Hnasko, R., and Brunkard, J.O. (2021). TOR coordinates nucleotide availability with ribosome biogenesis in plants. Plant Cell *33*, 1615–1632. 10.1093/plcell/koab043.

141. Schindelin, J., Rueden, C.T., Hiner, M.C., and Eliceiri, K.W. (2015). The ImageJ ecosystem: An open platform for biomedical image analysis. Mol. Reprod. Dev. *82*, 518–529. 10.1002/mrd.22489.

142. Schindelin, J., Arganda-Carreras, I., Frise, E., Kaynig, V., Longair, M., Pietzsch, T., Preibisch, S., Rueden, C., Saalfeld, S., Schmid, B., et al. (2012). Fiji: An open-source platform for biological-image analysis. Nat. Methods *9*, 676–682. 10.1038/nmeth.2019.

143. de Reuille, P.B., Routier-Kierzkowska, A.L., Kierzkowski, D., Bassel, G.W., Schüpbach, T., Tauriello, G., Bajpai, N., Strauss, S., Weber, A., Kiss, A., et al. (2015). MorphoGraphX: A platform for quantifying morphogenesis in 4D. eLife *4*, 1–20. 10.7554/eLife.05864.

144. Schäfer, M., Brütting, C., Baldwin, I.T., and Kallenbach, M. (2016). High-throughput quantification of more than 100 primary- and secondary-metabolites, and phytohormones by a single solid-phase extraction based sample preparation with analysis by UHPLC-HESI-MS/MS. Plant Methods *12*, 30. 10.1186/s13007-016-0130-x.

145. Kojima, M., Kamada-Nobusada, T., Komatsu, H., Takei, K., Kuroha, T., Mizutani, M., Ashikari, M., Ueguchi-Tanaka, M., Matsuoka, M., Suzuki, K., et al. (2009). Highly sensitive and high-throughput analysis of plant hormones using ms-probe modification and liquid chromatographytandem mass spectrometry: An application for hormone profiling in oryza sativa. Plant Cell Physiol. *50*, 1201–1214. 10.1093/pcp/pcp057.

146. Novák, O., Antoniadi, I., and Ljung, K. (2017). High-resolution cell-type specific analysis of cytokinins in sorted root cell populations of *Arabidopsis thaliana*. Methods Mol. Biol. *1497*, 231–248. 10.1007/978-1-4939-6469-7_1.

147. R Core Team (2021). R: A language and environment for statistical computing. R Foundation for Statistical Computing, Vienna, Austria. URL https://www.R-project.org/.
148. Wickham, H. (2009). ggplot2: Elegant Graphics for Data Analysis R. Gentleman, K. Hornik, and G. Parmigiani, eds. (Springer) 10.1007/978-0-387-98141-3.

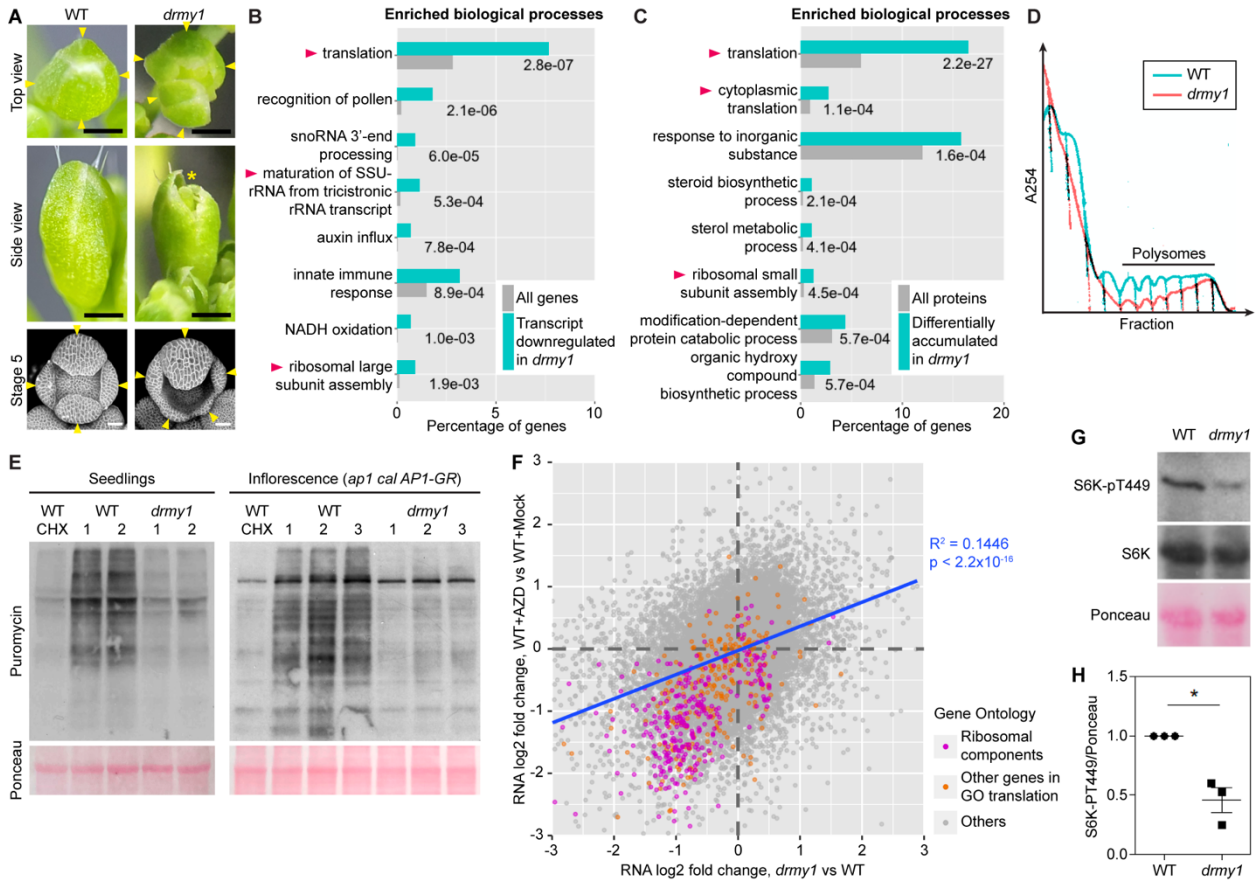

Figure 1. *drmy1* has reduced ribosome abundance, translation rate, and TOR activity.
(A) Top row, stage 12 buds of WT (left) and *drmy1* (right) viewed from the top. Arrowheads point to sepals. Note that the *drmy1* bud has 5 sepals of unequal size and unevenly spaced, exposing the stamens and carpels. Middle row, stage 12 buds of WT (left) and *drmy1* (right) viewed from the side. Asterisk shows the gap between sepals with petals and carpels exposed. Bottom row, stage 5 buds of WT (left) and *drmy1* (right) containing *35S::mCitrine-RCI2A* (plasma membrane marker). Arrowheads point to sepal primordia. Note that the *drmy1* bud has 5 sepal primordia of different sizes. Scale bars are 0.5 mm for stage 12 bud images and 25 µm for stage 5 bud images.
(B-C) Gene ontology (GO) enrichment of downregulated genes **(B)** and differentially accumulated proteins **(C)** in *drmy1* compared to WT, in the *ap1 cal AP1-GR* background. Shown are the top 8 GO terms and their enrichment p-values. A complete list can be found in Supplemental Dataset 1. Arrowheads highlight terms related to ribosome biogenesis or translation.
(D) Ribosome profiles of WT (blue) and *drmy1* (red) in the *ap1 cal AP1-GR* background, representative of 3 biological replicates each. Polysomal peaks are highlighted. All replicates can be found in Supplemental Dataset 2.
(E) Puromycin labeling of WT vs *drmy1*. Left, puromycin labeling in WT and *drmy1* seedlings. From left to right: WT pre-treated with CHX, two biological replicates of WT pre-treated with mock, and two biological replicates of *drmy1* pre-treated with mock. All groups were then treated with puromycin. For seedlings to match in size, WT seedlings were 8 days old and *drmy1* seedlings were 10 days old. Right, puromycin labeling in WT and *drmy1* inflorescences of induced *ap1 cal*

AP1-GR background. From left to right: WT co-treated with puromycin and CHX, three biological replicates of WT treated with puromycin, and three biological replicates of *drmy1* treated with puromycin. In both experiments, RuBisCO large subunit on Ponceau S-stained membrane is shown as a loading control (bottom).

(F) Coherent alteration of gene expression by *drmy1* and AZD-8055 TOR inhibitor treatment. Shown here is a scatterplot of RNA log 2 fold change in *drmy1* vs WT (x-axis), and WT+AZD vs WT+Mock (y-axis), in 7-day-old seedlings. Genes are color-coded based on the following categories: genes in "Structural constituents of the ribosome" (GO:0003735) and its offspring terms (magenta); all other genes in "Translation" (GO:0006412) and its offspring terms (orange); all other genes (gray). Blue line shows a linear regression of all points ($R^2 = 0.1446$, $p < 2.2x10^{-16}$). Note that the axes were trimmed to (-3,3) for ease of display.

(G-H) Phosphorylation of the direct TOR substrate, S6K-pT449, in WT and *drmy1*. Representative images are shown in **(G)**. Top, Western blot against S6K-pT449. Middle, Western blot against total S6K protein. Bottom, Ponceau S staining as a loading control. **(H)** Quantification of the intensity of S6K-pT449 over Ponceau normalized by WT, in three experiments, shows that TOR activity decreased by half in *drmy1*. (mean ± SD; *, $p<0.05$).

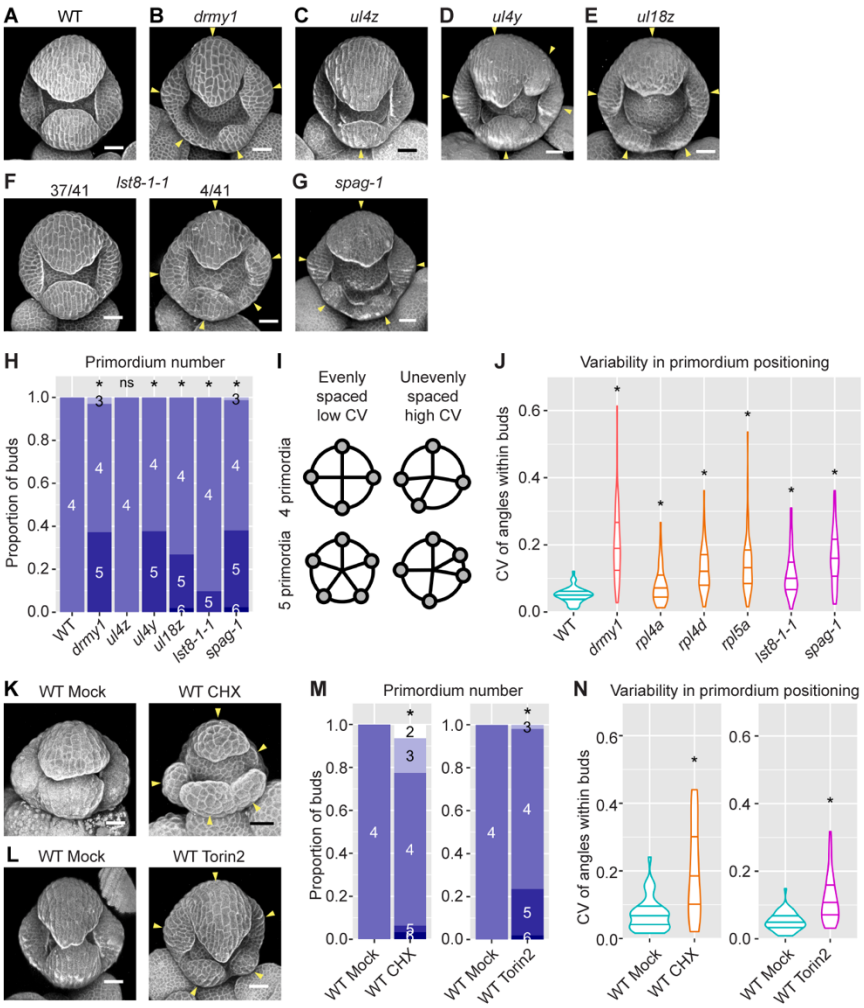

Figure 2. Defects in TOR activity, ribosome integrity, and translation cause variable sepal initiation.

(A-G) Representative images of stage 5 buds in WT (A), *drmy1* (B), *ul4z* (C), *ul4y* (D), *ul18z* (E), *lst8-1-1* (F), and *spaghetti-1* (G). Tissue morphology is visualized by either propidium iodide (a cell wall-staining dye) or a plasma membrane marker. Arrowheads indicate sepal primordia that are variable in number, position, and size. Note that *ul4z* flowers always develop four sepal primordia, although of different sizes; *lst8-1-1* occasionally (4/41, 9.8%) develops buds with more than four sepal primordia. Scale bars, 25 µm.

(H) Quantification of sepal primordium number, comparing *drmy1* (n = 67 buds), *ul4z* (n = 52 buds), *ul4y* (n = 53 buds), *ul18z* (n = 52 buds), *lst8-1-1* (n = 41 buds), and *spaghetti-1* (n = 84 buds) with WT (n = 51 buds). Asterisks indicate statistically significant ($p < 0.05$) differences from WT in Fisher's contingency table tests.

(I) Illustration of robust versus variable positioning of sepal primordia. Primordia are considered robustly positioned if they are evenly distributed around the edge of the bud. Within each bud, angles between adjacent primordia with respect to the center of the bud are measured, and coefficient of variation (CV) is calculated. A bud with robustly positioned primordia would have

similar angular values and a low CV value. A bud with variably positioned primordia would have very different angular values and a high CV value.

(J) Quantification of variability in primordium positioning (CV) in the same buds as in (H), following illustration in (I). Asterisks indicate statistically significant ($p < 0.05$) differences from WT in Wilcoxon's rank sum tests.

(K) Representative images of buds from *in vitro*-cultured WT inflorescences treated with mock or 2 μM CHX for 9-10 days (see Material and Methods). Arrowheads indicate sepal primordia that are variable in number, position, and size. Scale bars, 25 μm.

(L) Representative images of buds from WT plants treated with mock or 2 nmol Torin2 for 15 days (see Material and Methods). Arrowheads indicate sepal primordia that are variable in number, position, and size. Scale bars, 25 μm.

(M-N) Quantification of variability in primordium number (M) and positional variability (N) similar to (H,J), comparing CHX-treated (n = 31 buds), CHX-mock (n = 42 buds), Torin2-treated (n = 51 buds) and Torin2-mock buds (n = 56 buds).

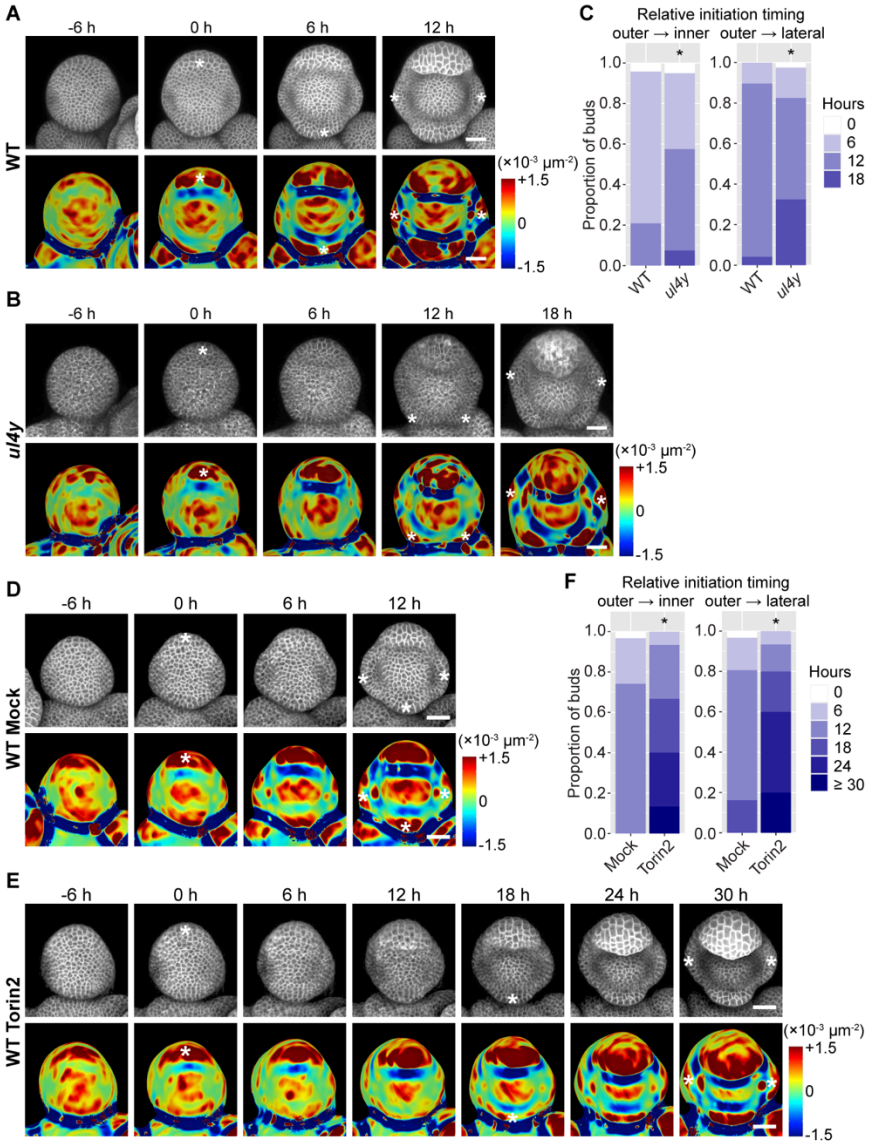

Figure 3. TOR and ribosomal defects cause variability in the timing of sepal initiation.

(A-C) 6h-interval live imaging of the sepal initiation process in WT (A) and *ul4y* (B), which is quantified in (C). n = 48 buds for WT; n = 40 buds for *ul4y*.

(D-F) 6h-interval live imaging of the sepal initiation process in buds from WT plants treated with mock or 2 nmol Torin2 bi-daily for 15 days, which is quantified in (F). n = 31 buds for mock; n = 15 buds for Torin2.

In **(A,B,D,E)**, top rows show the *35S::mCitrine-RCI2A* membrane marker, and bottom rows show Gaussian curvature heatmaps calculated from the same image stacks. Asterisks indicate sepal initiation events, defined as a dark red band (primordium with positive curvature) separated from the floral meristem by a dark blue band (boundary with negative curvature) in the Gaussian curvature heatmap. Scale bars, 25 µm.

In **(C,F)**, the amount of time between outer and inner sepal initiation (left) and between outer and lateral sepal initiation (right) were calculated for each bud, and summarized over all the buds.

Asterisks indicate statistically significant ($p < 0.05$) differences in the distribution of relative initiation timing in Fisher's contingency table tests.

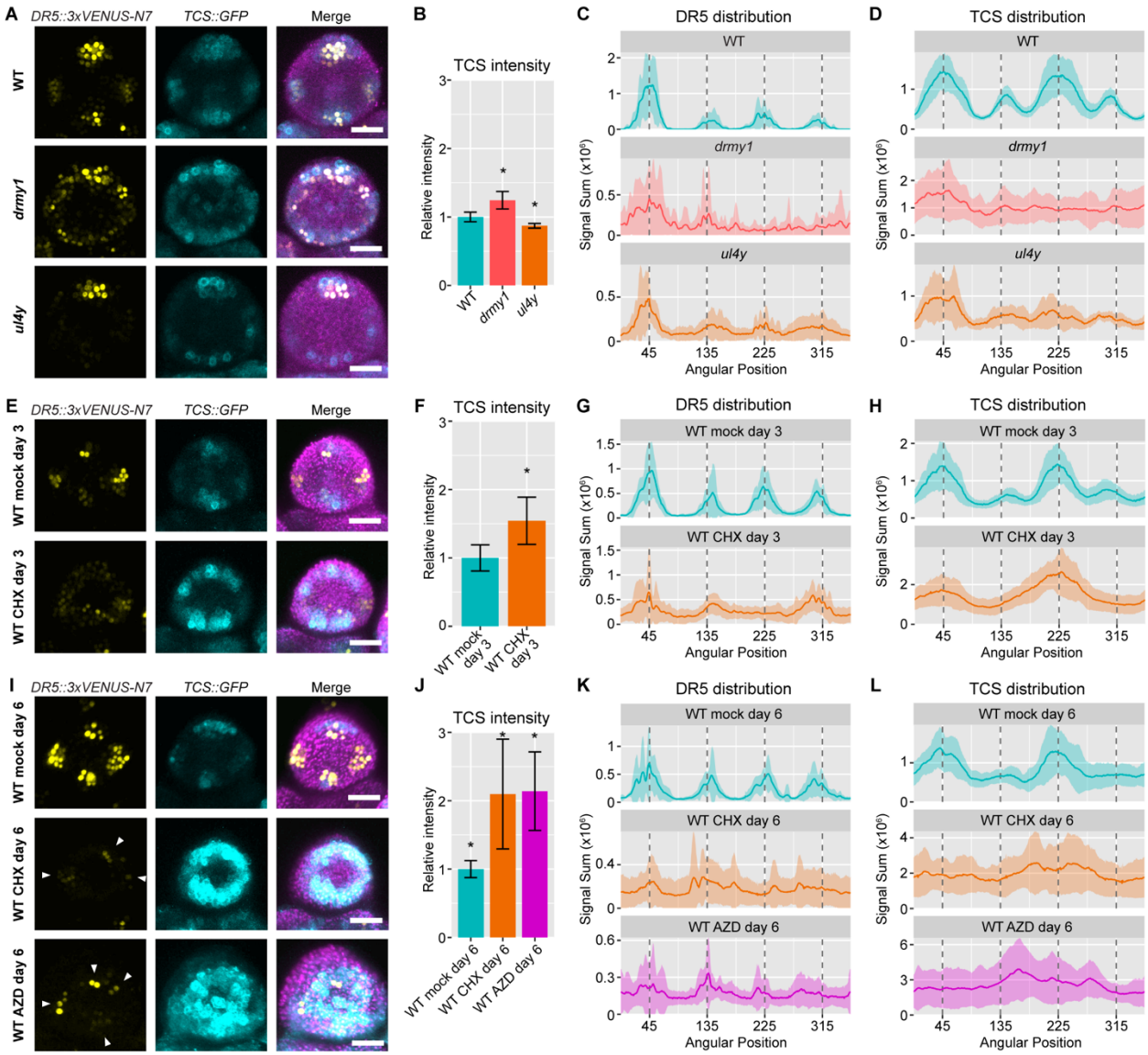

Figure 4. Defects in TOR activity, ribosome integrity, and translation cause variability in auxin and cytokinin signaling.

(A-D) The ribosomal mutant *ul4y* loses robustness in auxin and cytokinin signaling. (A) Representative images of late stage 2 buds of WT, *drmy1*, and *ul4y*, showing the auxin signaling reporter *DR5::3xVENUS-N7* in yellow, the cytokinin signaling reporter *TCS::GFP* in cyan, and both merged with Chlorophyll (in WT) or *UBQ10::mCherry-RCI2A* (in *drmy1* and *ul4y*) in magenta. (B) Quantification of TCS intensity (integrated density divided by area) from maximum intensity projection images, normalized to mean of WT. Shown are mean ± SD. Asterisks show statistically significant differences from WT in two-tailed Student's t-tests (*drmy1*, $p = 2.1 \times 10^{-6}$; *ul4y*, $p = 3.4 \times 10^{-5}$). (C) Circular histogram of DR5 distribution around the bud. Each bud was divided into 360 sectors of 1° each. Within each sector, DR5 signal measured in pixel intensity units (0-255 range) was summed. This sum was plotted along the x-axis starting from the sector at 1:30 position (between the incipient outer sepal and incipient lateral sepal on the right) going

counterclockwise. I.e. in WT, the outer sepal is near 45°, the inner sepal near 225°, and the lateral sepals near 45° and 135° (vertical dotted lines). The mean was plotted as a solid line, and mean ± SD was plotted as a shaded area. (D) Circular histogram of TCS distribution around the bud. Sample size for (A-D): WT, n = 12 buds; *drmy1*, n = 15 buds; *ul4y*, n = 10 buds.

(E-H) 3 days of translation inhibition causes increased and diffuse cytokinin signaling, and diffuse auxin signaling. (E) Representative images of late stage 2 buds from dissected and cultured WT inflorescences treated with mock or 2 µM CHX for 3 days. Shown are *DR5::3xVENUS-N7* in yellow, *TCS::GFP* in cyan, and both merged with Chlorophyll in magenta. (F) Quantification of TCS intensity from maximum intensity projection images, normalized to mean of WT mock day 3. Shown are mean ± SD. Asterisk shows statistically significant difference in a two-tailed Student's t-test ($p = 2.0x10^{-4}$). (G) Circular histogram of DR5 distribution around the bud. (H) Circular histogram of TCS distribution around the bud. Sample size for (E-H): WT mock day 3, n = 10 buds; WT CHX day 3, n = 12 buds.

(I-L) 6 days of TOR or translation inhibition causes increased and diffuse cytokinin signaling, and randomly positioned auxin signaling maxima. (I) Representative images of late stage 2 buds from dissected and cultured WT inflorescences treated with mock, 2 µM CHX, or 2 µM AZD for 6 days. Shown are *DR5::3xVENUS-N7* in yellow, *TCS::GFP* in cyan, and both merged with Chlorophyll in magenta. Arrowheads point to randomly positioned auxin maxima in buds of the CHX or AZD group. (J) Quantification of TCS intensity from maximum intensity projection images, normalized to mean of WT mock day 6. Shown are mean ± SD. Asterisks show statistically significant differences from mock in two-tailed Student's t-tests (CHX, $p = 1.0x10^{-3}$; AZD, $p = 1.2x10^{-4}$). (K) Circular histogram of DR5 distribution around the bud. (L) Circular histogram of TCS distribution around the bud. Sample size for (I-L): WT mock day 6, n = 12 buds; WT CHX day 6, n = 11 buds; WT AZD day 6, n = 10 buds. Scale bars in (A,E,I) represent 25 µm.

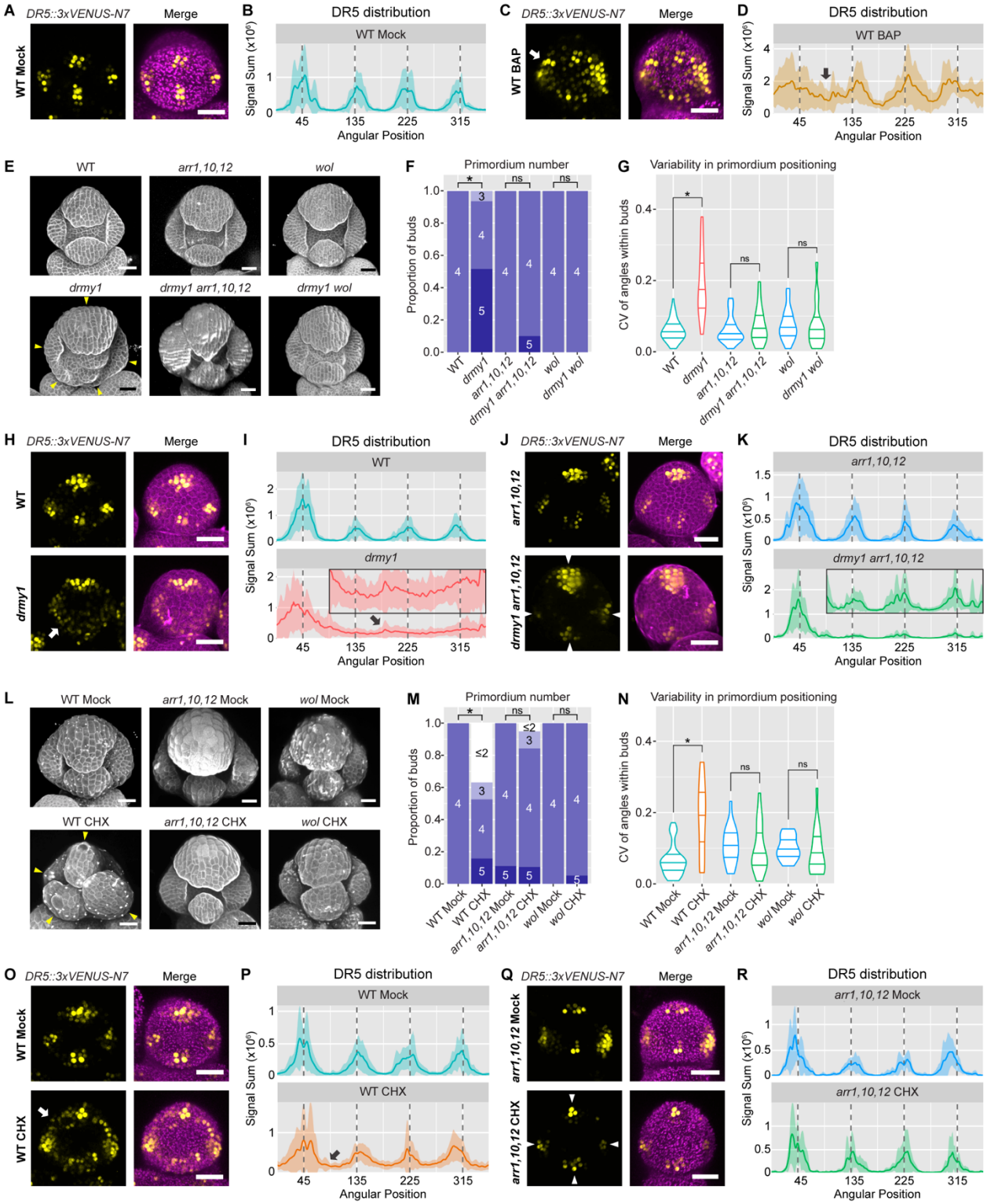

Figure 5. Cytokinin signaling is required for variability in auxin signaling and sepal initiation under translation inhibition.

(A-D) Cytokinin treatment makes auxin signaling diffuse. Shown are late stage 2 WT buds under mock (A,B) or 5 µM cytokinin (BAP) treatment (C,D) for 4 days. (A,C) Representative images of

the auxin signaling reporter *DR5::3xVENUS-N7* in yellow, and *DR5* merged with Chlorophyll in magenta. (B,D) Circular histograms of the *DR5::3xVENUS-N7* signal, showing mean (solid line) and mean ± SD (shaded area). Arrows point to DR5 signal in variable positions. Sample size: WT Mock n = 10, WT BAP n = 10. Also see Zhu et al. (2020), Extended Data Figure 7e.

(E-G) Cytokinin signaling is required for variable sepal initiation in *drmy1*. (E) Representative images of stage 5 buds in WT, *drmy1*, *arr1,10,12*, *drmy1 arr1,10,12*, *wol*, and *drmy1 wol*. Arrowheads indicate initiated sepal primordia that are variable in number, position, and size. (F,G) Quantification of sepal primordium number (F) and positional variability (G), comparing WT (n = 58) with *drmy1* (n = 31), *arr1,10,12* (n = 24) with *drmy1 arr1,10,12* (n = 20), and *wol* (n = 36) with *drmy1 wol* (n = 39). Asterisks indicate statistically significant ($p < 0.05$) differences in Fisher's contingency table tests (F) and Wilcoxon's rank sum tests (G) respectively. ns indicates no significant difference.

(H-K) Cytokinin signaling is required for variable patterning of auxin signaling in *drmy1*. Shown are late stage 2 buds of WT vs *drmy1* (H,I), and *arr1,10,12* vs *drmy1 arr1,10,12* (J,K). (H,J) Representative images of the auxin signaling reporter *DR5::3xVENUS-N7* in yellow, and *DR5* merged with propidium iodide in magenta. Arrows point to diffuse DR5 signal in variable positions in the *drmy1* bud. Arrowheads show four robust DR5 maxima in *drmy1 arr1,10,12*. (I,K) Circular histograms of the *DR5::3xVENUS-N7* signal, showing mean (solid line) and mean ± SD (shaded area). For ease of visualization, circular histograms of *drmy1* and *drmy1 arr1,10,12* between 90 and 360 degrees are enlarged and shown as insets (y-axis range 0-0.4). Sample size: WT n = 19, *drmy1* n = 16, *arr1,10,12* n = 13, *drmy1 arr1,10,12* n = 9.

(L-N) Cytokinin signaling is required for variable sepal initiation under translation inhibition. (L) Representative images of stage 6 buds in WT, *arr1,10,12*, and *wol*, treated with Mock or 2 μM CHX for 10 days. Arrowheads indicate variable initiation of sepal primordia. (M,N) Quantification of sepal primordium number (M) and positional variability (N), comparing Mock and CHX within each genotype. Sample size: WT Mock n = 29, WT CHX n = 19, *arr1,10,12* Mock n = 18, *arr1,10,12* CHX n = 19, *wol* Mock n = 15, *wol* CHX n = 19. Asterisks indicate statistically significant ($p < 0.05$) differences in Fisher's contingency table tests (M) and Wilcoxon's rank sum tests (N) respectively. ns indicates no significant difference.

(O-R) Cytokinin signaling is required for diffuse auxin signaling under translation inhibition. Shown are late stage 2 buds of WT (O,P) and *arr1,10,12* (Q,R), treated with Mock or 2 μM CHX for 3 days. (O,Q) Representative images of the auxin signaling reporter *DR5::3xVENUS-N7* in yellow, and *DR5* merged with Chlorophyll in magenta. Arrows point to diffuse DR5 signal in variable positions in CHX-treated WT. Arrowheads show four robust DR5 maxima in CHX-treated *arr1,10,12*. (P,R) Circular histograms of the *DR5::3xVENUS-N7* signal, showing mean (solid line) and mean ± SD (shaded area). Sample size: WT Mock n = 17, WT CHX n = 18, *arr1,10,12* Mock n = 7, *arr1,10,12* CHX n = 7. Scale bars in (A,C,E,H,J,L,O,Q) represent 25 μm.

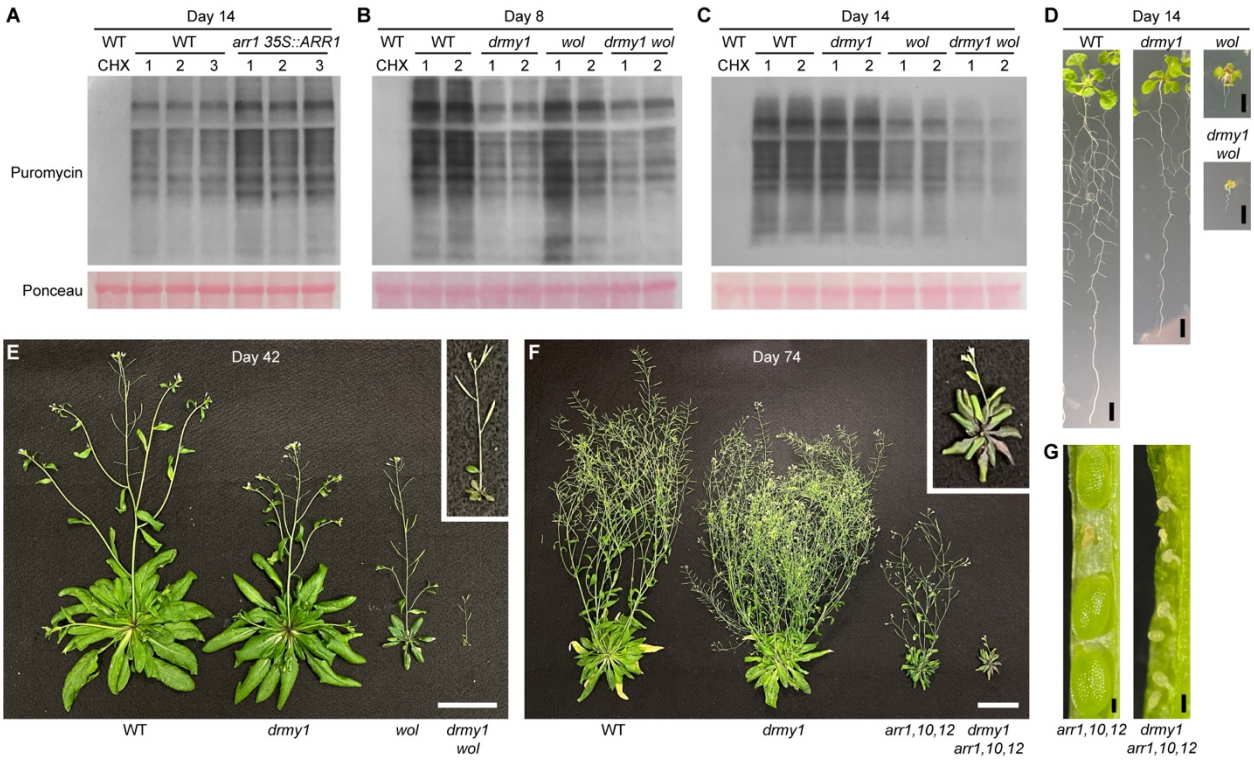

Figure 6. Upregulation of cytokinin signaling is required to maintain translation and fitness in *drmy1*.

(A) Puromycin labeling of WT seedlings with 4 h CHX pre-treatment (control), and three biological replicates each of WT and *arr1 35S::ARR1* seedlings with 4 h mock pre-treatment. All seedlings are 14 days old. RuBisCO large subunit in Ponceau S-stained membrane is shown as a loading control. Also see Karunadasa et al. (2020).

(B,C) Puromycin labeling of WT seedlings with 4 h CHX pre-treatment (control), and two biological replicates of WT, *drmy1*, *wol*, and *drmy1 wol* seedlings with 4 h mock pre-treatment. Seedlings are 8 days old in (B) and 14 days old in (C). RuBisCO large subunit in Ponceau S-stained membrane is shown as a loading control.

(D) Representative 14 days old seedling images of WT, *drmy1*, *wol*, and *drmy1 wol* used in (C). Notice that *drmy1 wol* is very small and pale. Scale bars, 5 mm.

(E) Representative aerial part images of 42 days old plants of WT, *drmy1*, *wol*, and *drmy1 wol*. Inset shows enlarged *drmy1 wol* plant; notice that it has a tiny rosette and inflorescence. Scale bars, 5 cm. See also Supplemental Figure 6F.

(F) Representative aerial part images of 74 days old plants of WT, *drmy1*, *arr1*,*10*,*12*, and *drmy1 arr1*,*10*,*12*. Inset shows enlarged *drmy1 arr1*,*10*,*12* plant; notice its pale leaves accumulating anthocyanin, and short inflorescence. Scale bars, 5 cm. See also Supplemental Figure 6E.

(G) Dissected siliques of *arr1,10,12* (left) and *drmy1 arr1,10,12* (right) showing developing seeds. Notice that while *arr1,10,12* occasionally have aborted seeds, all seeds in the *drmy1 arr1,10,12* silique were aborted. Scale bars, 0.2 mm.

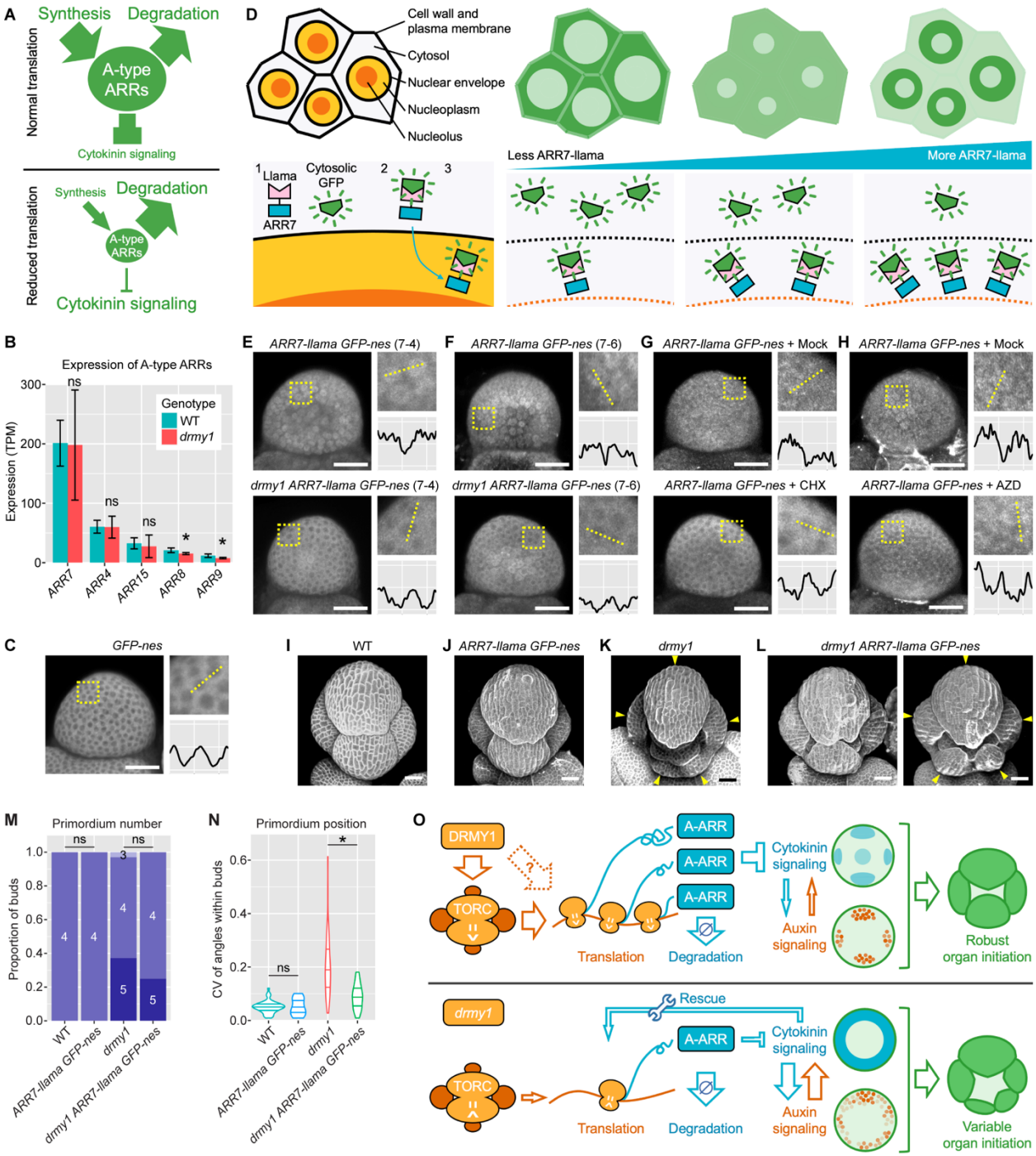

Figure 7. A-type ARR protein levels are sensitive to TOR and translation inhibition.
(A) The hypothesis. A-type ARRs are rapidly synthesized and degraded to dampen cytokinin signaling. Translation inhibition causes inability to rapidly synthesize these proteins in response to cytokinin signaling, resulting in an upregulation of cytokinin signaling.
(B) Expression of A-type ARR genes in WT vs *drmy1* inflorescences (*ap1 cal AP1-GR*) measured in RNA-seq. Shown are the five A-type ARR genes with the highest expression, ranked by mean expression level in WT. Asterisk indicates statistically significant difference, while ns means no

201 significant difference. P-values: ARR7, p = 0.807; ARR4, p = 0.611; ARR15, p = 0.532; ARR8, p
202 = 0.0115; ARR9, p = 0.0416.
203 **(C)** A GFP-channel image of a stage 2 bud of GFP-nes (*pUBQ10::sfGFP-nes-UBQ3ter*). For this
204 panel and (E-H), each image was brightened to reveal GFP distribution patterns. A square region
205 taken from the image containing 5-10 cells is enlarged and shown on the top right. Within the
206 enlargement, GFP intensity was quantified along the dotted line and plotted on the bottom right.
207 X-axis, pixels (range 0-238). Y-axis, GFP intensity in gray value (smoothened by taking the
208 average intensity of 11-pixel neighborhoods; range 90-210). Scale bars, 25 μm.
209 **(D)** Illustration of the Llama Tag system used in this study. Plants were co-transformed with *ARR7-*
210 *llama* (*pARR7::ARR7-linker-llama-ARR7ter*) and *GFP-nes* (*pUBQ10::sfGFP-nes-UBQ3ter*).
211 Without ARR7-llama, the GFP is localized in the cytosol. ARR7-llama is produced in the cytosol
212 and translocates into the nucleus. When this happens, the Llama Tag capable of binding GFP
213 drags GFP into the nucleus (note that from our observation it is excluded from the nucleolus).
214 Therefore, at low ARR7-llama levels, GFP signal is mainly seen in the cytosol. At intermediate
215 ARR7-llama levels, GFP is at comparable intensities between the cytosol and the nucleus, and
216 no clear pattern can be seen. At high ARR7-llama levels, GFP is mainly seen in the nucleus.
217 **(E,F)** GFP channel images of stage 2 buds from two independent transgenic lines of *ARR7-llama*
218 *GFP-nes*, 7-4 (E) and 7-6 (F), in WT (top) vs *drmy1* (bottom). Images are representative of n =
219 17 (line 7-4, WT), n = 40 (line 7-4, *drmy1*), n = 9 (line 7-6, WT), and n = 6 (line 7-6, *drmy1*) buds.
220 **(G)** GFP channel images of WT *ARR7-llama GFP-nes* buds treated with mock (top) or 2 μM CHX
221 (bottom) for 24 hours. The mock image is representative of n = 20 buds (12 from line 7-4, 5 from
222 line 7-6, and 3 from line 7-12). The CHX image is representative of n = 19 buds (11 from line 7-4,
223 5 from line 7-6, and 3 from line 7-12).
224 **(H)** GFP channel images of WT *ARR7-llama GFP-nes* buds treated with mock (top) or 2 μM AZD-
225 8055 (bottom) for 72 hours. The mock image is representative of n = 13 buds (8 from line 7-4 and
226 5 from line 7-6). The AZD-8055 image is representative of n = 11 buds (8 from line 7-4 and 3 from
227 line 7-6).
228 **(I-N)** *ARR7-llama* partially restores robustness in *drmy1* sepal primordia. (I-L) Representative
229 stage 5 or 6 buds from WT (I), WT with the *ARR7-llama* and *GFP-nes* constructs (J), *drmy1* (K),
230 and *drmy1* with these constructs (L). (M) Quantification of sepal primordium number. ns indicates
231 no significance difference in a Fisher's exact test (WT vs *ARR7-llama*, p = 1; *drmy1* vs *drmy1*
232 *ARR7-llama*, p = 0.44). (N) Quantification of variability in sepal primordium position. Asterisk
233 indicates statistically significant difference ($p = 5.7 \times 10^{-6}$), while ns indicates no statistically
234 significant difference (p = 0.91). Data for WT and *drmy1* were reused from Figure 2H, 2J. Data
235 for *ARR7-llama GFP-nes* and *drmy1 ARR7-llama GFP-nes* were pooled from line 7-4 and 7-6.
236 Sample size: WT n = 51, *ARR7-llama GFP-nes* n = 16, *drmy1* n = 67, *drmy1 ARR7-llama GFP-*
237 *nes* n = 20. Scale bars, 25 μm.
238 **(O)** Working model. In WT, DRMY1 maintains TOR activity and translation, which sustains the
239 rapid translation of A-type ARRs in response to cytokinin signaling. This suppresses excessive
240 cytokinin signaling, allowing auxin and cytokinin signaling to interact and form robust spatial
241 patterns. Robust patterning of auxin and cytokinin signaling gives rise to robustly numbered,
242 positioned, and sized sepal primordia. In *drmy1*, A-type ARR protein levels are reduced due to

243 insufficient TOR activity, ribosome content, and translation rate. Cytokinin signaling is upregulated,
244 which rescues the translation rate reduction in a homeostatic mechanism. This upregulation of
245 cytokinin signaling disrupts the robust spatial pattern of both cytokinin and auxin signaling, which
246 in turn causes variable sepal initiation.
247